Crack propagation on highly heterogeneous composite materials

A catalogue record is available from the Eindhoven University of Technology Library

ISBN: 978-90-386-1367-3

Crack propagation on highly heterogeneous composite materials

PROEFSCHRIFT

ter verkrijging van de graad van doctor aan de
Technische Universiteit Eindhoven, op gezag van de
Rector Magnificus, prof.dr.ir. C.J. van Duijn, voor een
commissie aangewezen door het College
voor Promoties in het openbaar te verdedigen
op dinsdag 23 september 2008 om 16.00 uur

door

Miguel José Patrício Dias

geboren te Coimbra, Portugal

Dit proefschrift is goedgekeurd door de promotor:

prof.dr. R.M.M. Mattheij

Copromotor:
dr. M.E. Hochstenbach

Acknowledgment

This thesis is the product of research that was carried out at the Eindhoven University of Technology in the period ranging from October 2004 to August 2008. I find great pleasure in expressing my gratitude to the people who have contributed to this work.

I would like to start by thanking my promotor prof.dr. (Bob) Mattheij for offering me the opportunity to join a very interesting research project and for believing in me always. I will never forget how much I have learned from the many interesting conversations we had about maths, history, languages and life in general. I am sincerely grateful to my co-promotor dr. (Michiel) Hochstenbach for all the useful comments, discussions and the occasional game playing. Also, I greatly appreciate the kindness of prof.dr. (Bert) de With. Our conversations were very enlightening for me.

I am indebted to dr.ir. (Fons) van de Ven for the many times I went to him with a question. My thanks go to dr. (Sorin) Pop, ms. Enna van Dijk, dr. (Jos) Maubach and all the other members of CASA for their great help and friendship.

It's been great working and having fun with Mark van Kraaij, with whom I've had the privilege of sharing an office. I would also like to mention Remo, Dragan, Vincent, Evgeny, Willem, Yves, Kakuba, Kamyar and all the colleagues and friends that I've been fortunate to meet. I greet all the friends that I've kept throughout the years at home and abroad, in particular João, António, Mikael, Ana and Sandra. Thank you for bringing joy and balance to my life.

Most of all I am grateful to my family, my brother Ricardo, my sister-in-law Marta and my lovely niece Sofia. The loving support of my parents has been beyond words. I am blessed to have them in my life and I would like to dedicate this thesis to them.

Contents

Chapter 1

Introduction

1.1 Motivation

Engineering structures are designed to withstand the loads they will be subjected to while in service. Large stress concentrations are avoided and a reasonable margin of security is taken to ensure that values close to the maximum admissible stress are never attained. However, material imperfections that arise at the time of production or usage of the material are unavoidable and must be taken into account. Indeed, there are many unfortunate examples of situations where microscopic flaws have caused seemingly safe structures to fail, cf. [15, 53, 95].

In the past, when a component of some structure exhibited a crack, it was either repaired or simply retired from service. Such precautions are nowadays often deemed unnecessary, not possible to enforce, or may prove too costly. On one hand, the safety margins assigned to structures have to be smaller, due to increasing demands for energy and material conservation. On the other hand, the detection of a flaw in a structure does not automatically mean that it is not safe to use anymore. This is particularly relevant for expensive materials or components of structures whose usage it would be inconvenient to interrupt.

In this setting fracture mechanics plays a central role, as it provides useful tools allowing an analysis of materials that exhibit cracks. The goal is to predict whether and in which manner failure might occur. The origins of this branch of science in the western world can be traced back to at least as early as the work of Leonardo da Vinci, cf. [77,86]. He did a study of fracture strength of materials using a device described in the Codex Atlanticus [57,89], as represented in Figure 1.1. The experience consisted of suspending a basket on a wire of a given thickness and length and allowing it to be slowly filled with sand from an adjacently suspended hopper. A spring placed on the opening of the hopper ensured that the sand would stop dropping once the wire broke. The weight of

the basket with sand provided a measure of the tensile strength of the wire. By repeating the experience for wires of different lengths, da Vinci observed that shorter wires supported greater weight than longer wires. This conflicts with the classical theory of mechanics of materials that states that the stress in each unit of the wire should be the same regardless of its length. An explanation for this can be provided by the likelihood of larger fluctuations in the width of longer wires or in other words, by the idea that a chain is only as strong as its weakest link. The width of a presumably homogeneous wire actually varies with the position along it and the wire breaks in the region where its width is smallest.

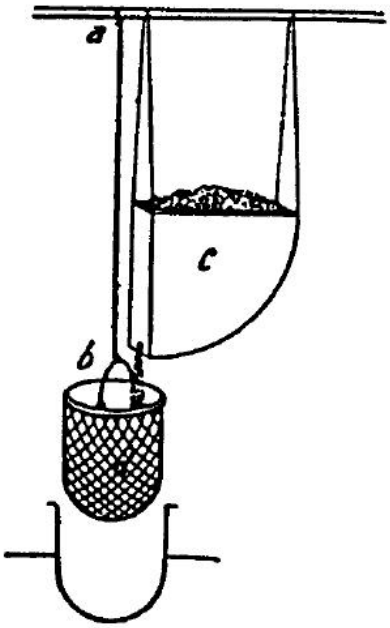

Figure 1.1: Basket (b) hanging on a wire (a), being filled up by sand falling from a hopper (c).

More than a century later Galileo investigated the influence of the size of structures in fracture, cf. [16,23,32]. Much more recently, the English aeronautical engineer Alan Griffith was able to theorise on the failure of brittle homogeneous linear elastic materials, see [34]. The classic model of a linear elastic material had been given by Robert Hook's work in the late XVII century. He related the force applied to a perfect spring to the extension of the spring, cf. [86]. Hook's law for *linear elastic* materials states that the stress on a solid medium is directly proportional to the strain produced, as long as the limit of elasticity is not exceeded. As a consequence, in the absence of stresses, a solid elastic body remains in its undeformed reference state. Also, no permanent deformations occur. After loading, when the stresses are again zero, the body returns to its original configuration.

Griffith used a thermodynamic approach to analyse the centrally cracked glass plate present in an earlier work of Inglis [41]. His theory was strictly restricted to elastic *brittle* materials like glass, in which virtually no plastic deformation near the tip of the crack occurs. However, extensions that account for such a deformation and further extend this theory were later suggested, for example in [42–45, 65].

Up to the present day fracture mechanics has remained a hot topic, with many open and intriguing questions. In particular there is great interest in predicting *crack propagation* on *composite* materials. Composites consist of two or more chemically or physically dissimilar constituents that are bonded together along interior material interfaces and do not dissolve or blend into each other, cf. [48, 52]. The idea is that by putting together the right ingredients a material with a better performance can be obtained. Composites are heterogeneous at the microscale, by which we mean the scale of the constituents, but they can be considered homogeneous at the macroscale. When the constituents are finely mixed, the materials are said to be highly *heterogeneous*.

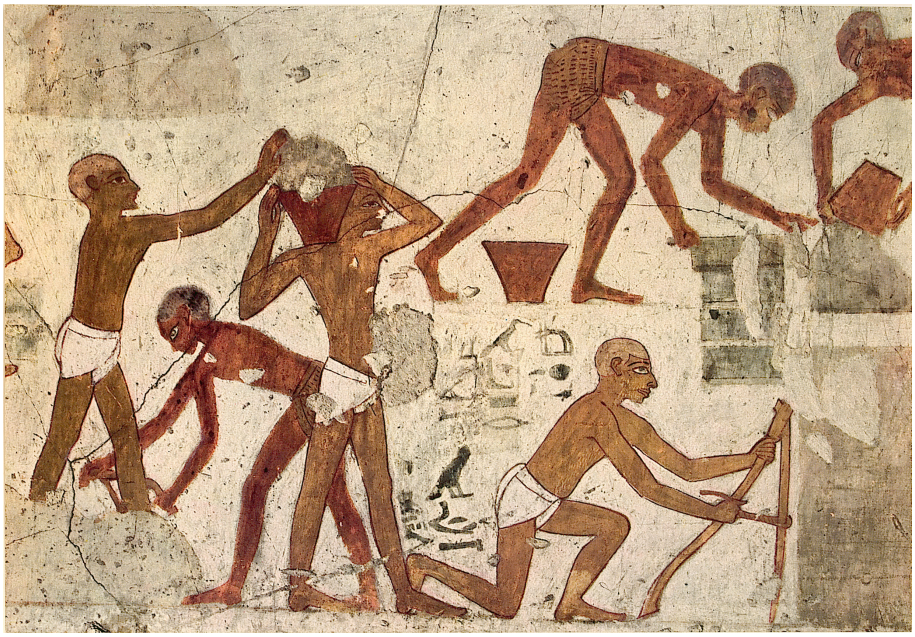

Figure 1.2: Manufacturing of bricks in Egypt; tomb of Rekhmire.

Nowadays composites such as fiber reinforced polymers or plywood are very common and can be found in many daily life products. But composites have actually been used by humans for thousands of years. An early example are the bricks made of mud and straw used in Ancient Egypt and mentioned in the Bible in the book Exodus. The manufacturing process of these bricks is represented in Figure 1.2.

1.2 Problem setting

To discuss the problem of crack propagation further, we begin by considering a simple example related to the cracked plate represented in Figure 1.3, which is loaded along its upper and lower edges so that the crack surfaces are pulled apart in the x_2-direction. We want to know under which conditions the initially stationary crack will start to grow, assuming the plate to be isotropic, homogeneous, brittle and linearly elastic.

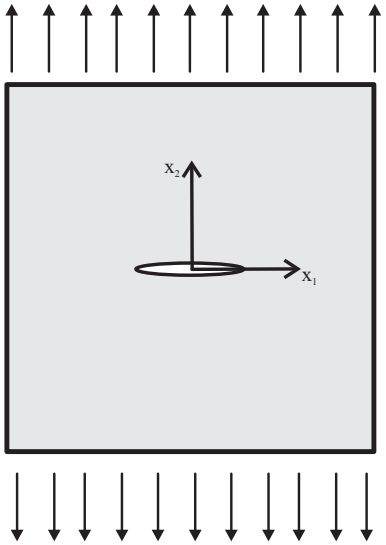

Figure 1.3: Finite plate with a centre through crack under tension.

The analysis of the fracture phenomenon focuses on the behaviour of the stress field in the crack tip region. Each stress component displays a singular behaviour characterised by local parameters called stress intensity factors (*SIFs*). These parameters are related to the geometry, the constitution of the material and the external boundary conditions, cf. for example [15, 94]. In particular, for the plate we have considered the horizontal tensile stress ahead of the crack tip and along the x_1-axis is characterised by the mode I SIF denoted by K_I. A fracture criterion tells us that the crack will propagate when K_I reaches a critical value that is material dependent, see [15, 37, 94].

In this simple example the crack may only grow in the direction of the x_1-axis. In more general situations the direction of propagation is not known a priori. The previous fracture criterion can then be naturally extended and the crack growth assumed to occur in a direction given as a function of the SIFs, cf. for example [30, 90]. In turn, the SIFs can be computed from the displacement and stress fields so that solving the elasticity problem is the first step in predicting whether and how a crack present on a homogeneous material will propagate. In general, the solutions of elasticity problems are obtained in terms of the displacements. There are many situations in which these solutions are either known [49] or can be easily approximated using classical numerical techniques

such as *finite element methods* or boundary element methods, cf. [7,10,11].

Given a cracked plate, an incremental approach to predict the future *crack path* can then be implemented, [30,37,55,67]. The crack is modelled as a very thin and long hole in the geometry, along which stress-free boundary conditions are prescribed. Assuming the crack to be static, the elasticity problem is solved and the direction for crack propagation determined. The crack is then incremented by updating the geometry. The procedure is repeated to determine the path further.

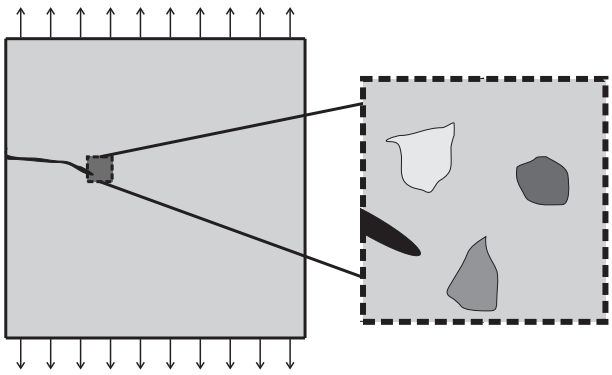

Figure 1.4: Cracked thin plate subject to vertical loading (left). Zoom in of the crack tip region displaying the various constituents of the composite (right).

Having considered crack propagation on homogeneous materials only is a rather large simplification. It is a much more complicated problem to know whether and how a pre-existent crack on a composite material may grow, see Figure 1.4. For now let us consider the situation in which the crack is propagating inside a homogeneous component of the composite and far from any internal material interfaces. As before, to model the crack propagation, we would have to first solve the elasticity problem. When dealing with composites, the coefficients of the underlying PDEs are material dependent and it is often the case that the constituents of the composite are finely mixed so that these coefficients jump between different values along the spatial coordinates very rapidly. This gives rise to very complicated problems with PDEs that have highly oscillatory coefficients. These are usually very hard to solve also numerically. When an accurate representation of the evolution of cracks is necessary, alternatives have to be found.

Many strategies that extend and adapt the method of finite elements for problems involving PDEs with coefficients that oscillate very rapidly have been developed, cf. [5,6, 28,38,39]. A different approach is given by the theory of *homogenisation*. It can be efficiently applied to PDEs with periodic coefficients. It allows for the approximation of the solutions of the original heterogeneous problem in terms of the solutions of the homogeneous problem comprised by the same boundary conditions but simplified PDEs, the *homogenised* or *effective* equations. The idea is to establish the *macroscopic* behaviour of a system that has heterogeneities on the *microscopic* level. The starting point is then a PDE with ϵ-periodic coefficients, with $\epsilon \ll 1$. The crucial step of the homogenisation process

consists of taking ϵ to zero. This is the same as assuming that the heterogeneities in the composite are so small that we may replace it by a fictitious homogeneous material. This asymptotic process, together with solving the *homogenised problem*, is in general computationally much easier than solving the original problem. The concept of homogenisation has been associated to other techniques and looked at from different points of view, giving rise to very efficient algorithms, cf. for example [2, 46, 71]. We like to cite [21] in particular, which updates the earlier writings of [8, 12, 78].

For periodic composite materials, this upscaling procedure has permitted significant progress. In particular it allows for an enormous simplification in the study of *layered* materials, cf. [68]. This type of materials is singled out due to their simplicity and because they are very commonly employed in the construction of structures with high performance and are also used for a wide range of applications, from sensor devices to magnetic or optical imaging. As an example, one may think of multilayer capacitors [51, 93] or laminar composites [25, 54].

A distinct approach to tackle elasticity problems related to highly heterogeneous composites consists of employing *domain decomposition* methods, see for example [26, 72, 79]. Unlike homogenisation, the heterogeneities are now resolved, which leads to more accuracy but also more computational complexity. Domain decomposition allows the division of the computational domain into smaller subdomains where the differential equation is to be solved. The original problem is then split into problems set on these subdomains, coupled together by matching conditions. In this way, instead of solving one very complicated problem, several less complicated problems will be solved. Domain decomposition is a very versatile technique. It allows for a parallel implementation as well as the usage of different numerical schemes within distinct subdomains. It is also advantageous for dealing with irregular geometries, discontinuous coefficients, local grid refinements, boundary layers and coupling between equations of different types, cf. for example [72, 80].

Both homogenisation and domain decomposition were introduced to deal with the complexity of elasticity problems for composite materials. A *hybrid approach* that borrows concepts from these two techniques is further considered. The advantage of this alternative approach is that it allows for a microscopic analysis to be restricted to where it is relevant, thus reducing the computational complexity of the problems dramatically when compared to domain decomposition methods. On the other hand, it provides more accuracy than homogenisation, cf. [69, 70]. This hybrid approach is particularly useful if on one or more localised regions of the computational domain a phenomenon such as crack propagation is to be analysed, for which the microstructure plays an important role. The study of these critical regions may be performed separately from the remainder of the domain, where a macroscopic approximation is sufficient. Such a compromise between the techniques of domain decomposition and homogenisation proves very effective if one intends to describe the behaviour of a pre-existent crack on a composite. Indeed, this is a local phenomenon that is primarily affected by the microstructure in the vicinity of the crack tip.

Let us now go back to the problem of fracture on a composite. When the crack is prop-

agating inside one the the material components, the incremental approach for homogeneous materials can be used effectively by employing domain decomposition or the hybrid approach to solve the elasticity problems. However, the crack will eventually propagate on further to other materials and interact with internal boundaries. Unless we look at this problem at a macroscale and deal with a homogeneous material, factors such as the nature and distribution of the constituents or the effect of the interfaces have to be taken into account, cf. [19]. This yields an extremely complex problem, and actually other aspects such as the existence of defects, the possibility of branching, creation of new cracks or delamination may also have to be incorporated into the analysis, cf. [9, 24, 63].

To provide a concrete framework that captures the fundamental aspects of the problem of fracture on a composite we consider a crack propagating through a periodically layered material. The aforementioned incremental approach can be adapted and extended for this problem by accounting for the interaction with the interfaces and making use of the hybrid technique to solve the complex elasticity problems.

1.3 Thesis layout

The present thesis is constituted by 7 chapters. In Chapter 2 the basic concepts of the classical theory of linear elasticity are introduced. The governing equations are established in Section 2.1. The problem of linear elasticity is then presented in a general setting in Section 2.2. In particular this can be formulated to model the behaviour of composite materials. The situation of thin plates under plane stress is also addressed. We conclude this chapter by introducing a weak formulation of the problem of linear elasticity and indicating how numerical approximations for its solution can be found using finite element methods.

Being able to determine the stress and displacement fields of a given cracked plate is not sufficient to model the growth of a propagating crack. One further needs to decide on criteria to determine under which conditions cracks will propagate as well as the direction of propagation. This is the main topic of Chapter 3, which begins with a short introduction in Section 3.1. Subsequently, in Section 3.2 several fracture parameters are introduced. We distinguish between global parameters and local parameters. Fracture criteria given in terms of the fracture parameters are then introduced in Section 3.3. The chapter is concluded with a discussion of various numerical aspects in Section 3.4. Fracture parameters are computed using several numerical methods and it is shown that with the J-integral method one obtains accurate reliable approximations. Finally, an algorithm is set up to predict the path of a growing pre-existent crack on an isotropic homogeneous linear elastic plate loaded in a mixed mode situation. This chapter may be regarded as an overview of some aspects of linear elastic fracture mechanics and is an enlarged version of [67].

One of the main issues arising in modelling crack propagation on composite elastic ma-

terials is solving the related elasticity problems, which are often very complex. When these materials are periodically distributed, one may apply the homogenisation theory, which is the object of study of Chapter 4. We start in Section 4.1 by presenting a one-dimensional example of an elliptic differential equation with periodic oscillating coefficients. This is meant to show how homogenisation techniques provide an accurate approximation for the solution of this example problem without having to resolve the microscale, hence avoiding prohibitively large computational costs. It is also shown that if more accuracy is sought correctors can be employed to recover the heterogeneities. Next, in Section 4.2, the 2D elasticity problem for periodically distributed composite materials is considered. The asymptotic behaviour of the solution of the underlying equations is analysed and the necessary fundamental concepts of the homogenisation theory literature are introduced. The homogenised equations are presented, as well as the main convergence result. The elastic behaviour of layered composites, a prime example of periodically distributed composites due to their widespread applications, is investigated. Explicit formulae for the respective effective coefficients are found, allowing us to establish several useful properties. In particular it is shown that the homogenised material that corresponds to an isotropic elastic layered material is orthotropic, with engineering constants given as a function of those characterising the constituents of the composite. The chapter is concluded with a discussion of some numerical aspects. An efficient procedure to determine the effective solutions for elasticity problems related to periodic structures numerically is proposed and illustrated with several examples. We note that the novel results of this chapter, in particular sections 4.2.2 and 4.2.3, are contained in [68].

In Chapter 5 domain decomposition methods are studied. Like the homogenisation techniques these methods are considered to handle the computational complexity of elasticity problems related to highly heterogeneous materials. The key idea is to divide the computational domain into smaller subdomains where the original equation is to be solved. This permits the solution to be obtained with microscopic resolution throughout, eventually employing parallelisation. Following the same pattern as in the previous chapter, we begin by illustrating the basic principles of the domain decomposition methods with a one-dimensional example in Section 5.1. It is discussed how approximations for the solution of the problem can be found using either overlapping or non-overlapping methods. We conclude the section by establishing a convergence result. In Section 5.2 the extension to the planar elasticity problem is considered. Domain decomposition methods are related to an interface equation expressed in terms of the Steklov-Poincaré operator. The Dirichlet-Neumann method is presented and it is shown how it reduces to the preconditioned Richardson method for the Steklov-Poincaré equation, which allows us to establish the convergence. An algorithm expressing an overlapping scheme is presented. We conclude by studying the Dirichlet-Neumann method at the discrete level in Section 5.3 and it is discussed how the acceleration parameter for this method can be optimised.

In many problems where different length scales are involved the microstructure is only really relevant on a localised subdomain where the phenomena one wants to model occurs. Everywhere else a macroscopic analysis is deemed sufficient. A hybrid approach to deal with this class of problems is proposed in Chapter 6, combining ho-

mogenisation and domain decomposition to form a new method, cf. [69, 70]. The idea is to resolve the microstructure where necessary and homogenise elsewhere to obtain an accurate solution with reasonably small computational effort. We start by analysing a one-dimensional boundary value problem in Section 6.1. An iterative scheme to find numerical approximations for the solution of this problem is proposed and the associated error is studied. In Section 6.2 the hybrid approach is extended for the problem of linear elasticity. Finally examples of application for the two problems considered are presented in Section 6.3.

The numerical techniques presented in the three previous chapters allow us to extend the analysis of Chapter 3 to the study of cracked composite materials. We begin Chapter 7 by investigating how stress intensity factors are affected by the local microscopic structure. The advantages of employing the hybrid approach to solve the related elasticity problem are highlighted in Section 7.1. Finally, in Section 7.2 the influence of internal material boundaries on a propagating crack is analysed. An algorithm to predict the path of pre-existent cracks on highly heterogeneous materials, making use of the aforementioned hybrid approach, is proposed. The technique is illustrated for a periodic composite and shown to produce very satisfactory results when compared to a reference solution.

Chapter 2

Mathematical modelling of linear elastic materials

The behaviour of linear elastic materials such as steel or copper can be modelled by second order elliptic PDEs. These differential equations take into account the specific properties of the medium. This sometimes leads to very complicated problems, particularly for highly heterogeneous structures.

In this chapter we introduce the basic concepts and equations that allow the mathematical analysis of mechanics problems involving linear elastic materials. The general elasticity problem is presented. Special attention is devoted to thin plates under plane stress.

2.1 Governing equations

The deformation of a body is expressed in terms of the strain and stress tensors, as well as the displacement vector. These fields satisfy the kinematic relations, conservation laws and constitutive equations that we will introduce in this section.

2.1.1 Kinematics

To study the motion of a deformable 3-dimensional continuous body $\mathcal{B}$, we start by setting up a suitable kinematical framework that does not depend on the constitution of the body or the forces that act on it, cf. [33, 36, 87]. As a result of the action of several forces, the body $\mathcal{B}$ will move and deform. We refer to the configuration of $\mathcal{B}$ at time t,

i.e., the region Ω_t that $\mathcal{B}$ occupies at time t, as the current configuration. We assume that for $t = 0$, the body is both undeformed and unstressed. It is then said to be at its reference configuration Ω.

We identify each point P of $\mathcal{B}$ with the position $\mathbf{x} = (x_1, x_2, x_3) \in \Omega$ it occupies in the reference configuration, with respect to a Cartesian coordinate system with origin $\mathbf{O}$ and unit basis vectors $\{\mathbf{e}_1, \mathbf{e}_2, \mathbf{e}_3\}$. We refer to $\mathbf{x}$ as a material point. As the body moves, the position of this point will also vary and we denote by $\mathbf{y} = \mathbf{y}(\mathbf{x}, t)$ the position that it occupies at time t. The vector function $\mathbf{y}$ is called the motion.

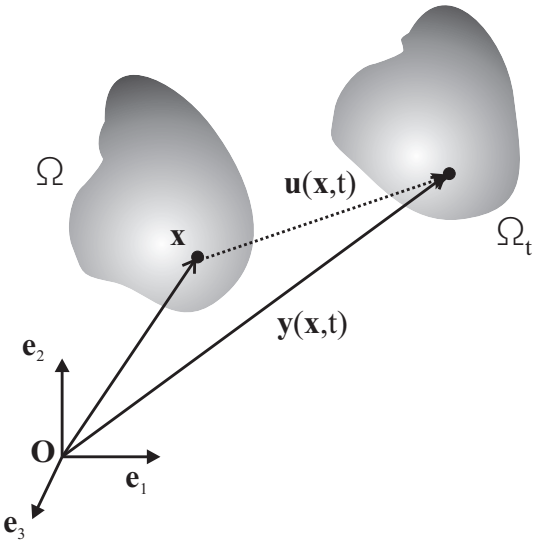

Figure 2.1: Motion and displacement of the material point $\mathbf{x}$.

For each point $\mathbf{x} \in \Omega$, clearly $\mathbf{y}(\mathbf{x}, 0) = \mathbf{x}$. Rather than working with $\mathbf{y}$ as a primary variable, it is useful to introduce the displacement vector field $\mathbf{u}(\mathbf{x}, t) = \mathbf{y}(\mathbf{x}, t) - \mathbf{x}$, see Figure 2.1. The displacement field characterises the motion of the body. It accounts for both the rigid body motions, i.e., translations and rotations and also for the deformations in which there are relative movements and distortions within the body. Not being interested in rigid body motions, we introduce a quantity that allows us to measure only deformation, the strain tensor $\boldsymbol{\eta} = (\eta_{ij})_{1 \le i,j \le 3}$ given by

$$\boldsymbol{\eta} = \frac{1}{2}(\nabla \mathbf{u} + (\nabla \mathbf{u})^T + (\nabla \mathbf{u})^T \nabla \mathbf{u}). \tag{2.1.1}$$

Here,

$$\nabla \mathbf{u} = \begin{pmatrix} \frac{\partial u_1}{\partial x_1} & \frac{\partial u_1}{\partial x_2} & \frac{\partial u_1}{\partial x_3} \\ \frac{\partial u_2}{\partial x_1} & \frac{\partial u_2}{\partial x_2} & \frac{\partial u_2}{\partial x_3} \\ \frac{\partial u_3}{\partial x_1} & \frac{\partial u_3}{\partial x_2} & \frac{\partial u_3}{\partial x_3} \end{pmatrix}$$

is the displacement gradient matrix. To interpret the physical meaning of $\boldsymbol{\eta}$, we start by considering the points $\mathbf{x} + \boldsymbol{\delta}\mathbf{x}_i$ in the reference configuration Ω, for $i = 1, 2$. In the current configuration, $\mathbf{x}$ and the two vectors $\boldsymbol{\delta}\mathbf{x}_i$ will be mapped to $\mathbf{y}$ and $\boldsymbol{\delta}\mathbf{y}_i = \mathbf{y}(\mathbf{x} + \boldsymbol{\delta}\mathbf{x}_i,\ t) - \mathbf{y}(\mathbf{x}, t)$ respectively, see Figure 2.2.

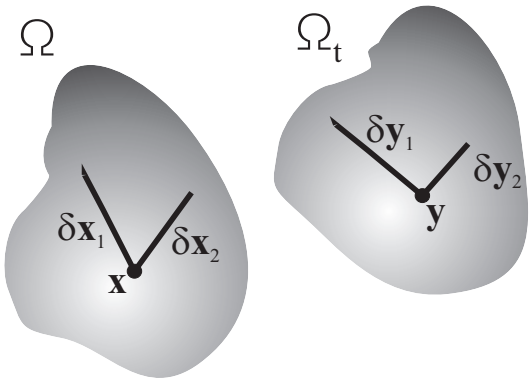

Figure 2.2: Configurations of $\mathcal{B}$.

To analyse the changes in both lengths and relative angles of the vectors $\boldsymbol{\delta}\mathbf{x}_1$ and $\boldsymbol{\delta}\mathbf{x}_2$ after deformation, we take the difference $\boldsymbol{\delta}\mathbf{y}_1 \cdot \boldsymbol{\delta}\mathbf{y}_2 - \boldsymbol{\delta}\mathbf{x}_1 \cdot \boldsymbol{\delta}\mathbf{x}_2$. We assume that it is possible to expand the functions $\mathbf{y}(\mathbf{x} + \boldsymbol{\delta}\mathbf{x}_1,\ t)$ and $\mathbf{y}(\mathbf{x} + \boldsymbol{\delta}\mathbf{x}_2,\ t)$ in Taylor series about $\mathbf{x}$, so that we can write

$$\begin{aligned} \boldsymbol{\delta}\mathbf{y}_1 \cdot \boldsymbol{\delta}\mathbf{y}_2 - \boldsymbol{\delta}\mathbf{x}_1 \cdot \boldsymbol{\delta}\mathbf{x}_2 \quad &= \quad (\nabla \mathbf{u} \boldsymbol{\delta}\mathbf{x}_1) \cdot \boldsymbol{\delta}\mathbf{x}_2 + (\nabla \mathbf{u} \boldsymbol{\delta}\mathbf{x}_2) \cdot \boldsymbol{\delta}\mathbf{x}_1 \\ &\quad + (\nabla \mathbf{u} \boldsymbol{\delta}\mathbf{x}_1) \cdot (\nabla \mathbf{u} \boldsymbol{\delta}\mathbf{x}_2) + \ldots \end{aligned} \tag{2.1.2}$$

Taking the limit in (2.1.2) as $\delta := \max\{\|\boldsymbol{\delta}\mathbf{x}_1\|, \|\boldsymbol{\delta}\mathbf{x}_2\|\}$ goes to zero, where $\|\cdot\|$ denotes the Cartesian norm, it follows that

$$\lim_{\delta \to 0} \frac{\boldsymbol{\delta}\mathbf{y}_1 \cdot \boldsymbol{\delta}\mathbf{y}_2 - \boldsymbol{\delta}\mathbf{x}_1 \cdot \boldsymbol{\delta}\mathbf{x}_2}{\delta^2} = 2\mathbf{m} \cdot \boldsymbol{\eta}(\mathbf{u})\mathbf{n}, \tag{2.1.3}$$

where $\mathbf{m} := \boldsymbol{\delta}\mathbf{x}_1/\delta$ and $\mathbf{n} := \boldsymbol{\delta}\mathbf{x}_2/\delta$ are fixed vectors, independent of h.

It is clear that if the body moves as a rigid body, then $\boldsymbol{\eta}(\mathbf{u}) = 0$, because the term on the left hand side of (2.1.2) must be zero. The converse is also true, as can be seen by interpreting the components of $\boldsymbol{\eta}$. To do so, we start by looking at the diagonal components of the strain tensor. These measure the relative elongation of vectors that are parallel to the coordinate axes. Indeed, assume for example that $\boldsymbol{\delta}\mathbf{x}_1 = \boldsymbol{\delta}\mathbf{x}_2 = \mathbf{e}_1$. Then from (2.1.3) we see that

$$\eta_{11} = \frac{1}{2} \lim_{\delta \to 0} \frac{\|\boldsymbol{\delta}\mathbf{y}_1\|^2 - \|\boldsymbol{\delta}\mathbf{x}_1\|^2}{\delta^2}.$$

As for the off-diagonal components of $\boldsymbol{\eta}$, they give a measure for the change in the angle between two vectors each parallel to a different coordinate axes. To illustrate this, assume that $\boldsymbol{\delta}\mathbf{x}_1$ and $\boldsymbol{\delta}\mathbf{x}_2$ have the same length δ and that they are parallel to $\mathbf{e}_1$ and $\mathbf{e}_2$, respectively. Then

$$\eta_{12} = \frac{1}{2} \lim_{\delta \to 0} \frac{\boldsymbol{\delta}\mathbf{y}_1 \cdot \boldsymbol{\delta}\mathbf{y}_2}{\delta^2}.$$

Throughout this thesis we will assume that the components of the displacement gradient are small. The material body $\mathcal{B}$ is then said to undergo infinitesimal deformation. The nonlinear term in (2.1.1) can be neglected and the strain tensor $\boldsymbol{\eta}$ may be replaced by the symmetric infinitesimal strain tensor $\boldsymbol{\epsilon}$ given by

$$\boldsymbol{\epsilon}(\mathbf{u}) = \frac{1}{2}(\nabla\mathbf{u} + (\nabla\mathbf{u})^T). \tag{2.1.4}$$

Henceforth we will simply refer to $\boldsymbol{\epsilon}$ as the strain tensor. The relationships expressed by (2.1.4), relating the strain tensor to the displacement vector, are known as the kinematic equations.

2.1.2 Conservation laws

Classical continuum mechanics is based upon a system of fundamental laws that apply for all material bodies, both solid and fluid. These express the balances of mass, momentum, moment of momentum and energy by postulating that in the absence of a source, these quantities remain unchanged. Here we present the laws of balance in their global form and introduce the notion of the stress tensor. The equations of motion for a continuum are deduced.

The global balance laws are formulated for an arbitrary sub-body $\mathcal{B}'$ of a body $\mathcal{B}$. At all times during the motion, $\mathcal{B}'$ contains the same set of points. We denote by $\Omega' \subset \Omega$ and $\Omega'_t \subset \Omega_t$ the regions occupied by $\mathcal{B}'$ in the undeformed state and at the time instant

t, respectively. Amongst the forces acting on $\mathcal{B}'$, we distinguish between the *body force* $\mathbf{f} = \rho\mathbf{b}(\mathbf{x}, t)$ and the surface traction $\mathbf{s_n}(\mathbf{x}, t)$, where ρ is the mass density and $\mathbf{b}$ is the specific external force field, or specific volume force field. The body force is due to external forces, e.g. the gravity. It represents the force per unit of volume acting at the time instant t on each particle $\mathbf{x}$ of $\mathcal{B}'$. As for the surface traction, also called the *stress vector*, it is the force per unit of area exerted by the part of $\mathcal{B}$ outside of $\mathcal{B}'$ across the border of $\mathcal{B}'$, see Figure 2.3. It depends on the point of action $\mathbf{x} \in \partial\Omega'_t$, on the time t and also on the outward pointing normal $\mathbf{n}$ in $\mathbf{x}$ on $\partial\Omega'_t$.

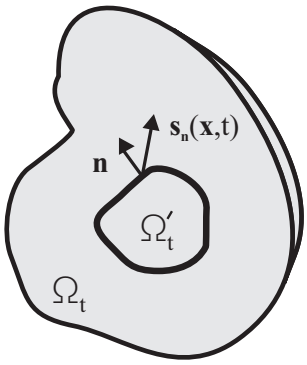

Figure 2.3: Stress vector field defined over the border of Ω'_t.

We are now ready to state the mechanical global balance laws.

Conservation of mass: in the absence of mass sources, the mass of the material contained in Ω' is constant,

$$\frac{d}{dt}\int_{\Omega'_t} \rho dV = 0. \tag{2.1.5}$$

Conservation of linear momentum: the rate of change of momentum of the material contained in $\mathcal{B}'$, due to the movement of the material with velocity $\dot{\mathbf{u}}$, is equal to the sum of the body forces and surface forces acting on the material,

$$\frac{d}{dt}\int_{\Omega'_t} \rho\dot{\mathbf{u}} dV = \int_{\Omega'_t} \rho\mathbf{b} dV + \oint_{\partial\Omega'_t} \mathbf{s_n} dS \tag{2.1.6}$$

Conservation of angular momentum: the rate of change of angular momentum in Ω', when the control volume moves with the continuum, is equal to the sum of the moment

of the body forces and the moment of the surface forces acting on it,

$$\frac{d}{dt}\int_{\Omega_t'} \mathbf{x}\times\rho\dot{\mathbf{u}}dV = \int_{\Omega_t'} \mathbf{x}\times\rho\mathbf{b}dV + \oint_{\partial\Omega_t'} \mathbf{x}\times\mathbf{s_n}dS. \tag{2.1.7}$$

Conservation of energy: the rate of change of kinetic energy and internal energy is equal to the mechanical power of the stresses and body forces acting on the material added to the heat supplied by internal sources and exchanged around the border,

$$\frac{d}{dt}\int_{\Omega_t'} \rho E dV = \oint_{\Omega_t'} \mathbf{s_n}\cdot\dot{\mathbf{u}}ds + \int_{\Omega_t'} \rho\mathbf{b}\cdot\dot{\mathbf{u}}dV - \oint_{\Omega_t'} \mathbf{q}\cdot\mathbf{n}dS + \int_{\Omega_t'} \rho r dV. \tag{2.1.8}$$

In (2.1.8), $\mathbf{q}$ is the heat flux vector, r the specific heat supply and E is the specific energy, cf. [62].

Since we assume the deformations to be infinitesimal, the distinction between the reference and current configurations may be ignored, cf. [36]. One would like to extract local relationships, valid for each of the material points in the body, from the global laws. Following [62, 87], we first introduce the second order tensor field $\sigma = (\sigma_{ij})_{1\le i,j\le 3}$ called the Cauchy stress, which verifies the Cauchy law

$$\boldsymbol{\sigma}\cdot\mathbf{n} = \mathbf{s_n}, \tag{2.1.9}$$

for each unit vector $\mathbf{n}$. The Cauchy stress characterises the state of stress for each point of $\mathcal{B}$. Now, using (2.1.9) and Gauss' theorem, we can rewrite (2.1.6) in the form

$$\int_{\Omega_t'} \rho\ddot{\mathbf{u}} - \rho\mathbf{b} - \nabla\cdot\boldsymbol{\sigma}dV = 0, \tag{2.1.10}$$

attending to the fact that by the transport theorem

$$\frac{d}{dt}\int_{\Omega_t'} \rho\dot{\mathbf{u}}dV = \int_{\Omega_t'} \rho\ddot{\mathbf{u}}dV. \tag{2.1.11}$$

Since (2.1.10) holds for any subdomain Ω_t' of Ω_t, the integrand must vanish and

$$\nabla\cdot\ \boldsymbol{\sigma} + \rho\mathbf{b} = \rho\ddot{\mathbf{u}}. \tag{2.1.12}$$

This equation is known as Cauchy's equation of motion. In the static case, when $\ddot{\mathbf{u}} = 0$, it reduces to the equation of equilibrium

$$\nabla \cdot \boldsymbol{\sigma} + \rho \mathbf{b} = \mathbf{0}. \tag{2.1.13}$$

We note that (2.1.7) allows us to show that the tensor σ is symmetric, cf. [62].

2.1.3 Constitutive equations

The kinematic equations (2.1.4) and the Cauchy's equation of motion (2.1.12) hold for any continuous medium. However, the mechanical properties of the material must also be taken into account. These are expressed by the *constitutive equations* or material laws. For linear elastic materials, the stress $\boldsymbol{\sigma}$ depends linearly on the strain $\boldsymbol{\epsilon}$. They are related by the generalised Hook's law

$$\boldsymbol{\sigma} = \mathbf{A}\boldsymbol{\epsilon}, \tag{2.1.14}$$

where $\mathbf{A} = \mathbf{A} = (a_{ijkh})_{1 \le i,j,k,h \le 2}$ is a fourth-order tensor called the *elasticity tensor*, see [36, 87]. It is convenient to write (2.1.14) in the matrix form

$$\begin{pmatrix} \sigma_{11} \\ \sigma_{22} \\ \sigma_{33} \\ \sigma_{12} \\ \sigma_{23} \\ \sigma_{31} \end{pmatrix} = \begin{pmatrix} a_{1111} & a_{1122} & a_{1133} & a_{1112} & a_{1123} & a_{1131} \\ a_{2211} & a_{2222} & a_{2233} & a_{2212} & a_{2223} & a_{2231} \\ a_{3311} & a_{3322} & a_{3333} & a_{3312} & a_{3323} & a_{3331} \\ a_{1211} & a_{1222} & a_{1233} & a_{1212} & a_{1223} & a_{1231} \\ a_{2311} & a_{2322} & a_{2333} & a_{2312} & a_{2323} & a_{2331} \\ a_{3111} & a_{3122} & a_{3133} & a_{3112} & a_{3123} & a_{3131} \end{pmatrix} \begin{pmatrix} \epsilon_{11} \\ \epsilon_{22} \\ \epsilon_{33} \\ \epsilon_{12} \\ \epsilon_{23} \\ \epsilon_{31} \end{pmatrix}. \tag{2.1.15}$$

The elasticity tensor is a function of position in the body, but it is independent of time as long as the material remains elastic, $\mathbf{A} = \mathbf{A}(\mathbf{x})$. Due to the symmetry of the stress and strain tensors, the components of $\mathbf{A}$ satisfy

$$a_{ijkh} = a_{jikh} = a_{khij}, \quad \text{for } i, j, k, h = 1, 2, 3.$$

The body $\mathcal{B}$ with elastic behaviour characterised by $\mathbf{A}$ is called homogeneous if both ρ and $\mathbf{A}$ are independent of spacial coordinates. Another classification arises from the

fact that some materials have certain properties of symmetry which allow the number of independent components of the elasticity tensor to be reduced, cf. [33]. A medium is then called *isotropic* if at each material point its mechanical properties are identical in all directions and *anisotropic* otherwise. It is called *orthotropic* if it has different materials properties along different orthogonal directions. In particular, for isotropic materials, (2.1.14) can be rewritten as

$$\boldsymbol{\sigma} = \lambda(\mathrm{tr}\boldsymbol{\epsilon})\mathbf{I} + 2\mu\boldsymbol{\epsilon}, \tag{2.1.16}$$

where λ and μ are the so called *Lamé moduli*. These are related to the relevant material parameters *Young's modulus* E, the *Poisson's ratio* ν and the *shear modulus* G by

$$E = \frac{\mu(2\mu+3\lambda)}{\mu+\lambda}, \quad \nu = \frac{\lambda}{2(\mu+\lambda)} \text{ and } G = \frac{E}{2(1+\nu)}.$$

2.2 The problem of linear elasticity

The governing equations that have been introduced allow the mechanical behaviour of linear elastic materials to be translated into a mathematical formulation. In particular, the *elasticity problem* for composite materials may be considered.

2.2.1 Problem formulation

In the dynamic case, the linear elastic behaviour of a material body $\mathcal{B}$ can be expressed in terms of the displacement vector $\mathbf{u}$ and the strain and stress tensors $\boldsymbol{\epsilon}$ and $\boldsymbol{\sigma}$ by the following equations, cf. for example [58, 62, 94].

$$\nabla \cdot \boldsymbol{\sigma} + \mathbf{f} = \rho\ddot{\mathbf{u}}, \tag{2.2.1}$$

$$\boldsymbol{\epsilon}(\mathbf{u}) = \frac{1}{2}(\nabla\mathbf{u} + (\nabla\mathbf{u})^T), \tag{2.2.2}$$

$$\boldsymbol{\sigma} = \mathbf{A}\boldsymbol{\epsilon}. \tag{2.2.3}$$

We note that the static case is obtained replacing $\rho\ddot{\mathbf{u}}$ by $\mathbf{0}$ in (2.2.1). In order for the elasticity problem to be complete and consistent, suitable boundary conditions are needed at each point of $\partial\Omega$, cf. [61, 87]. For this the equations (2.2.1)-(2.2.3) are supplemented by boundary conditions

$$\mathbf{u} = \boldsymbol{\varphi}_D, \quad \mathbf{x} \in \Gamma_D, \tag{2.2.4}$$

$$\boldsymbol{\sigma} \cdot \mathbf{n} = \boldsymbol{\varphi}_N, \quad \mathbf{x} \in \Gamma_N, \tag{2.2.5}$$

related to the undeformed boundary $\Gamma = \partial\Omega$. Here, Γ_D and Γ_N are the subsets of Γ where the displacements and the stress vectors are prescribed and the indices in $\boldsymbol{\varphi}_D$ and $\boldsymbol{\varphi}_N$ refer to Dirichlet and Neumann, respectively. We note that for the dynamic case initial boundary conditions must be added for the displacements and their time derivatives. The existence and uniqueness of the solution for this problem is ensured, possibly apart from rigid body motions, [87].

The equations of the problem of elasticity can be reduced to a system of three equations in which the displacement vector field is the primary unknown. We eliminate the stress and strain from the governing equations by substitution to obtain the Navier equations for the displacements. These read

$$\nabla \cdot \ (\mathbf{A}\boldsymbol{\epsilon}(\mathbf{u})) + \mathbf{f} = \rho\ddot{\mathbf{u}}.$$

As for the boundary condition expressed by (2.2.5) it is given by

$$\mathbf{A}\boldsymbol{\epsilon}(\mathbf{u}) \cdot \mathbf{n} = \boldsymbol{\varphi}_N, \quad \mathbf{x} \in \Gamma_N. \tag{2.2.6}$$

When dealing with composite materials, the components of the elasticity tensor vary with the spacial coordinates, giving rise to highly oscillatory PDEs. At the internal material interfaces, the coefficients of the differential equation display a discontinuity. The mathematical problem for composites is increasingly complex for more heterogeneous materials. It is still formulated as (2.2.1)-(2.2.5), but at the internal boundary no-jump conditions are prescribed, i.e., it is assumed that the displacements and the tractions are continuous.

2.2.2 Plane stress

The elasticity problem for the three-dimensional case is not easy to solve. However, under certain conditions, the problem may be simplified. This is the case for situations of *plane stress*, where thin plate-like structures are considered. For these, the normal and shear stresses in the x_3-direction can be assumed to be zero.

In this thesis we will consider the static elasticity problem for thin plates in a plane stress situation that reads

$$\begin{cases} -\nabla \cdot (\mathbf{A}(\mathbf{x})\boldsymbol{\epsilon}(\mathbf{u})) = \mathbf{f}, & \mathbf{x} \in \Omega, \\ \mathbf{u} = \mathbf{0}, & \mathbf{x} \in \Gamma_D, \\ \boldsymbol{\sigma}(\mathbf{u}) \cdot \mathbf{n} = \boldsymbol{\varphi}_N, & \mathbf{x} \in \Gamma_N. \end{cases} \tag{2.2.7}$$

The primary variable is the displacement vector $\mathbf{u} = (u_i)_{1 \le i \le 2}$. The elasticity tensor $\mathbf{A}$ which relates $\boldsymbol{\sigma}$ and $\boldsymbol{\epsilon}$ can be represented by a 3×3 matrix. For isotropic materials we have

$$\mathbf{A} = \begin{pmatrix} E/(1-\nu^2) & (E\nu)/(1-\nu^2) & 0 \\ (E\nu)/(1-\nu^2) & E/(1-\nu^2) & 0 \\ 0 & 0 & E/(2(1+\nu)) \end{pmatrix}, \tag{2.2.8}$$

where the Young's modulus E and the Poisson's ratio ν are the material parameters introduced earlier. For orthotropic materials $\mathbf{A}$ is given in terms of the Young's moduli E_{xy}, E_{yx}, the Poisson's ratios ν_{xy}, ν_{yx} and the shear modulus G_{xy}, so that

$$\mathbf{A} = \begin{pmatrix} E_x/(1-\nu_{xy}\nu_{yx}) & (E_x\nu_{xy})/(1-\nu_{xy}\nu_{yx}) & 0 \\ (E_y\nu_{yx})/(1-\nu_{xy}\nu_{yx}) & E_y/(1-\nu_{xy}\nu_{yx}) & 0 \\ 0 & 0 & G_{xy} \end{pmatrix}. \tag{2.2.9}$$

where $\nu_{xy}E_y = \nu_{yx}E_x$.

For future convenience we introduce the weak formulation for (2.2.7). Let Ω be a connected bounded open set in R^n. Moreover, let $\partial\Omega = \Gamma_N \cup \Gamma_D$ be Lipschitz continuous such that Γ_D is of measure greater than zero. From a Green's formula, we obtain the following variational formulation

$$a(\mathbf{u}, \mathbf{v}) = \langle \mathbf{l}, \mathbf{v} \rangle, \forall\, \mathbf{v} \in \mathcal{V}, \tag{2.2.10}$$

where we define

$$a(\mathbf{u}, \mathbf{v}) := \int_\Omega \sum_{i,j=1}^{2} \sigma_{ij}(\mathbf{u})\epsilon_{ij}(\mathbf{v}) dV, \tag{2.2.11}$$

$$\langle \mathbf{l}, \mathbf{v} \rangle := \int_\Omega \sum_{i=1}^{2} f_i v_i dV + \oint_{\Gamma_D} \sum_{i=1}^{2} \boldsymbol{\varphi}_{N,i} v_i dS. \tag{2.2.12}$$

Here, $\boldsymbol{\varphi}_N = (\boldsymbol{\varphi}_{N,i})_{i=1,2}$ and $\mathbf{v} = (v_i)_{i=1,2}$. As for $\mathcal{V}$ it is such that

$$\mathcal{V} := \{\mathbf{v} \mid \mathbf{v} \in (H^1(\Omega))^2,\ \boldsymbol{\gamma}(\mathbf{v}) = 0 \text{ on } \Gamma_D\}, \tag{2.2.13}$$

where $\boldsymbol{\gamma}(\mathbf{v}) := \mathbf{v}|_{\partial\Omega}$ is the trace of $\mathbf{v}$ on $\partial\Omega$. Furthermore, we assume that $\mathbf{f} \in (L^2(\Omega))^2$ and $\boldsymbol{\varphi}_N \in (L^2(\Gamma_N))^2$. The bilinear form a is $\mathcal{V}$-elliptic and continuous, whereas the linear functional $\mathbf{l}$ is bounded and linear, cf. [21]. The Lax-Milgram lemma assures that (2.2.10)-(2.2.12) has a unique solution.

A numerical approximation $\mathbf{u}_h$ for the solution $\mathbf{u} \in \mathcal{V}$ of (2.2.10) can be obtained by using *finite elements*. The domain Ω is triangulated into non-overlapping elements, typically triangles, rectangles or tetrahedra. We consider a finite dimensional subspace of $\mathcal{V}$ of dimension N, which we denote by $\mathcal{V}_h$. The parameter h in subscript expresses the maximum width of the side of the elements. A nodal basis $\{\boldsymbol{\phi}_j\}_{j=1,\dots,N}$ is defined for $\mathcal{V}_h$ such that at the finite element nodes denoted by $\mathbf{a}_j$ we have

$$\boldsymbol{\phi}_i(\mathbf{a}_j) = \delta_{ij},$$

where δ_{ij} is the Kronecker symbol. A finite element approximation $\mathbf{u}_h$ to $\mathbf{u}$ consists of a linear combination of elements of the nodal basis,

$$\mathbf{u}_h = \sum_{j=1}^{N} y_j \boldsymbol{\phi}_j.$$

Inserting this into the variational problem yields

$$a(\sum_{j=1}^{N} y_j \boldsymbol{\phi}_j, \boldsymbol{\phi}_k) = \langle \mathbf{l}, \boldsymbol{\phi}_k \rangle, \forall\, k = 1, \dots, N. \tag{2.2.14}$$

This produces a linear system for the vector of unknowns $\mathbf{y} = (y_i)_{i=1,\dots,N}$ that reads

$$\mathbf{D}\mathbf{y} = \mathbf{b},$$

where we define the *stiffness matrix* $\mathbf{D} = [d_{ij}]_{i,j=1,\dots,N}$ and the *load* $\mathbf{b} = (b_i)_{i=1,\dots,N}$ by

$$d_{ij} := a(\boldsymbol{\phi}_i, \boldsymbol{\phi}_j), \quad b_i := \langle \mathbf{l}, \boldsymbol{\phi}_i \rangle.$$

For a more thorough analysis of the finite element method, cf. for example [7, 10].

Chapter 3

The mechanics of crack propagation

Many tragic examples have shown that the slightest flaws in engineering structures might lead to major catastrophes. There is then great need of understanding the mechanics of fracture. This branch of science plays a central role in providing useful tools that allow for an analysis of materials exhibiting cracks. A main goal is to predict whether and in which manner failure might occur.

In this chapter we focus on the brittle fracture of thin plates in a plane stress situation, subject to in-plane loading. We start by introducing the relevant fracture parameters, the energy release rate, the J-integral and the stress intensity factors. Different fracture criteria are presented and related. We conclude by looking into numerical techniques for determining the fracture parameters and by predicting the path for a crack propagating on a homogeneous material.

3.1 Elastic failure

Let us consider a plate displaying a pre-existent crack. We can distinguish several ways in which a force may be applied to the plate causing the crack to propagate. In [45] a classification is proposed corresponding to the three situations represented in Figure 3.1. We will refer to these as mode I, mode II and mode III, respectively.

In the *mode I*, or opening mode, the body is loaded by tensile forces, such that the crack surfaces are pulled apart in the x_2-direction. The deformations are symmetric with respect to planes perpendicular to the x_2-axis and the x_3-axis.

In the *mode II*, or sliding mode, the body is loaded by shear forces parallel to the crack surfaces, which slide over each other in the x_1-direction. The deformations are symmetric with respect to a plane perpendicular to the x_3-axis and skew-symmetric with respect to a plane perpendicular to the x_2-axis.

Finally, in the *mode III*, or tearing mode, the body is loaded by shear forces parallel to the crack surfaces. These slide over each other in the x_3-direction. The deformations are skew-symmetric with respect to planes perpendicular to the x_3-axis and the x_2-axis.

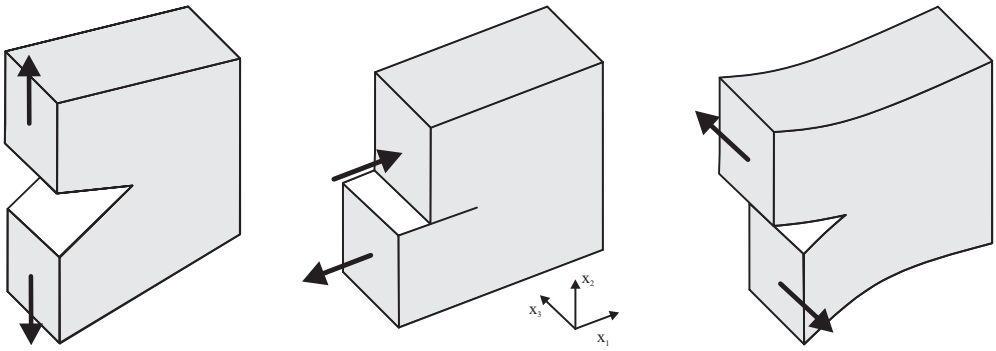

Figure 3.1 - a) *Opening.* ***b)*** *Sliding.* ***c)*** *Tearing.*

For each of these modes crack extension may only take place in the direction of the x_1-axis, the original orientation of the crack. More generally, we typically find a *mixed mode* situation, where there is a superposition of the modes and the crack may propagate in any direction. For such a problem the principle of stress superposition states that the individual contributions to a given stress component are additive, so that if σ_{ij}^{I}, σ_{ij}^{II} and σ_{ij}^{III} are the stress components associated to the modes I, II and III respectively, then the stress component σ_{ij} of a plate in a mixed mode situation is given by

$$\sigma_{ij} = \sigma_{ij}^{I} + \sigma_{ij}^{II} + \sigma_{ij}^{III}, \text{ for } i, j = 1, 2. \tag{3.1.1}$$

Within the scope of the theory of linear elasticity, a crack introduces a discontinuity in the elastic body such that the stresses tend to infinity as one approaches the crack tip. Using the semi-inverse method as in [91], Irwin [43,44] related the singular behaviour of the stress components to the distance to the crack tip r. In particular, when we consider a Cartesian coordinate system centred at the crack tip, in the opening mode and in polar coordinates we have

$$\sigma_{ij} \simeq \frac{K_I}{\sqrt{2\pi r}} f_{ij}^{I}(\theta), \tag{3.1.2}$$

where the angular variation function f_{ij}^{I} , which will be introduced later, depends only on θ. The parameter K_I, the stress intensity factor (*SIF*), plays a fundamental role in fracture mechanics, as it characterises the stress field, reflecting the geometry of the structure and the loading it is subject to. This approximation for the stresses is assumed to be valid in the vicinity of the crack tip for linearly elastic materials. Actually, the materials yield or deform inelastically very near the crack tip and so there is a region of validity of the approximation, cf. [73, 95].

Henceforth we will consider problems of linear elastic, isotropic, homogeneous and brittle cracked plates loaded under plane stress conditions. Both pure and mixed mode III situations will not be considered.

3.2 Fracture parameters

We begin by introducing the concepts of the strain release rate and the J-integral. These are global fracture parameters, based on an energetic approach. Next we focus on the stress intensity factors, which arise from the local distribution of the stresses in the vicinity of the crack tip.

3.2.1 Global approach

The failure of brittle materials, characterised by having virtually no plastic deformation near the tip of the crack, was first explained by Griffith using a thermodynamic approach, cf. [34, 92]. He used the mathematical work of Inglis [41], who had earlier analysed the case of an elastic infinite plate under uniform tensile stress. This had a central elliptic flaw of semi-major axis $a = c\cosh\xi$, and semi-minor axis $b = c\sinh\xi$, for given values of c, see Figure 3.5 a). The key idea is that when $\xi \to 0$, the elliptical flaw degenerates into a line of length $2a$ which can be considered to represent a crack. Under the assumption that the faces of the crack are free of stress, it can be assumed that crack propagation will occur if the energy required to form a new crack can be delivered by the system, see [15, 94]. Mathematically, this can be translated in terms of the quantities

$$\mathcal{U} = \frac{\sigma^2 \pi a^2}{2E}, \text{ and } \mathcal{W} = 2a\gamma. \tag{3.2.1}$$

Here, $\mathcal{U}$ is the strain energy released in the formation of a crack of length a and $\mathcal{W}$ is the corresponding surface energy increase, both per unit thickness of plate. The Young's modulus is denoted by E and γ is the material surface energy density or surface tension. The criterion for crack growth is then given by the equality

$$\mathcal{G} = \mathcal{R}, \text{ where } \mathcal{G} = -\frac{\partial \mathcal{U}}{\partial a} \text{ and } \mathcal{R} = \frac{\partial \mathcal{W}}{\partial a}. \tag{3.2.2}$$

This holds if the strain *energy release rate* $\mathcal{G}$ during crack growth is large enough to exceed the rate of increase in surface energy $\mathcal{R}$ associated with the formation of new crack surfaces.

The energy release rate can also be given in terms of the path-independent *J-integral*, cf. [74]. This is defined as a line integral along a counterclockwise contour C which surrounds the crack tip, see Figure 3.2. Its components are given in terms of the strain energy density $W_e = \sum_{i,j=1,2} \sigma_{ij}\epsilon_{ij}$ and the stresses by

$$J_k = \oint_C (W_e n_k - \sum_{i,j=1,2} \sigma_{ij} n_j \frac{\partial u_i}{\partial x_k}) dS, \tag{3.2.3}$$

for $k = 1, 2$ and where $\mathbf{n} = (n_1, n_2)$ is the outward-pointing normal vector defined over C, cf. [37, 90, 95]. The vector $\mathbf{J} = (J_k)_{k=1,2}$ can be regarded as the energy flux per unit length into the crack tip. It is called path-independent because it does not depend on the choice of the curve C, cf. [37].

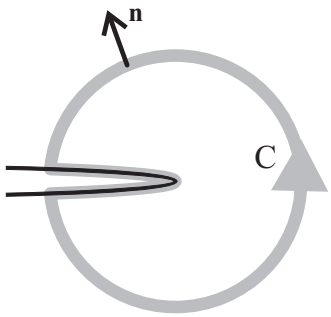

Figure 3.2: Integration path (gray) around the crack tip.

In the local coordinate system with the crack tip as origin and the crack located along the negative x_1-axis represented in Figure 3.3 the J-integral and the strain release rate are related by

$$J_1 = \mathcal{G}, \tag{3.2.4}$$

cf. for example [50].

3.2.2 Local approach

Let us consider a static crack in a plate which is in a plane stress situation. Assume that the crack surfaces are free of stress and that the axes are positioned as in Figure 3.3.

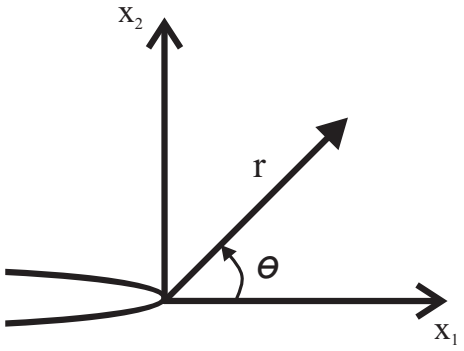

Figure 3.3: Crack tip coordinates.

For linearly elastic materials, the *stress field* in the vicinity of the crack tip is given in polar coordinates by

$$\boldsymbol{\sigma}(r,\theta) = \frac{K_I}{\sqrt{2\pi r}}\mathbf{f}^I(\theta) + \frac{K_{II}}{\sqrt{2\pi r}}\mathbf{f}^{II}(\theta), \tag{3.2.5}$$

up to an error of order of $\sqrt{r}$ for each component, cf. for example [15, 20, 31, 45]. In (3.2.5), the angular variation functions $\mathbf{f}^I = (f^I_{ij})_{i,j=1,2}$ for mode I are given by

$$f^I_{11}(\theta) = \cos(\frac{1}{2}\theta)\left(1 - \sin(\frac{1}{2}\theta)\sin(\frac{3}{2}\theta)\right), \tag{3.2.6}$$

$$f^I_{22}(\theta) = \cos(\frac{1}{2}\theta)\left(1 + \sin(\frac{1}{2}\theta)\sin(\frac{3}{2}\theta)\right), \tag{3.2.7}$$

$$f^I_{12}(\theta) = f^I_{21}(\theta) = \cos(\frac{1}{2}\theta)\sin(\frac{1}{2}\theta)\cos(\frac{3}{2}\theta), \tag{3.2.8}$$

while the equivalent functions $\mathbf{f}^{II} = (f^{II}_{ij})_{i,j=1,2}$ for mode II are

$$f^{II}_{11}(\theta) = -\sin(\frac{1}{2}\theta)\left(2 + \cos(\frac{1}{2}\theta)\cos\frac{3}{2}\theta)\right), \tag{3.2.9}$$

$$f_{22}^{II}(\theta) = \cos(\frac{1}{2}\theta)\sin(\frac{1}{2}\theta)\cos(\frac{3}{2}\theta), \tag{3.2.10}$$

$$f_{12}^{II}(\theta) = f_{21}^{II}(\theta) = \cos(\frac{1}{2}\theta)\left(1 - \sin(\frac{1}{2}\theta)\sin\frac{3}{2}\theta)\right). \tag{3.2.11}$$

As for K_I and K_{II}, they represent the SIFs for the modes I and II respectively and are defined by

$$K_I := \lim_{r\to 0} K_I^*(r), \text{ where } K_I^*(r) = \sqrt{2\pi r}\sigma_{22}(r,0), \tag{3.2.12}$$

$$K_{II} := \lim_{r\to 0} K_{II}^*(r), \text{ where } K_{II}^*(r) = \sqrt{2\pi r}\sigma_{12}(r,0). \tag{3.2.13}$$

It is also possible to obtain equations for the corresponding *displacement field* near the crack tip, cf. [20,45,66]. Again up to an error of order of $\sqrt{r}$, this is given by

$$\mathbf{u}(r,\theta) = \frac{K_I}{G}\sqrt{\frac{r}{2\pi}}\bar{\mathbf{f}}^I(\theta) + \frac{K_{II}}{G}\sqrt{\frac{r}{2\pi}}\bar{\mathbf{f}}^{II}(\theta). \tag{3.2.14}$$

The angular variation functions $\bar{\mathbf{f}}^I = (\bar{f}_i^I)_{i=1,2}$ and $\bar{\mathbf{f}}^{II} = (\bar{f}_i^{II})_{i=1,2}$ in (3.2.14) are

$$\bar{f}_1^I(\theta) = \cos(\frac{1}{2}\theta)\left(\frac{1-\nu}{1+\nu} + \sin^2(\frac{1}{2}\theta)\right), \tag{3.2.15}$$

$$\bar{f}_2^I(\theta) = \sin(\frac{1}{2}\theta)\left(\frac{2}{1+\nu} - \cos^2(\frac{1}{2}\theta)\right), \tag{3.2.16}$$

$$\bar{f}_1^{II}(\theta) = \sin(\frac{1}{2}\theta)\left(\frac{2}{1+\nu} + \cos^2(\frac{1}{2}\theta)\right), \tag{3.2.17}$$

$$\bar{f}_2^{II}(\theta) = \cos(\frac{1}{2}\theta)\left(-\frac{1-\nu}{1+\nu} + \sin^2(\frac{1}{2}\theta)\right). \tag{3.2.18}$$

These formulae allow us to have a characterisation of the stresses and the displacements in the vicinity of a crack tip.

3.3 Fracture criteria

Two different types of fracture criteria must be distinguished. Global criteria are based on an energy balance and are related to the energy release strain and the J-integral. Local criteria, on the other hand, make use of the key role of the SIFs in the stress state near the tip of the crack, see for example [37, 90, 94].

We proceed to present global and local criteria for a stationary semi-infinite line crack, loaded in a mode I situation. The symmetry of the deformations then implies that the crack may only propagate in a direction perpendicular to the loading. All that is required is a condition for crack growth.

A possible criterion, so-called *global criterion*, states that the crack will propagate when the energy stored is sufficient to break the material. This is expressed by the following equation for the energy release rate

$$\mathcal{G} = \mathcal{G}_c. \tag{3.3.1}$$

Here, $\mathcal{G}_c$ is the *critical energy release rate*. It is a material parameter that may be determined experimentally. Given that the first component of $\mathbf{J}$ equals the energy release rate, (3.3.1) can also be expressed in terms of the J-integral.

It is also possible to establish a different criterion making use of the fact that the singular stresses are characterised by K_I in the region surrounding the tip of the crack. This *local criterion* reads

$$K_I = K_{I_c}. \tag{3.3.2}$$

Here K_{I_c}, which behaves as a threshold value for K_I, is called the *critical stress intensity factor* or the mode I fracture toughness. We include in Table 3.1 examples of experimental data for the fracture toughness of some materials, as taken from [4].

The criteria (3.3.1) and (3.3.2) are actually equivalent, as the energy release rate and the stress intensity factor are related by

$$\mathcal{G} = \frac{K_I^2}{E}. \tag{3.3.3}$$

Naturally the critical energy release rate and the critical stress intensity factor are also similarly related.

We now turn our attention to the more general case when the loading is a combination of modes I and II, assuming that $K_I > 0$. Now there is a fundamental difference to the

Material	K_{I_c} $(MN/m^{3/2})$
Mild steel	140
Titanium alloys	$55-120$
High carbon steel	30
Nickel, copper	>100
Concrete (steel reinforced)	$10-15$
Concrete (unreinforced)	0.2
Glasses, rocks	1
Ceramics (Alumina, SiC)	$3-5$
Nylon	3
Polyester	0.5

Table 3.1: Examples of fracture toughness.

mode I loading situation, where the direction of the crack growth is trivially determined. In a mixed mode situation, criteria on whether the crack will propagate but also on which direction it will do so must be decided upon.

A *global criterion* for propagation, expressed in terms of the J-integrals defined earlier, is given by

$$\|\mathbf{J}\|_2 = G_c, \tag{3.3.4}$$

which can be seen as a generalisation of (3.3.1) when written in terms of J_1. The direction $\theta_p^{(J)}$ of the crack extension is the same as the direction of the vector $\mathbf{J}$

$$\theta_p^{(J)} = \arctan\left(\frac{J_2}{J_1}\right). \tag{3.3.5}$$

Moreover, a *local criterion* based on the *circumferential tensile stress* $\sigma_{\theta\theta}$ given by

$$\sigma_{\theta\theta} = \frac{\sigma_{11}+\sigma_{22}}{2} - \frac{\sigma_{11}-\sigma_{22}}{2}\cos(2\theta) - \sigma_{12}\sin(2\theta), \tag{3.3.6}$$

also known as the *tangential stress*, can be obtained by rewriting the stresses in (3.2.5) into local polar coordinates, cf. [15, 20]. We thus obtain, up to an order of $\sqrt{r}$,

$$\sigma_{\theta\theta}(r,\theta) = \frac{K_{\theta\theta}(\theta)}{\sqrt{2\pi r}}, \tag{3.3.7}$$

where

$$K_{\theta\theta}(\theta) = K_I \cos^3(\frac{1}{2}\theta) - 3K_{II}\sin(\frac{1}{2}\theta)\cos^2(\frac{1}{2}\theta), \tag{3.3.8}$$

is the *circumferential stress intensity factor*. By the *maximum circumferential tensile stress criterion*, crack growth will occur when

$$\max_{\theta} K_{\theta\theta}(\theta) = K_{I_c}, \tag{3.3.9}$$

which can be seen as a generalisation of (3.3.2). This criterion states that the direction of propagation is given by the angle $\theta_p^{(K)}$ which maximises $K_{\theta\theta}(\theta)$,

$$\theta_p^{(K)} = 2\arctan\left(\frac{K_I - \sqrt{K_I^2 + 8K_{II}^2}}{4K_{II}}\right), \tag{3.3.10}$$

cf. [30,55]. This formula can be used to rewrite the condition for crack extension (3.3.9). Indeed, $\max_\theta K_{\theta\theta}(\theta)$ can be calculated by inserting the value of the angle given by (3.3.10) in the circumferential tensile stress expressed in (3.3.8). We thus obtain

$$\frac{4\sqrt{2}K_{II}^3\left(K_I + 3\sqrt{K_I^2 + 8K_{II}^2}\right)}{\left(K_I^2 + 12K_{II}^2 - K_I\sqrt{K_I^2 + 8K_{II}^2}\right)^{\frac{3}{2}}} = K_{I_c}. \tag{3.3.11}$$

In a mixed mode situation the components of the J-integral are related to the stress intensity factors

$$J_1 = \frac{k+1}{8G}(K_I^2 + K_{II}^2); \qquad J_2 = -\frac{k+1}{4G}K_I K_{II}, \tag{3.3.12}$$

where $k = (3-\nu)/(1+\nu)$, ν is the material's Poisson's ratio and G its shear modulus, cf. [37,90]. These relations allow the comparison between the global fracture criterion (3.3.4) - (3.3.5) and the local fracture criterion (3.3.10) - (3.3.11) for a mixed mode situation. When the fracture is dominated by mode I, i.e., when $|K_{II}/K_I|$ is small, these

criteria are nearly equivalent, cf. [90]. This is illustrated in Figure 3.4, where the propagation angles are displayed.

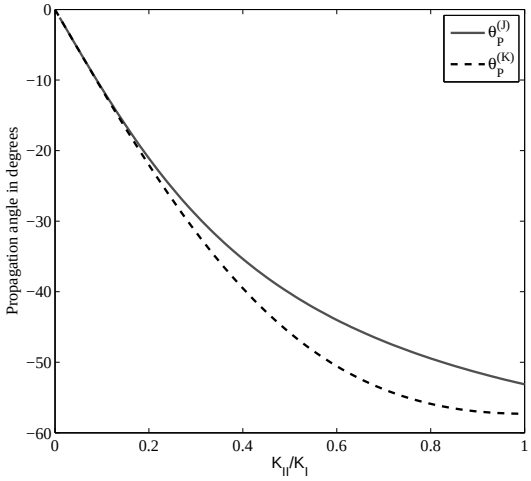

Figure 3.4: Crack propagation angles.

Henceforth we adopt the local criterion (3.3.10) - (3.3.11) and denote the propagation angle $\theta_P^{(K)}$ simply by θ_P.

3.4 Numerical aspects

The fracture parameters which were introduced earlier are usually computed applying numerical techniques. Once they have been determined, the fracture criteria allow the prediction of the consecutive positions of the crack tip of a propagating crack.

3.4.1 Stress intensity factors

As we have seen the criteria for crack propagation can be given in terms of the SIFs. It is then important to be able to approximate these accurately. There are classical examples of cracked geometries for which the stress intensity factors have been computed or approximated explicitly, cf. [83].

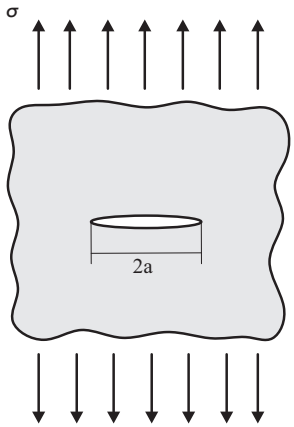

Figure 3.5 - a) *Infinite plate with a centre through crack under tension.*

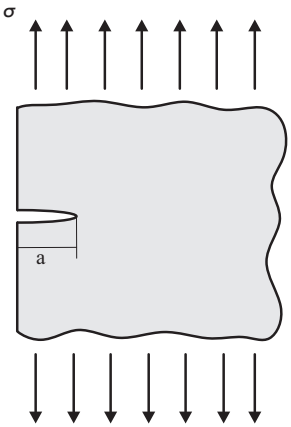

b) *Semi-Infinite plate with a centre through crack under tension.*

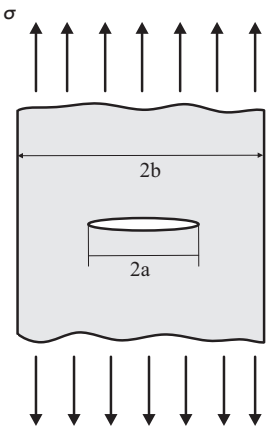

c) *Infinite stripe with a centre through crack under tension.*

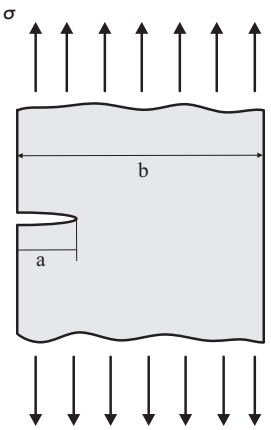

d) *Infinite stripe with an edge through crack under tension.*

As an example we include the values of the SIFs for the various geometries represented in Figure 3.5, each subject to a uniform tensile stress σ. These values are as follows, where the letters a) - d) used to identify the formulae correspond to those of the figure.

a) $K_I = \sigma\sqrt{\pi a}$;

b) $K_I = 1.1215\sigma\sqrt{\pi a}$;

c) $K_I = \sigma\sqrt{\pi a}\left(1 - 0.025\rho^2 + 0.06\rho^4\sqrt{\sec\frac{\pi\rho}{2}}\right)$;

d) $K_I = \sigma\sqrt{\pi a}\left(\sqrt{\frac{2}{\pi\rho}\tan\frac{\pi\rho}{2}}\ \frac{0.752+2.02\rho+0.37(1-\sin(\pi\rho/2))^3}{\cos(\pi\rho/2)}\right)$.

Here, $\rho = a/b$. The previous examples involve geometries of infinite dimensions. In this section, we will instead focus on a finite geometry. Consider a square plate, of side length $2b$, with a central crack of length $2a$, see Figure 3.6. Let the plate be loaded from its upper and lower edges again by a uniform tensile stress σ.

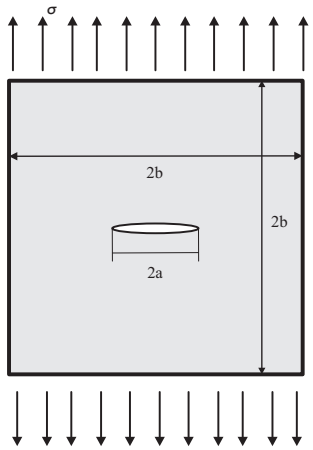

Figure 3.6: Finite plate with a centre through crack under tension.

For this cracked plate, the SIF has been estimated in [1] to be given by

$$\begin{aligned} K_I &= \sigma\sqrt{\pi a}(1 + 0.043\rho + 0.491\rho^2 + 7.125\rho^3 - 28.403\rho^4 \\ &\quad +59.583\rho^5 - 65.278\rho^6 + 29.762\rho^7). \end{aligned} \tag{3.4.1}$$

From this formula we compute reference solutions for the stress intensity factors for several values of $\rho = a/b$. The values of K_I/K_0, where $K_0 := \sigma\sqrt{\pi a}$, are displayed in the second line of Table 3.2. Note that K_I/K_0 does not depend on the loading applied to the plate, but only on the geometrical ratio ρ. In what follows we discuss several methods to compute the SIFs numerically, namely the stress correlation method, the displacement correlation method and the J-integral method, cf. for example [95].

Earlier we presented formulae that allow us to characterise the stress field in the vicinity of a crack tip. In turn, if the stress field is known, this allows determining the SIFs using (3.2.12) and (3.2.13). This is the key idea of the *stress correlation method*. The technique is applied as follows: one simply finds the functions $K_I^*(r)$ and $K_{II}^*(r)$ for values of the stress computed ahead of the crack tip, using finite elements for instance, and extrapolates back to $r = 0$ to find approximations for K_I and K_{II} respectively. This method is quite simple, but its accuracy depends on the mesh refinement and also on how well

the solution of the elasticity problem captures the crack singularity.

An alternative technique is given by the *displacement correlation method*. It makes use of the equations for the displacement field near the crack tip, from which it can be shown that

$$K_I = \lim_{r\to 0} K_I^{**}(r), \text{ where } K_I^{**}(r) = \frac{E}{4}u_2(r,\pi)\sqrt{\frac{2\pi}{r}}, \tag{3.4.2}$$

$$K_{II} = \lim_{r\to 0} K_{II}^{**}(r), \text{ where } K_{II}^{**}(r) = \frac{E}{4}u_1(r,\pi)\sqrt{\frac{2\pi}{r}}. \tag{3.4.3}$$

The determination of the SIFs then follows a similar procedure to the one described for the stress correlation method.

Finally, the *J-integral method* makes use of the J-integral. This can be computed along a path surrounding the crack tip by means of (3.2.3). In turn the SIFs can be determined using (3.3.12). The main advantage of the J-integral method is that it is very accurate in general without requiring the usage of very fine meshes. This is because capturing the crack tip singular stress field is no longer necessary. It suffices to be able to find a good approximation for the stress and strain fields over the curve of the J-integral. It is in that sense a global approach.

To illustrate the usage of these techniques we consider once again the problem of the plate illustrated in Figure 3.6. For each value of ρ we start by finding an approximation for the SIF by applying the displacement correlation method. We first solve the elasticity problem by a finite element method. A mesh with quadratic triangular elements with maximum width of the element side $h = 0.01$ is generated. Next, we approximate the function K_I^{**} by a linear polynomial within an interval contained in $[0, a]$. The choice of the interval is not arbitrary. Indeed, since the limit when $r \to 0$ is sought, we want to consider the function in a domain where the values of r are small. On the other hand the crack tip singularity affects the accuracy of the results near $r = 0$. This means that the values of K_I^{**} when r is too small must be disregarded.

To illustrate this procedure, we take $\rho = 0.4$. Without loss of generality, let $b = 1$. The values of K_I^{**}/K_0 can be plotted versus the values of r, see the full line in Figure 3.7.

We use a linear interpolator, represented by a dashed line, to fit the function in the interval $[0.03, 0.2]$. The data over the interval $[0, 0.03]$ are neglected due to the crack tip singularity and the consequent non-linear behaviour of K_I^{**}. To proceed, we extrapolate the value of the interpolator back to $r = 0$ and obtain the desired approximation. The SIFs computed using this method yield the results displayed in the third line of Table 3.2 for the various values of ρ contained in the first line of the table.

The stress correlation method works similarly. The results are shown in the fourth line of Table 3.2. They are not as accurate as those obtained using the displacement cor-

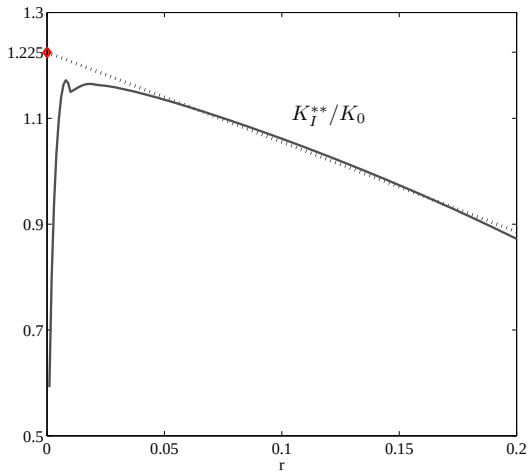

Figure 3.7: Extrapolation using the displacement correlation method, $\rho = 0.4$.

$SIF/K_0 \quad \backslash \quad \rho$	0.1	0.2	0.4	0.6
K_I/K_0	1.014	1.055	1.216	1.481
$K_I(\mathbf{u})/K_0$	1.004	1.058	1.225	1.525
$K_I(\boldsymbol{\sigma})/K_0$	1.226	1.145	1.211	1.802
$K_I(\mathbf{J})/K_0$	1.004	1.051	1.212	1.477

Table 3.2: Stress intensity factors.

relation method. This is to be expected, because now we are using the stresses to approximate the SIFs, whereas the primary result of the finite element computation is the displacement field.

It should also be pointed out that the two previous methods require a choice to be made for the interval where the linear interpolator is to be applied. This is not completely objective and requires intuition, which does affect the results. The inherent subjectivity of the choice of an interval is no longer a problem for the method employing the J-integral, as this fracture parameter is path-independent. In this sense this is a much more reliable method than the previous two as it allows for quite accurate approximations of the SIFs. The results obtained using this method can be seen in the last line of Table 3.2. They are the average of a number of J-integrals, each computed over a small circle centred at the crack tip.

3.4.2 Simulation of crack growth

Earlier a static fracture analysis was performed, where the goal was merely to compute the stress intensity factors. With the fracture criteria introduced in section 3.3, we can now look into the actual propagation of the crack.

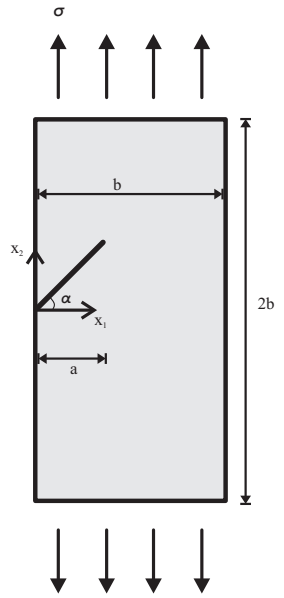

Figure 3.8: Finite plate with a crack subject to mixed mode loading.

Consider the cracked rectangular linear elastic plate of width b and height $2b$, represented in Figure 3.8. Let the ratio between the length of the crack measured along the x_1-axis and the width of the plate be such that $a/b = 1/5$. In order to consider a mixed mode situation the inclined initial crack is considered to be at a $\alpha = 45°$ angle with the horizontal axis. Without loss of generality, we take $b = 1$.

If the uniform tensile stress σ, which is applied at the lower and upper horizontal boundaries of the plate, is large enough so that the fracture criterion (3.3.11) holds, we do know that the initial crack will propagate. We assume it will do so in the direction given by (3.3.10).

We are now ready to set up a procedure for the prediction of the crack path. Denote the initial crack tip coordinates by $\mathbf{x}_{tip}^{(0)} = (x_{tip}^{(0)}, y_{tip}^{(0)})$ and the initial crack angle by $\theta^{(0)}$. Following an incremental approach to keep track of the position of the crack tip as the crack grows as suggested in [37, 55, 67], the crack path is determined step by step. At each step the direction of propagation is determined and the crack is incremented with a line segment of length Δa. This procedure is structured as follows.

Algorithm 3.1

Set $n = 0$. Given: Δa, $\mathbf{x}_{tip}^{(0)}$, $\theta^{(0)}$.

1- Solve the elasticity problem.

2- Compute the values of the stress intensity factors, K_I and K_{II}.

3- Determine the angle of propagation $\theta_p = \theta_p^{(K)}$ using equation (3.3.10).

4- Update the crack angle and the crack tip coordinates

$$\theta^{(n+1)} := \theta^{(n)} + \theta_P, \tag{3.4.4}$$

$$\mathbf{x}_{tip}^{(n+1)} = \mathbf{x}_{tip}^{(n)} + \Delta a(\cos(\theta^{(n+1)}), \sin(\theta^{(n+1)})). \tag{3.4.5}$$

5- Increment n, $n \to n + 1$.

6- If required to determine the path further, repeat steps 1 to 6.

This algorithm can be employed to determine the set of consecutive crack tip coordinates $\mathbf{x}_{tip}^{(n)} = (x_{tip}^{(n)}, y_{tip}^{(n)})$ for the propagating crack of the plate illustrated in Figure 3.8, with $\Delta a = 0.025$. We use the numerical package *Abaqus* to solve the elasticity problem in the first step of the algorithm. Quadratic rectangular elements are employed everywhere except near the crack tip, where quadratic triangular elements are used. The SIFs are determined using the J-integral method. The results obtained using the aforementioned algorithm are displayed in Table 3.3.

n	$x_{tip}^{(n)}$	$y_{tip}^{(n)}$	n	$x_{tip}^{(n)}$	$y_{tip}^{(n)}$	n	$x_{tip}^{(n)}$	$y_{tip}^{(n)}$
0	0.100	0.100	5	0.225	0.101	10	0.350	0.101
1	0.125	0.102	6	0.250	0.101	11	0.375	0.101
2	0.150	0.101	7	0.225	0.101	12	0.400	0.102
3	0.175	0.101	8	0.300	0.101	13	0.425	0.102
4	0.200	0.101	9	0.325	0.101	14	0.475	0.102

Table 3.3: Crack tip positions.

The discretisation elements of the crack tip region are illustrated in Figure 3.9, where the crack is represented by the darker region.

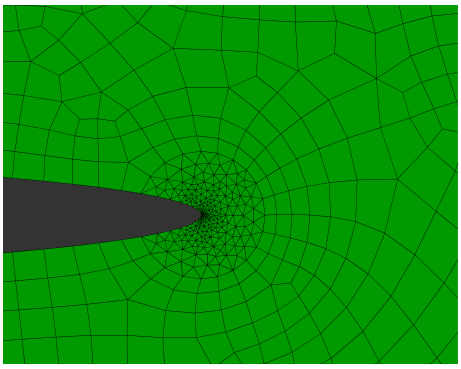

Figure 3.9: Crack tip region.

The deformed state of the plate before propagation and the deformed plate geometry obtained after 15 steps of the algorithm are displayed in Figure 3.10 a) and b), respectively.

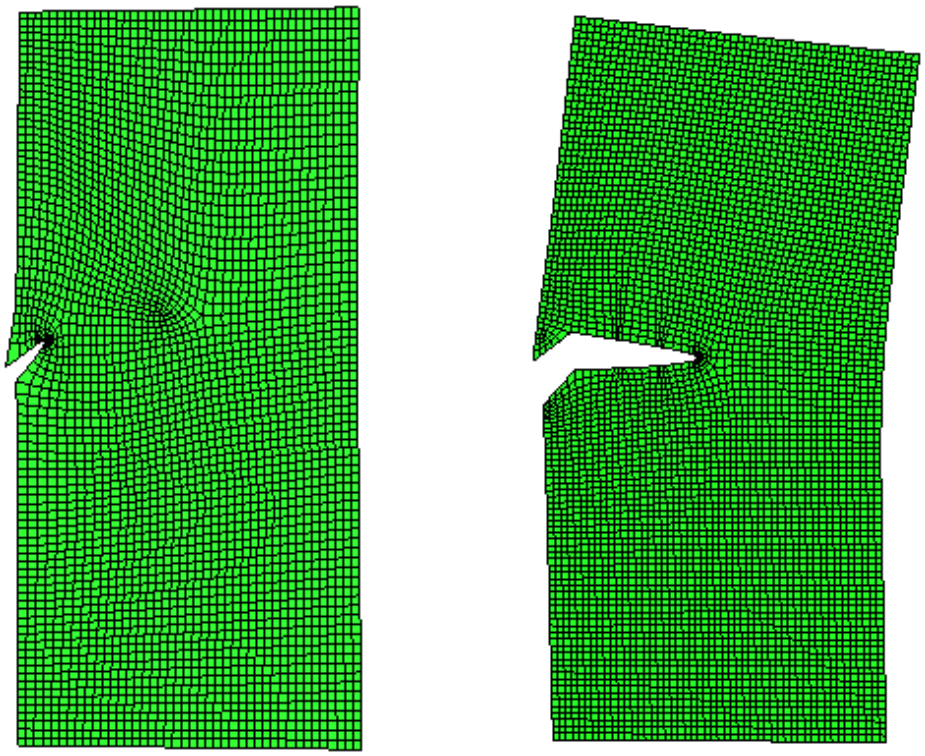

Figure 3.10 - a) *Deformed initial plate.* ***b)*** *Deformed plate for* $n = 15$.

Finally, the crack path can be seen in Figure 3.11. In a) we plot the initial crack segment

and in b) the crack path as it was determined after 15 steps.

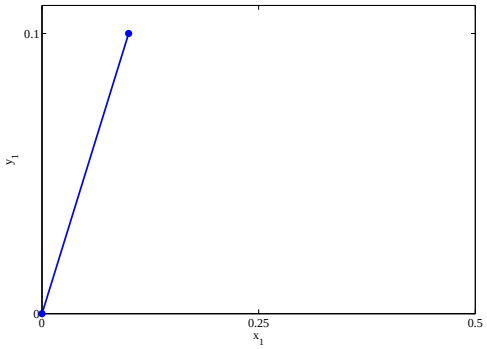

Figure 3.11 - a) *Initial crack position.*

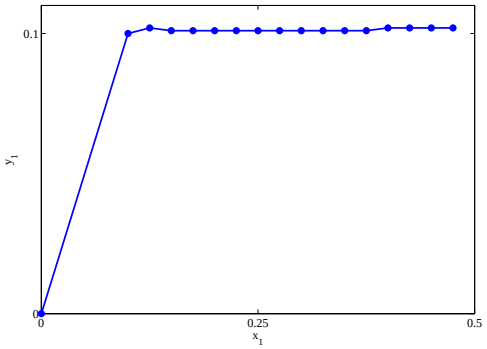

b) *Crack path for* $n = 15$.

There appears to be a strong tendency for the crack to propagate mainly in mode I, during continued fracture. This agrees with the predictions of [20,37]. We also observe that this simulation of crack growth is based on the static stress intensity factors. Dynamic effects such as wave propagation are not taken into account. A dynamic analysis is presented in [90].

Chapter 4

Homogenisation for periodic structures

Earlier the elliptic PDEs that model the behaviour of composite linear elastic materials were introduced. When these materials are very heterogeneous the coefficients of the differential equations become highly oscillatory. Classical numerical techniques such as finite elements or boundary elements are then computationally too expensive to obtain accurate approximations for the solutions of the PDEs. An alternative is provided by the theory of homogenisation when the coefficients are periodic. This converts the original problems into simpler homogenised problems, which provide good macroscopic approximations for the solutions of the heterogeneous problems.

In this chapter the basic ideas of homogenisation are introduced. Analytical expressions for the coefficients of the homogenised problem are obtained for layered materials and some properties of the homogenised materials are analysed. An efficient algorithm for the numerical determination of the effective coefficients is proposed.

4.1 One-dimensional model

Let us consider the one-dimensional Dirichlet boundary value problem with periodically oscillating coefficients

$$a^\epsilon(x) := \tilde{a}(\frac{x}{\epsilon}), \tag{4.1.1}$$

which is given by

$$\begin{cases} -\frac{d}{dx}\left[a^\epsilon(x)\frac{d}{dx}u^\epsilon(x)\right] &= f(x),\ x \in (0,1), \\ u^\epsilon(0) = 0, \\ u^\epsilon(1) = 0. \end{cases} \tag{4.1.2}$$

Here, a^ϵ is an ϵ-periodic function and $\epsilon \ll 1$. We assume that there exist two real constants α and β such that

$$0 < \alpha < \tilde{a}(x/\epsilon) < \beta.$$

The analysis of this problem will give us insight into many of the relevant issues present in the sophisticated problems dealt with by the theory of homogenisation. To illustrate this approach let

$$a^\epsilon(x) := \frac{1}{2 + \sin(\frac{2\pi x}{\epsilon})}. \tag{4.1.3}$$

We observe that a^ϵ is an oscillating function, see Figure 4.1. For smaller values of ϵ, it oscillates more rapidly.

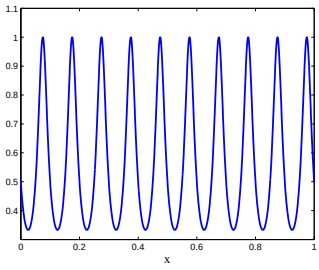

Figure 4.1: Oscillating behaviour of a^ϵ, $\epsilon = 0.1$.

The exact solution u^ϵ of (4.1.2) with $f(x) = 1$, represented in Figure 4.2 taking a^ϵ of the form (4.1.3), is given by

$$u^\epsilon(x) = \int_0^x \left(\frac{-y + c_0}{\tilde{a}(y/\epsilon)}\right) dy,\ c_0 = \frac{\int_0^1 [\tilde{a}(y/\epsilon)]^{-1} y\, dy}{\int_0^1 [\tilde{a}(y/\epsilon)]^{-1} dy}. \tag{4.1.4}$$

In general it is hard and often even impossible to find the analytical solution for problems with oscillating coefficients like (4.1.2). We must then resort to numerical methods, such as *finite element methods*.

Let $\{x_i\}_{i=0,\,\ldots,\,N+1}$, with $x_i = i/(N+1)$, be a discretisation of the interval $[0,1]$ and denote by h the distance between two adjacent points. We represent by V_0^h the subspace of $H^1(0,1)$ given by the functions that are linear in every interval $[x_{i-1},\ x_i]$, for $i = 1,\ \ldots,\ N+1$, and assume that $f \in L^2(0,1)$. Then the finite element approximation $u_h \in V^1(0,1)$ to $u^\epsilon \in H_0^1(0,1)$ satisfies

$$\int_0^1 \tilde{a}(x/\epsilon)\frac{du_h}{dx}(x)\frac{dv_h}{dx}(x)dx = \int_0^1 f(x)v_h(x)dx,\ \forall v_h \in V_0^h, \tag{4.1.5}$$

and its error is estimated by

$$\|u^\epsilon - u_h\|_{H^1(0,1)} \leq c\frac{\beta^2}{\alpha^3}\frac{h}{\epsilon}\|f\|_{L^2(0,1)}, \tag{4.1.6}$$

with $c \in \mathbb{R}$, cf. [60]. For a fixed value of ϵ, it is clear that u_h converges to u^ϵ when $h \to 0$. However, the convergence of this method is not uniform in ϵ, see [76]. This implies that when finite elements are used the grid size h must be taken sufficiently smaller than ϵ, cf. [39].

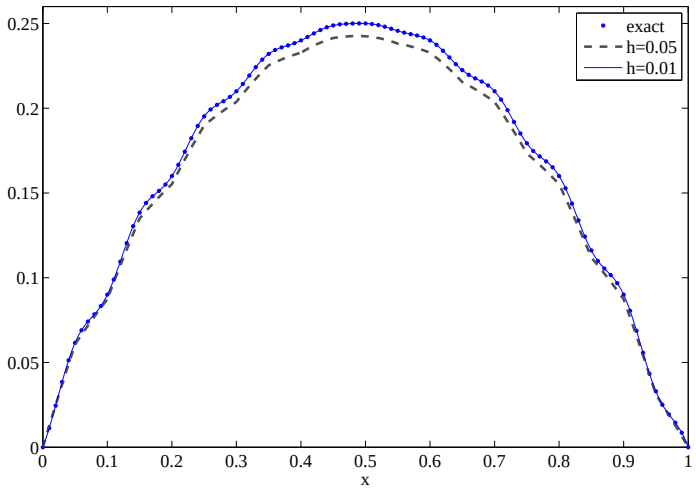

Figure 4.2: Solutions for the heterogeneous problem.

This behaviour is illustrated in Figure 4.2, again taking a^ϵ of the form (4.1.3). Here we show numerical approximations of (4.1.2) with $f(x) = 1$, for some values of h. Note that an accurate approximation for the exact solution is only obtained for $h = 0.01 < \epsilon = 0.1$.

Observe that taking $h < \epsilon$ to obtain an accurate approximation is computationally very expensive when ϵ takes small values, particularly for problems in higher dimensions.

In that case, even with heavy computer efforts it is impossible to obtain the desired accuracy.

4.1.1 Multiple scales method

One alternative approach to obtain an accurate numerical approximation for (4.1.2) in a cheap manner, using a mesh size $h > \epsilon$, is given by the homogenisation theory. It allows for the formulation of a second problem, still of the form of (4.1.2) but with constant coefficients, called *homogenised* or *effective coefficients*, so we are rid of the oscillations. The homogenised or *effective solution* $\overline{u}$ of the new problem should capture the macroscopic behaviour of u^ϵ, but not the oscillations on the microscopic scale.

In order to look for the homogenised approximation for the solution of (4.1.2), we use the multiple scale method. Following [2], consider the ansatz

$$u^\epsilon(x, y) = u_0(x, y) + \epsilon u_1(x, y) + \epsilon^2 u_2(x, y) + \dots, \tag{4.1.7}$$

where we assume the functions u_i to be 1-periodic in y and sufficiently smooth. They depend explicitly on x and $y := x/\epsilon$. This is a mathematical translation of the idea that u^ϵ depends on two length scales, macroscopic and microscopic. We will treat x and y as independent variables. By restricting ourselves to the first three terms of the last expansion and substituting the ansatz in the differential equation in (4.1.2) we obtain

$$\frac{1}{\epsilon^2}\mathcal{A}_0 u_0 + \frac{1}{\epsilon}(\mathcal{A}_1 u_0 + \mathcal{A}_0 u_1) + \frac{1}{\epsilon^0}(\mathcal{A}_2 u_0 + \mathcal{A}_1 u_1 + \mathcal{A}_0 u_2) + \dots = f. \tag{4.1.8}$$

Here we define the operators

$$\mathcal{A}_0 := -\frac{\partial}{\partial y}(\tilde{a}(y))\frac{\partial}{\partial y}, \tag{4.1.9}$$

$$\mathcal{A}_1 := -\frac{\partial}{\partial y}(\tilde{a}(y))\frac{\partial}{\partial x} - \frac{\partial}{\partial x}(\tilde{a}(y))\frac{\partial}{\partial y}, \tag{4.1.10}$$

$$\mathcal{A}_2 := -\frac{\partial}{\partial x}(\tilde{a}(y))\frac{\partial}{\partial x}. \tag{4.1.11}$$

Equating coefficients of equal power in ϵ in (4.1.8), we obtain the equalities

$$\mathcal{A}_0 u_0 = 0, \tag{4.1.12}$$

$$\mathcal{A}_0 u_1 = -\mathcal{A}_1 u_0, \tag{4.1.13}$$

$$\mathcal{A}_0 u_2 = -\mathcal{A}_1 u_1 - \mathcal{A}_2 u_0 + f, \tag{4.1.14}$$

The existence of u_i, $i = 0, 1, 2$, up to constants in y is ensured by the Fredholm alternative, cf. [71]. Now, it can be shown that the solution of (4.1.12) actually does not depend on y. Indeed, multiplying $\mathcal{A}_0 u_0$ by u_0 and integrating over $[0, 1]$ yields

$$\begin{aligned} 0 &= \int_0^1 u_0 A_0 u_0 \, dy \\ &= -\int_0^1 u_0 \frac{\partial}{\partial y}(\tilde{a}(y)\frac{\partial u_0}{\partial y}) dy = -\int_0^1 \tilde{a}(y)(\frac{\partial u_0}{\partial y})^2 dy, \end{aligned} \tag{4.1.15}$$

where the last equality was obtained using integration by parts. Since $\tilde{a}(y) > \alpha$, then $\partial u_0/\partial y$ must be zero. We conclude that the first term of the ansatz does not actually depend on the microscopic variable. It is the homogenised solution we are looking for. We proceed to finding a way to compute u_0, which we now denote as $\overline{u} := u_0$. To do so, we start by using separation of variables and seeking a solution of (4.1.13) of the form

$$u_1(x, y) = \chi(y)\frac{\partial \overline{u}}{\partial x}. \tag{4.1.16}$$

Inserting (4.1.16) in (4.1.13), we obtain the *cell problem*

$$\begin{cases} -\frac{d}{dy}(\widetilde{a}(y)\frac{d\chi}{dy}) = -\frac{d\widetilde{a}(y)}{dy}, & y \in (0,\ 1), \\ \chi \text{ is periodic}, \\ \int_0^1 \chi(y) dy = 0, \end{cases} \tag{4.1.17}$$

where the last condition is added to ensure the problem is well-posed. Finally we use (4.1.14) to look for the homogenised solution. Because the function u_2 is 1-periodic, it can be shown by using the fundamental theorem of calculus that $\int_0^1 A_0 u_2 dy = 0$, and so from (4.1.14) we have

$$\int_0^1 -\mathcal{A}_1 u_1 - \mathcal{A}_2 u_0 + f dy = 0. \tag{4.1.18}$$

Using the fact that the function $\overline{u}$ depends only on x and that u_1 is given by (4.1.16), the previous equation yields the *homogenised problem*

$$\begin{cases} -\overline{a}\frac{d}{dx}(\frac{d\overline{u}}{dx}) &= f(x),\ x \in (0,1), \\ \overline{u}(0) = 0, \\ \overline{u}(1) = 0, \end{cases} \tag{4.1.19}$$

where the *homogenised coefficient* $\overline{a}$ is given by

$$\overline{a} = \int_0^1 \widetilde{a}(y)dy - \int_0^1 \widetilde{a}(y)\frac{d\chi}{dy}(y)dy. \tag{4.1.20}$$

In summary, we obtain the homogenised problem (4.1.19) which corresponds to (4.1.2). This allows us to find an approximation $\overline{u}$ for the solution u^ϵ of the original problem without having to solve the microscale. Instead we are left to deal with the simpler homogenised problem, once the effective coefficient $\overline{a}$ in (4.1.20) has been determined.

We may now relate $\overline{u}$ and u^ϵ and estimate the approximation error, cf. [21, 60]. The following theorem justifies the validity of approximating the solution of a problem with highly oscillating periodic coefficients by the solution of the corresponding homogeneous problem, cf. [82].

Theorem 4.1.1 *Let $\widetilde{a} = \widetilde{a}(x)$ be a function in $L^\infty(0, l_1)$ which we extend to* IR *such that it is l_1-periodic, and $f \in L^2(d_1, d_2)$ a given function. Define $a^\epsilon(x) := \tilde{a}(x/\epsilon)$. Assume that there exist two real constants α and β such that*

$$0 < \alpha < \tilde{a}(y) < \beta.$$

Moreover, let $u^\epsilon \in H_0^1(d_1, d_2)$ be the unique solution of the problem

$$\begin{cases} -\frac{d}{dx}\left[a^\epsilon(x)\frac{d}{dx}u^\epsilon(x)\right] &= f(x),\ x \in (d_1, d_2), \\ u^\epsilon(d_1) = 0, \\ u^\epsilon(d_2) = 0, \end{cases} \tag{4.1.21}$$

and $\overline{u} \in H_0^1(d_1, d_2)$ be the unique solution of the homogenised problem

$$\begin{cases} -\overline{a}\frac{d^2}{dx^2}\overline{u}(x) &= f(x),\ x \in (d_1, d_2), \\ \overline{u}(d_1) = 0, \\ \overline{u}(d_2) = 0, \end{cases} \tag{4.1.22}$$

where the effective coefficient $\overline{a}$ *is given by*

$$\overline{a} = \frac{1}{\int_0^{l_1} [\widetilde{a}(y)]^{-1} dy}. \tag{4.1.23}$$

Then the solution of problem (4.1.21) converges to the solution of problem (4.1.22) in $H_0^1(d_1, d_2)$*, i.e.*

$$u^\epsilon \to \overline{u} \text{ weakly in } H_0^1(d_1, d_2). \tag{4.1.24}$$

Finally, let $a \in W^{1,p}(IR)$, for some $p > 2$. Under the conditions of the previous theorem it can be shown that there exists a constant $c \in IR$ such that

$$\|u^\epsilon - \overline{u}\|_{H^1(d_1,d_2)} \leq c\epsilon \|\overline{u}\|_{H^2(d_1,d_2)}. \tag{4.1.25}$$

4.1.2 Recovering the heterogeneities

The *homogenised solution* $\overline{u}$ captures the macroscopic behaviour of u^ϵ and disregards the oscillations. We would like to be able to recover these without having to employ finite elements with a very fine mesh. In order to do so we consider one more term in the asymptotic expansion (4.1.7), the *first order corrector* u_1.

Though we might expect $\overline{u} + \epsilon u_1$ to be a better approximation than $\overline{u}$, it does not necessarily verify the same boundary conditions as the heterogeneous solution u^ϵ. A function C which we call the *boundary corrector* should then be introduced so that $\overline{u} + \epsilon u_1 + C$ is the sought approximation that recovers the oscillations and at the boundaries $\overline{u} + \epsilon u_1 + C = u^\epsilon$. Let C satisfy the original heterogeneous equation with source term equal to zero

$$\begin{cases} -\frac{d}{dx}\left[a^\epsilon(x)\frac{d}{dx}C(x)\right] = 0, \ x \in (0,1), \\ C(0) = -\epsilon u_1(0), \\ C(1) = -\epsilon u_1(1). \end{cases} \tag{4.1.26}$$

In practice C may be approximated by a function that satisfies (4.1.26) with a^ϵ replaced by $\overline{a}$. It can be shown that there exists a constant d such that we have

$$\|u^\epsilon - (\overline{u} + \epsilon u_1 + \epsilon C)\|_0 \leq d\epsilon^2 \|\overline{u}\|_3, \tag{4.1.27}$$

and

$$\|u^\epsilon - (\overline{u} + \epsilon u_1 + \epsilon C)\|_1 \leq d\epsilon \|\overline{u}\|_2, \tag{4.1.28}$$

cf. [88]. The heterogeneities neglected by $\overline{u}$ can be recovered up to a point by the *corrected homogenised solution*. This is an advantageous process as it allows for a cheap solution to be obtained for a problem that would otherwise require a large computational effort.

4.1.3 Numerical example

Let us consider the boundary value problem (4.1.2) with (4.1.3) and $f(x) = 1$, as well as the corresponding homogenised problem (4.1.19). The solutions of these problems are given by (4.1.4) and

$$\overline{u}(x) = -\left[\frac{1}{2}(x^2 - x)\right] \int_0^1 \frac{1}{\widetilde{a}(y)} dy, \tag{4.1.29}$$

respectively. We can then determine the error $\overline{E} = u^\epsilon - \overline{u}$, which is displayed in the second line of the Table 4.1, in the norms $\|\cdot\|_\infty$ and $\|\cdot\|_{L^2(0,1)}$, for $\epsilon = 0.01$ and $\epsilon = 0.1$. We obtain better approximations when the period of the heterogeneities is small. This was to be expected, as the homogenisation procedure works better for materials that are finely mixed.

Better approximations for u^ϵ can be achieved using the first order corrector u_1 given by (4.1.16) and the boundary corrector C which solves (4.1.26). The latter can be approximated by the solution of the homogenised problem

$$\begin{cases} -\overline{a}\frac{d}{dx}\left[\frac{d}{dx}C(x)\right] & = & 0,\ x \in (0,1), \\ C(0) = -\epsilon u_1(0), \\ C(1) = -\epsilon u_1(1), \end{cases} \tag{4.1.30}$$

where $\overline{a}$ is given by (4.1.20). We display the norms of the error $E_C = u^\epsilon - (\overline{u} + \epsilon u_1 + C)$ in the last line of Table 4.1. Note that in this case it was possible to determine both u_1 and C analytically.

	$\epsilon = 0.01$		$\epsilon = 0.1$	
	$\|\cdot\|_\infty$	$\|\cdot\|_{L^2(0,1)}$	$\|\cdot\|_\infty$	$\|\cdot\|_{L^2(0,1)}$
$\overline{E}$	$1.6E-3$	$5.6E-4$	$1.5E-2$	$5.6E-3$
E_C	$4.1E-6$	$2.4E-6$	$4.1E-4$	$2.4E-4$

Table 4.1: Error of the approximations.

As expected, the corrected homogenised solution is a better approximation for u^ϵ than $\overline{u}$. This is better illustrated in Figure 4.3. The exact solution u^ϵ is depicted as dots. The homogenised solution $\overline{u}$ and its corrected counterpart $\overline{u} + \epsilon u_1 + C$ are represented as the darker and lighter solid lines, respectively.

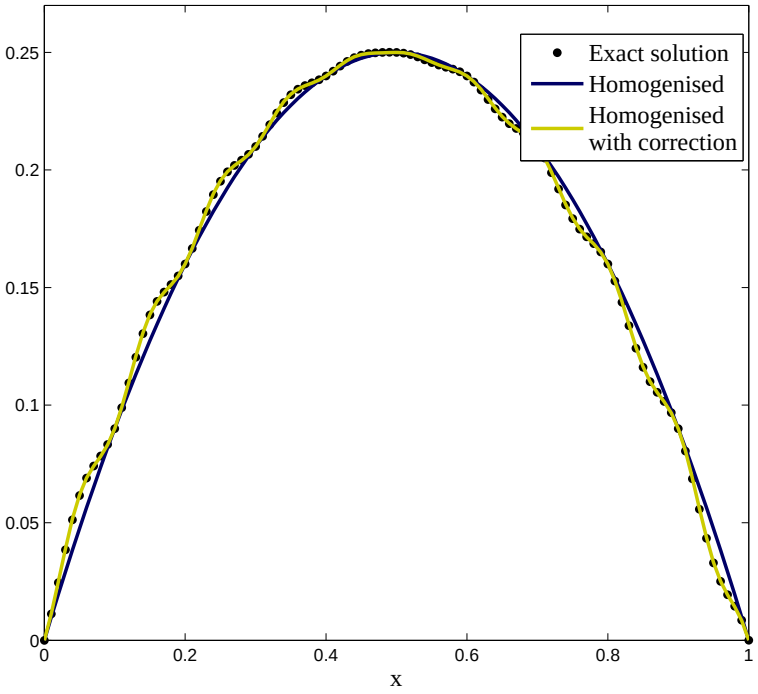

Figure 4.3: Solution of the heterogeneous problem and corresponding homogenised approximations, $\epsilon = 0.1$.

4.2 Homogenisation for elasticity

In this section we briefly analyse the asymptotic behaviour of the solution of *elasticity problems* associated to periodic composite materials using the theory of homogenisation, cf. [21, 71]. These results are presented for a 2D plane stress situation, though they can be extended to higher dimensions in a straightforward way.

Consider a composite plate with constituents periodically distributed over $\Omega \subseteq \mathbb{R}^2$. We can then define a reference cell $Y = [0, l_1] \times [0, l_2]$ such that Ω is covered by a mosaic of cells of the form $\epsilon Y = [0, \epsilon l_1] \times [0, \epsilon l_2]$, see Figure 4.4.

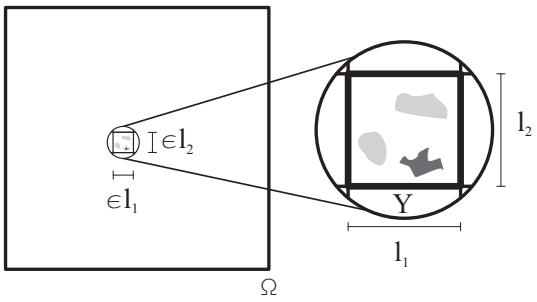

Figure 4.4: Domain Ω and reference cell Y.

The behaviour of the material is characterised by the fourth-order elasticity tensor $\tilde{\mathbf{A}} = \tilde{\mathbf{A}}(\mathbf{y}) = (\tilde{a}_{ijkh})_{1\le i,j,k,h\le 2}$ defined over the reference cell Y. Assume that there exist α, $\beta \in \mathbb{R}$ such that $\tilde{\mathbf{A}} \in M_e(\alpha, \beta, Y)$, i.e.,

- $\tilde{a}_{ijkh} \in L^\infty(Y)$, for any $i, j, k, h \in \{1, 2\}$;
- $\tilde{a}_{ijkh} = \tilde{a}_{jikh} = \tilde{a}_{khij}$, for any $i, j, k, h \in \{1, 2\}$;
- $\alpha\|\mathbf{M}\|^2 \le \tilde{\mathbf{A}}\mathbf{M}\mathbf{M}$, for any symmetric 2×2 matrix $\mathbf{M}$;
- $\|\tilde{\mathbf{A}}(\mathbf{y})\mathbf{M}\| \le \beta\|\mathbf{M}\|$, for any 2×2 matrix $\mathbf{M}$, almost everywhere on Y,

where for any fourth-order tensor $\mathbf{B} = (b_{ijkh})_{1\le i,j,k,h\le 2}$ and for any matrices $\mathbf{M} = (m_{ij})_{1\le i,j\le 2}$ and $\mathbf{N} = (n_{ij})_{1\le i,j\le 2}$, we denote

$$\begin{aligned} \|\mathbf{M}\| &:= (\sum_{i,j=1}^{2} m_{ij}^2)^{1/2}, \\ \mathbf{BM} &:= ((\sum_{k,h=1,2} b_{ijkh} m_{kh})_{ij})_{1\le i,j\le 2}, \\ \mathbf{BMN} &:= \sum_{i,j,k,h=1,2} b_{ijkh} m_{ij} n_{kh}. \end{aligned}$$

The functions $\tilde{a}_{ijkh}$ are extended to $\mathbb{R}^2$ periodically, which allows us to define an ϵ-*periodic tensor* $\mathbf{A}^\epsilon = \mathbf{A}^\epsilon(\mathbf{x}) = (a^\epsilon_{ijkh})_{1\le i,j,k,h\le N}$ such that for $\mathbf{x} = (x_1, x_2) \in \mathbb{R}^2$,

$$a^\epsilon_{ijkh}(\mathbf{x}) := \tilde{a}_{ijkh}(\mathbf{y}) = \tilde{a}_{ijkh}(\frac{\mathbf{x}}{\epsilon}), \tag{4.2.1}$$

where we denote $\mathbf{y} := \mathbf{x}/\epsilon$, for $\mathbf{y} = (y_1, y_2) \in \mathbb{R}^2$. It can be shown that if $\tilde{\mathbf{A}} \in M_e(\alpha, \beta, Y)$, then also $\mathbf{A}^\epsilon \in M_e(\alpha, \beta, Y)$.

We now formulate the linear elasticity problem for the periodically distributed composite material, that is stated as

$$\begin{cases} -\nabla \cdot \ (\mathbf{A}^\epsilon(\mathbf{x})\boldsymbol{\epsilon}(\mathbf{u}^\epsilon)) = \mathbf{f}, & \mathbf{x} \in \ \Omega, \\ \mathbf{u}^\epsilon = 0, & \mathbf{x} \in \Gamma_D, \\ \boldsymbol{\sigma}(\mathbf{u}^\epsilon) \cdot \mathbf{n} = \boldsymbol{\varphi}_N, & \mathbf{x} \in \Gamma_N, \end{cases} \tag{4.2.2}$$

where the functions $\boldsymbol{\varphi}_N$ and $\mathbf{f}$ are given and $\boldsymbol{\epsilon}$, $\boldsymbol{\sigma}$ and $\mathbf{u}$ denote the strain tensor, the stress tensor and the displacement vector respectively. We recall from Chapter 2 that these are such that for every function $\mathbf{w}$,

$$\boldsymbol{\epsilon}(\mathbf{w}) = \frac{1}{2}(\nabla \mathbf{w} + (\nabla \mathbf{w})^T), \ \ \boldsymbol{\sigma}(\mathbf{w}) = \mathbf{A}^\epsilon \boldsymbol{\epsilon}(\mathbf{w}). \tag{4.2.3}$$

We look for weak solutions of (4.2.2) in the space $\mathcal{V}$ defined by

$$\mathcal{V} = \{\mathbf{v} \mid \mathbf{v} \in (H^1(\Omega))^2, \ \boldsymbol{\gamma}(\mathbf{v}) = 0 \text{ on } \Gamma_D\}. \tag{4.2.4}$$

Moreover, we define the following norm

$$\|\mathbf{v}\|_{\mathcal{V}} = \left(\sum_{i=1}^{2} \|\nabla v_i\|^2_{L^2(\Omega)} \right)^{1/2}, \tag{4.2.5}$$

for $\mathbf{v} = (v_1, v_2) \in \mathcal{V}$, cf. [21].

4.2.1 Main result

Our objective is to determine the homogenised version for the problem (4.2.2), for which it is useful to introduce some auxiliary functions. Consider the family of vector-valued functions $\mathbf{P}^{lm}(\mathbf{y}) = (P_k^{lm}(\mathbf{y}))_{k=1,2}$ defined by

$$P_k^{lm}(\mathbf{y}) := y_m \delta_{kl}, \ k = 1, \ 2, \tag{4.2.6}$$

where δ_{kl} is the Kronecker symbol and $l, m \in \{1, 2\}$. Let $\boldsymbol{\chi}^{lm}(\mathbf{y}) = (\chi_k^{lm}(\mathbf{y}))_{k=1,2} \in (W_{per}(Y))^2$ be the unique solution of the *cell problem*

$$\begin{cases} -\nabla \cdot \ (\tilde{\mathbf{A}}(\mathbf{y})\nabla(\boldsymbol{\chi}^{lm} - \mathbf{P}^{lm})) = \mathbf{0}, & \mathbf{y} \in Y, \\ \boldsymbol{\chi}^{lm} \text{ is } Y\text{-periodic}, \\ M_Y(\chi_k^{lm}) = 0, \end{cases} \tag{4.2.7}$$

where

$$M_Y(f) := \frac{1}{|Y|}\int_Y f(y)dy \quad \text{and} \quad W_{per}(Y) := \{v \in H^1_{per}(Y) | M_Y(v) = 0\}. \tag{4.2.8}$$

Here, $H^1_{per}(Y)$ is the closure for the H^1-norm of $C^\infty_{per}(Y)$, the subset of $C^\infty(\mathbb{R}^2)$ of periodic functions over Y. In these conditions, it can be shown that the solution of (4.2.7) is unique.

We now aim at characterizing the homogeneous solution of the elasticity problem. The following result can be thought of as a generalisation of the theorem presented earlier on section 4.1 to the context of planar elasticity, cf. [21] for a proof.

Theorem 4.2.1 *Let us consider the heterogeneous elasticity problem*

$$\begin{cases} -\nabla \cdot \ (\mathbf{A}^\epsilon(\mathbf{x})\boldsymbol{\epsilon}(\mathbf{u}^\epsilon)) = \mathbf{f}, & \mathbf{x} \in \Omega, \\ \mathbf{u}^\epsilon = \mathbf{0}, & \mathbf{x} \in \Gamma_D, \\ \boldsymbol{\sigma}(\mathbf{u}^\epsilon) \cdot \mathbf{n} = \boldsymbol{\varphi}_N, & \mathbf{x} \in \Gamma_N, \end{cases} \tag{4.2.9}$$

where $\mathbf{f} \in \mathcal{V}'$, $\boldsymbol{\varphi}_N \in (H^{-1/2}(\Gamma_N))^2$ *and* $\mathbf{u}^\epsilon \in \mathcal{V}$ *is its unique solution. The corresponding homogeneous problem is given by*

$$\begin{cases} -\nabla \cdot \ (\overline{\mathbf{A}}\boldsymbol{\epsilon}(\overline{\mathbf{u}})) = \mathbf{f}, & \mathbf{x} \in \Omega, \\ \overline{\mathbf{u}} = \mathbf{0}, & \mathbf{x} \in \Gamma_D, \\ \overline{\mathbf{u}} \cdot \mathbf{n} = \boldsymbol{\varphi}_N, & \mathbf{x} \in \Gamma_N, \end{cases} \tag{4.2.10}$$

and it admits a unique solution $\overline{\mathbf{u}} \in \mathcal{V}$. *In these conditions,*

$$\mathbf{u}^\epsilon \to \overline{\mathbf{u}} \quad \textit{weakly in } \mathcal{V}, \tag{4.2.11}$$

$$\mathbf{A}^\epsilon \boldsymbol{\epsilon}(\mathbf{u}^\epsilon) \to \overline{\mathbf{A}}\boldsymbol{\epsilon}(\overline{\mathbf{u}}) \quad \textit{weakly in } (L^2(\Omega))^{2\times 2}. \tag{4.2.12}$$

Moreover, the homogenised tensor $\overline{\mathbf{A}} = (\overline{a}_{ijkh})$ *is symmetric and*

$$\overline{a}_{ijkh} = \frac{1}{|Y|}\int_Y \widetilde{a}_{ijkh}(\mathbf{y})d\mathbf{y} - \frac{1}{|Y|}\int_Y \sum_{l,m=1,2} \widetilde{a}_{ijlm}(\mathbf{y})\frac{\partial \chi_l^{kh}}{\partial y_m}(\mathbf{y})d\mathbf{y}. \tag{4.2.13}$$

This theorem is the fundamental result which allows us to analyse the behaviour of layered materials in the next subsection. In practical terms, one may avoid computing the solution of (4.2.9) directly. Instead we solve the cell problem (4.2.7) to find the *effective coefficients* $\overline{a}_{ijkh}$ and finally compute the approximation $\overline{\mathbf{u}}$ for $\mathbf{u}^\epsilon$ by means of (4.2.10).

As in the one dimensional case, correctors may be introduced to recover the heterogeneities that are disregarded by the homogenised solution. That will be done in Chapter 6.

4.2.2 Layered composites

We will now focus on layered periodic composite materials, which are such that their properties vary only along one spatial coordinate. We show how the effective coefficients can be determined analytically and use this result to characterise the homogenised material. Let us again consider the elasticity problem (4.2.2) where now the tensor components read

$$a^\epsilon_{ijkh}(\mathbf{x}) = \widetilde{a}_{ijkh}(\frac{\mathbf{x}}{\epsilon}) = \widetilde{a}_{ijkh}(\frac{x_1}{\epsilon}) = a^\epsilon_{ijkh}(x_1). \tag{4.2.14}$$

For the sake of simplicity and without loss of generality, we further assume that the reference cell is such that $|Y| = 1$. Then under the conditions of theorem 4.2.1, we make use of (4.2.14) to solve the cell problem analytically and find explicit expressions for the effective coefficients.

Theorem 4.2.2 *Consider the problem (4.2.2) with (4.2.14), where the components of the tensor* $\mathbf{A}^\epsilon$ *are such that*

$$\det(y_1) := \widetilde{a}_{1111}(y_1)\widetilde{a}_{2121}(y_1) - \widetilde{a}^2_{2111}(y_1) \neq 0, \quad \forall y_1 \in [0, l_1]. \tag{4.2.15}$$

Furthermore, denote

$$\mathrm{Det} =: [M_Y(\frac{\widetilde{a}_{2111}}{\det})]^2 - M_Y(\frac{\widetilde{a}_{1111}}{\det})M_Y(\frac{\widetilde{a}_{2121}}{\det}), \tag{4.2.16}$$

$$A_{ij} := -M_Y(\frac{\widetilde{a}_{ij11}\widetilde{a}_{2121}}{\det}) + M_Y(\frac{\widetilde{a}_{ij21}\widetilde{a}_{1121}}{\det}), \tag{4.2.17}$$

$$B_{ij} := M_Y(\frac{\widetilde{a}_{ij11}\widetilde{a}_{1121}}{det}) - M_Y(\frac{\widetilde{a}_{ij21}\widetilde{a}_{1111}}{det}). \tag{4.2.18}$$

Then the effective solution $\overline{\mathbf{u}}$ *for this problem satisfies*

$$\begin{cases} -\nabla \cdot (\overline{\mathbf{A}}\boldsymbol{\epsilon}(\overline{\mathbf{u}})) = \mathbf{f}, & \mathbf{x} \in \Omega, \\ \overline{\mathbf{u}} = 0, & \mathbf{x} \in \Gamma_D, \\ \boldsymbol{\sigma}(\overline{\mathbf{u}}) \cdot \mathbf{n} = \boldsymbol{\varphi}_N, & \mathbf{x} \in \Gamma_N, \end{cases} \tag{4.2.19}$$

where the components of $\overline{\mathbf{A}}$ *are symmetric and given by*

$$\overline{a}_{ijlm} = \frac{A_{ij}}{Det} M_Y(\frac{\widetilde{a}_{11lm}}{det}) + \frac{B_{ij}}{Det} M_Y(\frac{\widetilde{a}_{21lm}}{det}), \tag{4.2.20}$$

for all $i, j, l, m \in \{1, 2\}$ *with* $i + j \geq l + m$*, except for* $i = j = l = m = 2$*. In the later case,*

$$\begin{aligned} \overline{a}_{2222} = {} & M_Y(\widetilde{a}_{2222}) \\ & + M_Y(\frac{2\widetilde{a}_{2211}\widetilde{a}_{2221}\widetilde{a}_{2111} - \widetilde{a}_{2211}^2\widetilde{a}_{2121} - \widetilde{a}_{2221}^2\widetilde{a}_{1111}}{det}) \\ & - [\frac{A_{22}}{Det} M_Y(\frac{\widetilde{a}_{1111}}{det}) + \frac{B_{22}}{Det} M_Y(\frac{\widetilde{a}_{1121}}{det})] A_{22} \\ & - [\frac{B_{22}}{Det} M_Y(\frac{\widetilde{a}_{2121}}{det}) + \frac{A_{22}}{Det} M_Y(\frac{\widetilde{a}_{2111}}{det})] B_{22}. \end{aligned} \tag{4.2.21}$$

Proof:

Since $\widetilde{a}_{ijkh}(\mathbf{y}) = \widetilde{a}_{ijkh}(y_1)$, the homogenised coefficients given in (4.2.13) read

$$\overline{a}_{ijkh} = \frac{1}{|Y|}\int_Y \widetilde{a}_{ijkh}(y_1)dy_1 - \frac{1}{|Y|}\int_Y \sum_{l,m=1,2} \widetilde{a}_{ijlm}(y_1)\frac{\partial \chi_l^{kh}}{\partial y_m}(y_1)dy_1. \tag{4.2.22}$$

The family of functions $\partial\chi_l^{kh}/\partial y_m$ is determined by integrating the first equation in (4.2.7), which yields

$$\widetilde{a}_{1111}\frac{\partial \chi_1^{lm}}{\partial y_1} + \widetilde{a}_{1121}\frac{\partial \chi_2^{lm}}{\partial y_1} = -\widetilde{a}_{11lm} + c_1^{lm}, \tag{4.2.23}$$

$$\widetilde{a}_{2111}\frac{\partial \chi_1^{lm}}{\partial y_1} + \widetilde{a}_{2121}\frac{\partial \chi_2^{lm}}{\partial y_1} = -\widetilde{a}_{21lm} + c_2^{lm}. \tag{4.2.24}$$

The integration constants c_k^{lm} can be determined using the fact that the functions χ_k^{lm} are Y-periodic, for $k = 1, 2$. The result then follows from (4.2.22). □

This theorem allows us to compute the elasticity tensor $\overline{\mathbf{A}}$ explicitly for all media that are such that there exists a direction along which its properties are constant. In particular we can apply the previous result to a linear elastic isotropic non-homogeneous material with Poisson's ratio ν and with Young's modulus E. We recall from Chapter 2 that the symmetrical coefficients $\widetilde{a}_{ijkh}$ of the tensor $\widetilde{\mathbf{A}}$ that describe the material behaviour are

$$\widetilde{a}_{2222} = \widetilde{a}_{1111} = \frac{E}{1-\nu^2}; \qquad \widetilde{a}_{2211} = \frac{E\nu}{1-\nu^2}; \tag{4.2.25}$$

$$\widetilde{a}_{2121} = \frac{E}{2(1+\nu)}; \qquad \widetilde{a}_{2111} = \widetilde{a}_{2221} = 0. \tag{4.2.26}$$

We examine the situation when the material parameters are of the form

$$\nu = \nu(y_1) \text{ and } E = E(y_1). \tag{4.2.27}$$

We can then establish the following property.

Property 4.2.3 *The homogeneous problem related to (4.2.2) with (4.2.25)-(4.2.27) is*

$$\begin{cases} -\nabla \cdot (\overline{\mathbf{A}}\boldsymbol{\epsilon}(\overline{\mathbf{u}})) = \mathbf{f}, & \mathbf{x} \in \Omega, \\ \overline{\mathbf{u}} = 0, & \mathbf{x} \in \Gamma_D, \\ \boldsymbol{\sigma}(\overline{\mathbf{u}}) \cdot \mathbf{n} = \boldsymbol{\varphi}_N, & \mathbf{x} \in \Gamma_N, \end{cases} \tag{4.2.28}$$

where the effective coefficients $\overline{a}_{ijlm}$ are symmetric and given by

$$\overline{a}_{1111} = \frac{1}{M_Y(1/\widetilde{a}_{1111})}; \qquad \overline{a}_{2111} = \overline{a}_{2221} = 0; \tag{4.2.29}$$

$$\overline{a}_{2211} = \frac{M_Y(\widetilde{a}_{2211}/\widetilde{a}_{1111})}{M_Y(1/\widetilde{a}_{1111})}; \qquad \overline{a}_{2121} = \frac{1}{M_Y(1/\widetilde{a}_{2121})}; \tag{4.2.30}$$

$$\overline{a}_{2222} = M_Y(\widetilde{a}_{2222}) - M_Y(\frac{\widetilde{a}_{2211}^2}{\widetilde{a}_{1111}}) + \frac{[M_Y(\widetilde{a}_{2211}/\widetilde{a}_{1111})]^2}{M_Y(1/\widetilde{a}_{1111})}. \tag{4.2.31}$$

Proof: It is a consequence of Theorem 4.2.2. □

It is common to think of situations where the Poisson ratio is constant throughout the material, and only the Young's modulus varies as a function of x_1. We will show that in this situation the homogenised material is orthotropic. As was seen in Chapter 2 this means that the coefficients of the effective elasticity tensor $\overline{\mathbf{A}}$ are of the form

$$\overline{a}_{1111} = \frac{E_x}{1-\nu_{xy}\nu_{yx}}; \qquad \overline{a}_{2211} = \frac{E_x\nu_{yx}}{1-\nu_{xy}\nu_{yx}}, \tag{4.2.32}$$

$$\overline{a}_{2222} = \frac{E_y}{1-\nu_{xy}\nu_{yx}}; \qquad \overline{a}_{2121} = G_{xy}, \tag{4.2.33}$$

$$\overline{a}_{2111} = \overline{a}_{2221} = 0, \tag{4.2.34}$$

where $\nu_{xy}E_y = \nu_{yx}E_x$. Before we present this result in the form of a property, we state the following lemma.

Lemma 4.2.4 *In the conditions of Theorem 4.2.2 assume that there exist constants* c_{ijlm} *and a function* $E = E(y_1)$ *such that the coefficients* $\widetilde{a}_{ijlm}$ *read*

$$\widetilde{a}_{ijlm} = E(y_1)c_{ijlm}. \tag{4.2.35}$$

Then the effective coefficients are

$$\begin{aligned}\overline{a}_{ijlm} \quad = \quad & \frac{1}{[c_{2111}^2 - c_{1111}c_{2121}]M_Y(1/E)}\Big[c_{11lm}(-c_{ij11}c_{2121} + c_{ij21}c_{2111}) \\ & + c_{21lm}(c_{ij11}c_{2111} - c_{ij21}c_{1111})\Big],\end{aligned} \tag{4.2.36}$$

for all indices $i, j, l, m \in \{1, 2\}$ *not simultaneously* 2 *and* $i + j \geq l + m$. *In the later case,*

$$\begin{aligned}\overline{a}_{2222} &= M_Y(E)\Bigg[c_{2222} + \\ &\quad \frac{2c_{2211}c_{2221}c_{2111} - c_{2211}^2c_{2121} - c_{2221}^2c_{1111}}{c_{2111}^2 - c_{1111}c_{2121}}\Bigg] - \\ &\quad \Bigg[\frac{2c_{2211}c_{2111}^2(-c_{2211}c_{2121} + c_{2221}c_{2111})}{(c_{2111}^2 - c_{1111}c_{2121})^2} + \\ &\quad \frac{c_{2221}c_{1111}c_{2111}[c_{2211}c_{2121} - c_{2221}c_{1111}]}{(c_{2111}^2 - c_{1111}c_{2121})^2} + \\ &\quad \frac{c_{1111}(-c_{2211}c_{2121} + c_{2221}c_{2111})^2}{(c_{2111}^2 - c_{1111}c_{2121})^2} + \\ &\quad \frac{c_{2121}(c_{2211}c_{2111} - c_{2221}c_{1111})^2}{(c_{2111}^2 - c_{1111}c_{2121})^2}\Bigg]\frac{1}{M_Y(1/E)}. \end{aligned} \tag{4.2.37}$$

Proof: It is a consequence of Theorem 4.2.2. □

We are now ready to show that a finely mixed linear elastic material with constant Poisson's ratio ν and Young's modulus $E = E(y_1)$ can be replaced effectively by an orthotropic material, in the sense of homogenisation.

Property 4.2.5 *Let us consider the problem (4.2.2) with (4.2.25)-(4.2.26), where ν is a constant function and $E = E(y_1)$.*

The effective coefficients are such that the homogenised material is orthotropic. The corresponding material constants read

$$E_x = \frac{AB}{A + \nu^2(B - A)}, \qquad E_y = A, \tag{4.2.38}$$

$$\nu_{xy} = \frac{B\nu}{A + \nu^2(B - A)}, \qquad \nu_{yx} = \nu, \tag{4.2.39}$$

$$G_{xy} = \frac{B}{2(1 + \nu)}, \tag{4.2.40}$$

where

$$A = M_Y(E), \;\; B = \frac{1}{M_Y(1/E)}.$$

Proof: It is a consequence of Lemma 4.2.4. □

In the conditions of the previous property, the upper and lower bounds for the material constants given in (4.2.38)-(4.2.39) can be determined in terms of the Young's modulus and Poisson's ratio of the original heterogeneous material.

Property 4.2.6 *The material constants of the homogenised material satisfy*

$$\frac{1}{M_Y(1/E)} \leq E_x \leq M_Y(1/E), \tag{4.2.41}$$

$$\frac{1}{M_Y(E)M_Y(1/E)}\nu \leq \nu_{xy} \leq \nu. \tag{4.2.42}$$

Proof: Follows from using the Cauchy-Schwarz inequality. □

Finally we can think of a mixture of two isotropic homogeneous materials. Consider a composite layered material on Ω, which is such that a reference cell $Y = [0,1] \times [0,1]$ can be decomposed into two subdomains $Y_1 = [0,\ \frac{1}{2}] \times [0,\ 1]$, $Y_2 = [\frac{1}{2},\ 1] \times [0,\ 1]$. Suppose that for $i = 1,\ 2$, Y_i is occupied by a linear elastic material with Young's modulus E_i and Poisson's ratio ν_i.

Then, for a given value of $\epsilon > 0$ the domain Ω can be decomposed into two subdomains

$$\Omega_1^\epsilon = \{\mathbf{x} \in \Omega \,|\chi_1(\frac{\mathbf{x}}{\epsilon}) = 1\},$$

$$\Omega_2^\epsilon = \{\mathbf{x} \in \Omega \,|\chi_2(\frac{\mathbf{x}}{\epsilon}) = 1\}.$$

Here, χ_1 and χ_2 are the *characteristic functions* of the sets Y_1 and Y_2 given respectively by

$$\chi_i(\mathbf{y}) = \begin{cases} 1, & \mathbf{y} \in Y_i, \\ 0, & \mathbf{y} \in Y - Y_i, \end{cases} \tag{4.2.43}$$

that are extended by periodicity over Y. In this conditions, we state the following

Property 4.2.7 *Let us consider the problem (4.2.2) with (4.2.25) - (4.2.26), where*

$$E(\mathbf{y}) = E_1\chi_1(y_1) + E_2\chi_2(y_1), \tag{4.2.44}$$

$$\nu(\mathbf{y}) = \nu_1\chi_1(y_1) + \nu_2\chi_2(y_1). \tag{4.2.45}$$

Then the corresponding homogenised material is orthotropic with material constants given by

$$E_x = \frac{\overline{E}}{\overline{\nu}^2 + A\overline{E}},\ E_y = \overline{E}, \tag{4.2.46}$$

$$\nu_{xy} = \frac{\overline{\nu}}{\overline{\nu}^2 + A\overline{E}},\ \nu_{yx} = \overline{\nu}, \tag{4.2.47}$$

$$G = \frac{1}{(1+\nu_1)/E_1 + (1+\nu_2)/E_2}, \tag{4.2.48}$$

where

$$\overline{E} = \frac{1}{2}(E_1 + E_2),\ \ \overline{\nu} = \frac{1}{2}(\nu_1 + \nu_2),\ \ A = \frac{1}{2}(\frac{1-\nu_1^2}{E_1} + \frac{1-\nu_2^2}{E_2}). \tag{4.2.49}$$

Proof: It is a consequence of Property 4.2.3. □

We conclude this subsection with an example to illustrate the previous property. We consider an elastic plate occupying the region $\Omega = [0,1] \times [0,1]$. Let $\nu_1 = 0.1$, $\nu_2 = 0.3$, $E_1 = 1$, $E_2 = 10$ and the boundary conditions be such that:

$$\Gamma_D = \{0\} \times [0,1],\ \boldsymbol{\varphi}_N(\mathbf{x}) = \begin{cases} \mathbf{0}, & x_2 = 1, \\ \mathbf{0}, & x_2 = 0, \\ (1,0), & x_1 = 1. \end{cases} \tag{4.2.50}$$

We use a triangular grid with quadratic finite elements to solve the heterogeneous problem (4.2.2) with (4.2.25) - (4.2.26) for $\epsilon = 0.1$ and $\mathbf{f} = \mathbf{0}$. The vertical component of the displacements is plotted in Figure 4.5 a). We also plot the value of the horizontal displacement along the vertical line $x_2 = 0.5$ in Figure 4.5 b).

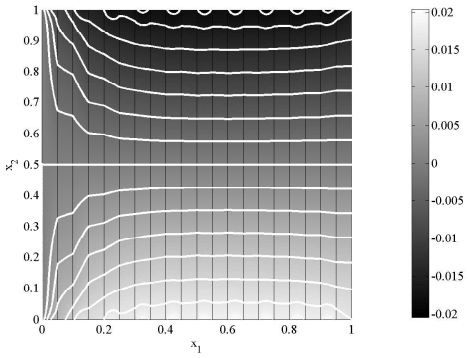

Figure 4.5 a) *Plot of the vertical component of* $\boldsymbol{u}^\epsilon$. *The contour lines highlight the oscillating behaviour.*

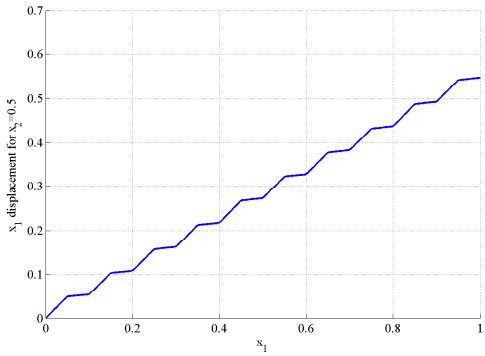

b) *Plot of the horizontal component of* $\boldsymbol{u}^\epsilon$ *along* $x_2 = 0.5$.

Finally we represent a plot of the solution of the corresponding homogenised problem in Figures 4.6 a) and b), obtained after applying Property 4.2.7. Again we used finite elements in the same manner as before.

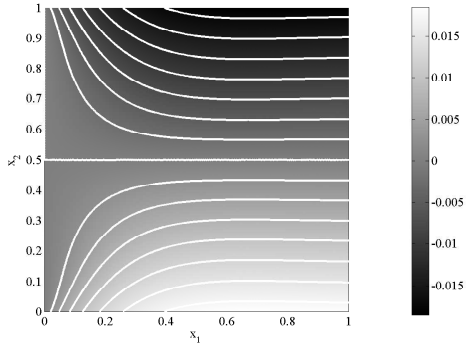

Figure 4.6 a) *Plot of the vertical component of* $\overline{\mathbf{u}}$, *which captures the essential behaviour of* $\boldsymbol{u}^\epsilon$.

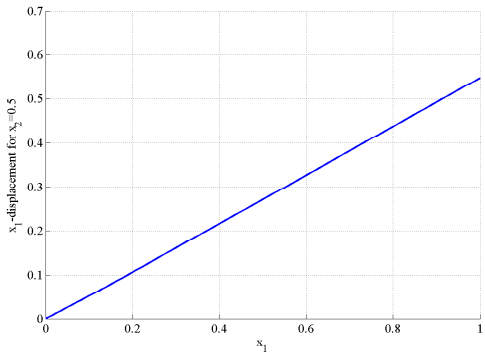

b) *Plot of the horizontal component of* $\overline{\mathbf{u}}$ *along* $x_2 = 0.5$.

As expected, the effective solution captures the essence of the behaviour of the original heterogeneous solution, disregarding only the oscillations.

4.2.3 Numerical aspects

Thus far our attention was devoted to finding explicit analytical expressions for the homogenised coefficients for layered materials. In this subsection we present a simple

procedure to find the homogenised solution related to (4.2.2) for any material with periodically distributed coefficients. This is applied to three different problems. The first two deal with layered materials. We start by considering an example where the coefficients of the underlying PDE are continuous functions of space. In the second example the coefficients are only piecewise continuous, as one would expect when dealing with composite materials. Finally we include another example where a more complicated structure is considered.

Let us again look at the elasticity problem (4.2.2). In order to determine the homogenised solution for this problem, it is necessary to first solve the cell problem and determine the effective coefficients. This procedure can be structured as the following algorithm.

Algorithm 4.1

1 - Solve the cell problem (4.2.7);

2 - Compute the coefficients $\overline{a}_{ijkh}$ by means of (4.2.13);

3 - Determine the solution of the homogenised problem (4.2.10).

We note that numerical techniques may have to be used at any of these steps. It is then important to estimate the error committed on each step, as the accuracy of the estimate $\overline{\mathbf{u}}$ allowed by Theorem 4.2.1 depends also on these errors.

Example 4.1 Continuous coefficients

Consider the problem (4.2.2) with (4.2.25)-(4.2.26), where the reference cell is now given by $Y = [-0.5, 0.5] \times [-0.5, 0.5]$ and the material properties characterised by

$$E(\mathbf{y}) = E(y_1) = 1 + y_1^2, \quad \nu = 0.3. \tag{4.2.51}$$

The non-trivial effective coefficients for this problem are easily determined using Property 4.2.3. The exact values of the coefficients are displayed in the second column of Table 4.2 with 6 significant digits.

To determine a numerical approximation for the coefficients, we follow steps 1 and 2 of Algorithm 4.1.

We use finite elements on a quadrangular mesh with quadratic elements with side size $h = 0.01$ in order to solve the cell problem. The solution functions χ_k^{lm} are either the

constant zero function or are similarly shaped to the function χ_1^{11}, which we represent over the reference cell in Figure 4.7.

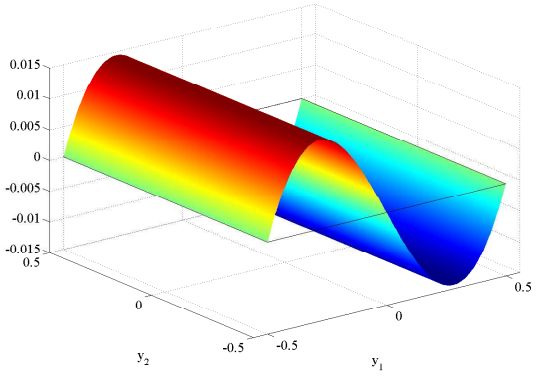

Figure 4.7: The periodic cell function χ_1^{11}.

For the second step two distinct strategies were followed in order to determine an approximation for the effective coefficients. Both aim at solving (4.2.13), but they differ in how the integrals

$$\int_Y \widetilde{a}_{ijlm}(y_1)dy_1, \quad \int_Y \sum_{l,m=1,2} \widetilde{a}_{ijlm}(y_1)\frac{\partial \chi_l^{kh}}{\partial y_m}dy_1, \tag{4.2.52}$$

are dealt with.

Coefficients	Exact	Ap_3	Ap_9
$\overline{a}_{1111}$	1.18506	1.18350	1.18506
$\overline{a}_{2121}$	0.41477	0.41423	0.41477
$\overline{a}_{2211}$	0.35552	0.35505	0.35552
$\overline{a}_{2222}$	1.18999	1.18985	1.18999

Table 4.2: Effective coefficients.

The first approach employs the expressions (4.2.25)-(4.2.26) of the heterogeneous coefficients $\widetilde{a}_{ijkh}$. Using these it is possible to compute the values of the integrals in (4.2.52) analytically when we use for example a least square polynomial approximation for χ_l^{kh}. In the third and fourth columns of Table 4.2 we display the approximations Ap_3 and Ap_9 for the relevant effective coefficients, obtained by using the mentioned polynomials with degree 3 and 9, respectively.

The values of the residuals of the approximations of the relevant non-zero functions χ_l^{kh}, denoted by Res_3 and Res_9, are given in Table 4.3.

Function	Res_3	Res_9
χ_1^{11}	$2.1\mathrm{E}-3$	$1.7\mathrm{E}-7$
χ_2^{21}	$2.1\mathrm{E}-3$	$1.7\mathrm{E}-7$
χ_1^{22}	$6.2\mathrm{E}-4$	$5.1\mathrm{E}-8$

Table 4.3: Residual of the approximation of χ_l^{kh}.

The second strategy that we adopt consists of computing the right hand side of (4.2.13) avoiding fitting. Instead, numerical differentiation and integration techniques are used. Firstly, for the approximation of $\partial\chi_l^{kh}/\partial y_m$, central differences are employed for all points except for the boundaries. Forward and backward differences are used for $x = -0.5$ and $x = 0.5$, respectively. To compute the integrals, the classical composite Trapezoidal and composite Simpson rules with 25 and 101 equidistant points are used. The values of the estimates for the coefficients are given in Table 4.4.

	Trapezoidal		Simpson	
Coefficients	25 points	101 points	25 points	101 points
$\overline{a}_{1111}$	1.18539	1.18508	1.18515	1.18507
$\overline{a}_{2121}$	0.41489	0.41478	0.41480	0.41477
$\overline{a}_{2211}$	0.35562	0.35552	0.35554	0.35552
$\overline{a}_{2222}$	1.19029	1.19001	1.19000	1.18998

Table 4.4: Effective coefficients.

We conclude that by using finite differences followed by the Simpson rule with 101 points one obtains results which are quite accurate. These are indeed nearly as accurate as the ones obtained by employing fitting with a polynomial of degree 9. Now, once the effective coefficients have been determined, the homogenised solution can be easily computed applying the third step of Algorithm 4.1.

Example 4.2 Piecewise coefficients

We consider the problem described in the previous example once again, but where now instead of (4.2.51) we have

$$E(\mathbf{y}) = E(y_1) = \chi_1(y_1) + 3\chi_2(y_1);\ \nu = 0.3, \tag{4.2.53}$$

where χ_1 and χ_2 are the characteristic functions of the sets $Y_1 = [-0.5, 0] \times [-0.5, 0.5]$ and $Y_2 = [0, 0.5] \times [-0.5, 0.5]$, respectively, as defined in (4.2.43). In order to deal with the discontinuous behaviour of $E(\mathbf{y})$, we approximate it by the continuous function

$$E_\lambda(y_1) = 2 + \frac{2}{\pi}\arctan(\lambda y_1). \tag{4.2.54}$$

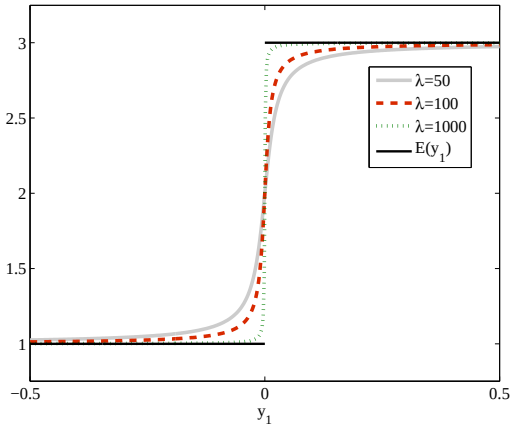

Figure 4.8: The functions E_λ.

Note that the approximation is more accurate as the value of λ grows, as illustrated in Figure 4.8.

Coefficients	Exact	Approximation		
		$\lambda = 50$	$\lambda = 100$	$\lambda = 1000$
$\overline{a}_{1111}$	1.64835	1.74169	1.70408	1.67335
$\overline{a}_{2121}$	0.57692	0.60959	0.59643	0.58907
$\overline{a}_{2211}$	0.49451	0.52251	0.51125	0.50200
$\overline{a}_{2222}$	2.14835	2.15675	2.15337	2.15192

Table 4.5: Effective coefficients.

We now use the second strategy described earlier. Table 4.5 contains the values of the approximations obtained for the non-zero coefficients of the homogenised PDE. These

can be compared to the exact solution given by Property 4.2.3, displayed in the second column of Table 4.5, with 6 significant digits.

As one would expect, the results are more accurate for larger values of λ. This parameter may be taken arbitrarily large, but at the cost of having to work with a fine mesh, locally around $y_1 = 0$, the material interface.

Example 4.3 A complicated structure

Let us again consider the elasticity problem (4.2.2) with (4.2.25)-(4.2.26) where over the reference cell $Y = [0,1] \times [0,1]$ the material properties now vary along both spatial coordinates. They are characterised by

$$E(\mathbf{y}) = 1.1 + \cos(2\pi y_1)\sin(2\pi y_2), \quad \nu = 0.3. \tag{4.2.55}$$

Let $\Omega = [0,1] \times [0,1]$, $\mathbf{f} = 0$ and the boundary conditions be such that

$$\Gamma_D = \{0\} \times [0,1], \ \boldsymbol{\varphi}_N(\mathbf{x}) = \begin{cases} (0,1), & x_2 = 1, \\ \mathbf{0}, & x_2 = 0, \\ (1,0), & x_1 = 1. \end{cases} \tag{4.2.56}$$

As before, we compute the solution functions χ_k^{lm} of the cell problem using finite elements. A fine triangular grid with 42778 quadratic elements is employed. For illustration, χ_1^{12} and χ_2^{12} are plotted in Figure 4.9.

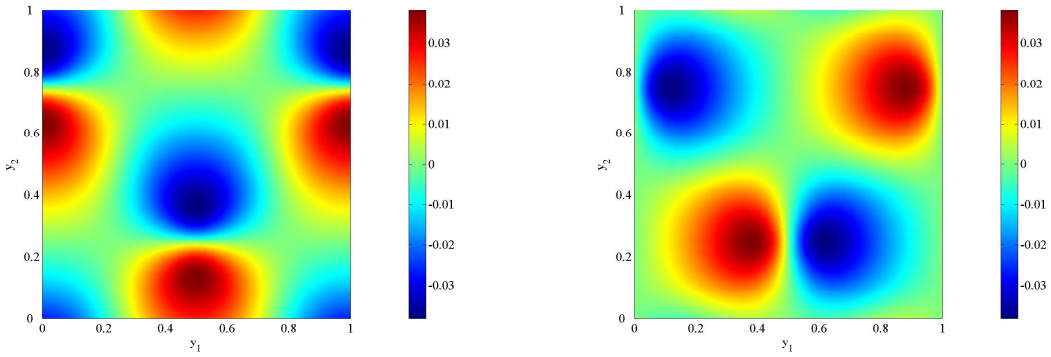

Figure 4.9 a) *The periodic cell function* χ_1^{12}. ***b)*** *The periodic cell function* χ_2^{12}.

We follow Algorithm 4.1 to approximate the value of the effective coefficients of the homogenised PDE. In Figure 4.10 a) we compare the horizontal components of the effective and the heterogeneous solutions along the line $x_2 = 0.5$ and in Figure 4.10 b) the

respective vertical components along $x_1 = 0.5$, for $\epsilon = 1/4$. The homogeneous solution is represented by the dashed lines.

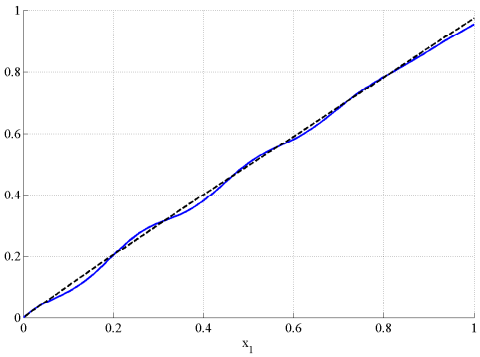

Figure 4.10 a) *Horizontal components of $\overline{\mathbf{u}}$ and the approximation $\mathbf{u}^\epsilon$ along $x_2 = 0.5$.*

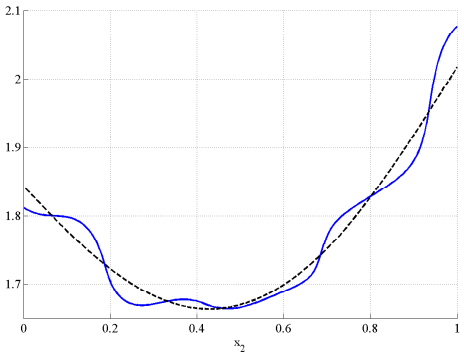

b) *Vertical components of $\overline{\mathbf{u}}$ and the approximation $\mathbf{u}^\epsilon$ along $x_1 = 0.5$.*

Finally, we compute the norms of the horizontal and vertical components of $\mathbf{u}^\epsilon - \overline{\mathbf{u}}$ for different values of ϵ, see Table 4.6.

	$\epsilon = 1/4$	$\epsilon = 1/8$	$\epsilon = 1/12$
$\|u_1^\epsilon - \overline{u}_1\|_{L^2(\Omega)}$	$1.4E-2$	$7.0E-3$	$4.6E-3$
$\|u_2^\epsilon - \overline{u}_2\|_{L^2(\Omega)}$	$9.5E-3$	$4.4E-3$	$3.0E-3$

Table 4.6: Error in $\|\cdot\|_{L^2(\Omega)}$.

As one would expect, for smaller values of ϵ, the heterogeneous solution is closer to the homogenised solution.

We have thus set up a procedure to compute a macroscopic approximation for the solution of complicated boundary value problems related to periodically distributed structures. In particular, this is useful to deal with the composite materials that we will consider in following chapters.

Chapter 5

Domain decomposition

Finding the numerical solutions of problems of practical interest such as elasticity problems related to highly heterogeneous composites often involves solving large-scale algebraic systems. Domain decomposition methods deal with this by partitioning the computational domain into a finite number of subdomains. The original PDEs are then solved on each of these subdomains. Instead of solving one complicated problem, one solves a number of simpler problems that require less computational effort. By patching together the subdomains, a sequence of numerical approximations converging to the sought solution is obtained.

In this chapter we analyse domain decomposition iterative schemes that employ either overlapping or non-overlapping subdomains. Several algorithms are presented and their convergence is established.

5.1 One dimensional example

The basic principles of the domain decomposition methods can be illustrated in a one dimensional setting. Let us consider the boundary value problem

$$\begin{cases} -\frac{d}{dx}\left[a^\epsilon(x)\frac{d}{dx}u^\epsilon(x)\right] = f(x), & x \in (0,1), \\ u^\epsilon(0) = 0, \\ u^\epsilon(1) = 0. \end{cases} \tag{5.1.1}$$

Suppose that

$$a^\epsilon(x) := \frac{1}{2+\sin(\frac{2\pi x}{\epsilon})}, \quad f(x) = 1. \tag{5.1.2}$$

The problem (5.1.1) with (5.1.2) was already introduced in the previous chapter. There we found that the oscillating behaviour of the coefficient a^ϵ leads to difficulties in solving (5.1.1) when classical numerical techniques are employed, particularly for $\epsilon \ll 1$. The theory of homogenisation was presented as a valid alternative which simplified the problem by replacing a^ϵ by an adequate constant function. The solution u^ϵ can then be approximated by the solution $\overline{u}$ of the homogenised problem

$$\begin{cases} -\bar{a}\frac{d^2}{dx^2}\overline{u}(x) = 1, & x \in (0,1), \\ \overline{u}(0) = 0, \\ \overline{u}(1) = 0. \end{cases} \tag{5.1.3}$$

Recall that the constant function $\bar{a}$ is given by (4.1.23). Homogenisation can be applied effectively to media with constituents that are finely mixed in such a way that the properties of any material sample are about the same. However, this excludes a great number of materials. One other drawback of this technique is that even using correctors, homogenisation may yield insufficiently accurate results if the local microscopic behaviour is sought. In those situations alternative ways of reducing the computational complexity of the original problem have to be used.

Domain decomposition methods are designed to take advantage of the architectural structure of modern parallel computers, cf. [47,80]. Though the distinction is not always clear, the algorithms are usually divided into Schwarz methods and substructing or Schur complement methods, cf. [3, 13, 79, 81]. The latter are associated with the usage of non-overlapping subdomains, while the former employ overlap. More details about the relationships between these different schemes are given in [14, 18, 40].

5.1.1 Substructuring iterative methods

To illustrate how (5.1.1) can be solved using domain decomposition methods, we start by splitting the computational domain $\overline{\Omega}$, with $\Omega = (0,1)$, into two non-overlapping subdomains $\overline{\Omega_1}$ and $\overline{\Omega_2}$, where

$$\Omega_1 = (0, 1/2), \quad \Omega_2 = (1/2, 1). \tag{5.1.4}$$

Denote by u_i the restriction of the solution u^ϵ of (5.1.1) to $\overline{\Omega_i}$, $i = 1, 2$. We suppress the superscript ϵ and write u_i instead of u_i^ϵ for simplicity reasons. Assuming that $u^\epsilon \in C^2(\overline{\Omega})$, (5.1.1) is equivalent to

$$\begin{cases} -\frac{d}{dx}\left[a^\epsilon(x)\frac{d}{dx}u_1(x)\right] = f(x), & x \in \Omega_1, \\ u_1(0) = 0, \\ u_1(1/2) = u_2(1/2), \\ \frac{\partial u_1}{\partial x}(1/2^-) = \frac{\partial u_2}{\partial x}(1/2^+), \\ -\frac{d}{dx}\left[a^\epsilon(x)\frac{d}{dx}u_2(x)\right] = f(x), & x \in \Omega_2, \\ u_2(1) = 0. \end{cases} \tag{5.1.5}$$

In fact, due to the continuity of u^ϵ and of its derivative in $x = 1/2$, the *matching conditions*

$$\begin{cases} u_1(1/2) = u_2(1/2), \\ \frac{\partial u_1}{\partial x}(1/2^-) = \frac{\partial u_2}{\partial x}(1/2^+), \end{cases} \tag{5.1.6}$$

are redundant. Splitting $\overline{\Omega}$ into $\overline{\Omega}_1$ and $\overline{\Omega}_2$, sequences of functions $\{u_i^{(k)}\}_k$ are generated, each defined on the subdomain $\overline{\Omega}_i$, $i = 1, 2$. The elements of each sequence satisfy a boundary value problem comprised by the original PDEs and the boundary condition $u_i^{(k)} = 0$ at $\partial\Omega \cap \partial\Omega_i$. As for the other boundary condition, there are different ways to prescribe it to ensure that $u_i^{(k)}$ converges to u_i as k increases. The common idea is to couple $u_1^{(k)}$ and $u_2^{(k)}$ by imposing one of the matching conditions and to iterate to achieve the other. If for example we impose continuity of derivatives by

$$\frac{\partial u_2^{(k)}}{\partial x}(1/2^+) = \frac{\partial u_1^{(k)}}{\partial x}(1/2^-),$$

the iterative process must be such that as k increases the quantity $|u_1^{(k)}(1/2) - u_2^{(k)}(1/2)|$ tends to zero. Accordingly we present the following algorithm to solve (5.1.1), where we represent by θ, $\alpha^{(0)}$ and *Tol* the acceleration parameter, the initial approximation for $u^\epsilon(1/2)$ and the tolerance for the stopping condition, respectively.

Algorithm 5.1

Set $k = 0$. Given: θ, $\alpha^{(0)}$, *Tol*.

1 - Solve

$$\begin{cases} -\frac{d}{dx}\left[a^\epsilon(x)\frac{d}{dx}u_1^{(k+1)}(x)\right] = f(x), & x \in \Omega_1, \\ u_1^{(k+1)}(0) = 0, \\ u_1^{(k+1)}(1/2) = \alpha^{(k)}, \end{cases} \tag{5.1.7}$$

and

$$\begin{cases} -\frac{d}{dx}\left[a^\epsilon(x)\frac{d}{dx}u_2^{(k+1)}(x)\right] = f(x), & x \in \Omega_2, \\ u_2^{(k+1)}(1) = 0, \\ \frac{\partial u_2^{(k+1)}}{\partial x}(1/2^+) = \frac{\partial u_1^{(k+1)}}{\partial x}(1/2^-). \end{cases} \tag{5.1.8}$$

2 - Update $\alpha^{(k)}$ and increment k

$$\alpha^{(k+1)} = \theta u_2^{(k+1)}(1/2) + (1-\theta)\alpha^{(k)}, \tag{5.1.9}$$

$$k \to k+1. \tag{5.1.10}$$

3 - Return to step 1 until $|u_1^{(k)}(1/2) - u_2^{(k)}(1/2)| < \mathit{Tol}$.

The so-called *Dirichlet-Neumann* procedure, described in Algorithm 5.1, will converge as long as θ is conveniently chosen. As we will see later, θ is an acceleration parameter that can be optimised for faster convergence. We note that in order to ensure faster convergence it is important to choose a value for $\alpha^{(0)}$ that is as good an approximation as possible to $u^\epsilon(1/2)$. An educated guess is given by the homogenised solution, $\alpha^{(0)} = \overline{u}(1/2)$. This has the advantage of being easy to compute.

We will now consider an example of application of the previous algorithm for which $\alpha^{(0)}$ will not be given by the homogenised solution. We do this because this educated guess would be an unrealistically good initial guess, much better than what is usually available in problems where homogenisation is not applicable. Moreover, we simply take $\theta = 0.4$.

Tol	$\|u^{(k)} - u^\epsilon\|_{L^2(\Omega)}$	k
$1E-3$	$2.31E-4$	5
$1E-4$	$9.24E-6$	7
$1E-5$	$1.85E-6$	8

Table 5.1: Error and number of iterations, $E_\alpha = 0.25$.

Using Algorithm 5.1 we approximate the solution of (5.1.1) with (5.1.2) and $\epsilon = 0.1$ by a sequence of functions $\{u^{(k)}\}_k$ defined by $u^{(k)}|_{(\overline{\Omega}_i \setminus \{1/2\})} := u_i^{(k)}$ and $u^{(k)}(1/2) := u_1^{(k)}(1/2)$. For each value of k, we employ finite elements to solve (5.1.7)-(5.1.8). Uniform meshes with width $h = 1E-4$ are used for each boundary value problem. The L^2 norms of the errors $u^{(k)} - u^\epsilon$ are displayed in the second column of Table 5.1 for the smallest number of iterations k that ensures the stopping condition is achieved, taking various values for *Tol*. The initial guess is taken $\alpha^{(0)} = 0$.

Tol	$\|u^{(k)} - u^\epsilon\|_{L^2(\Omega)}$	k
$1E-3$	$1.39E-4$	6
$1E-4$	$2.77E-5$	7
$1E-5$	$1.11E-6$	9

Table 5.2: Error and number of iterations, $E_\alpha = 0.75$.

Similar calculations are presented in Tables 5.2 and 5.3 for $\alpha^{(0)} = 1$ and $\alpha^{(0)} = 10$, respectively. The error $E_\alpha := |\alpha^{(0)} - u^\epsilon(1/2)|$ of the initial guesses, as indicated in the legends of the tables, is increasing. A larger number of iterations is then necessary to achieve the stopping condition.

Tol	$\|u^{(k)} - u^\epsilon\|_{L^2(\Omega)}$	k
$1E-3$	$7.21E-5$	8
$1E-4$	$1.44E-5$	9
$1E-5$	$2.88E-6$	10

Table 5.3: Error and number of iterations, $E_\alpha = 9.75$.

Finally, we note that the value of the tolerance *Tol* should be chosen carefully taking the expected behaviour of the error function into account. For instance, in the case of the problem we have considered, since the sign of a^ϵ is constant, it can easily be shown that when the desired tolerance is attained the maximum norm of the error $u^{(k)} - u^\epsilon$ is smaller than *Tol*. The reasoning is similar to the proof of the Theorem 5.1.1 that will be presented later.

5.1.2 Alternating Schwarz methods

Let us once again consider the problem (5.1.1) where we now take the following subdomains

$$\Omega_1 = (0, \gamma_2), \;\; \Omega_2 = (\gamma_1, 1), \tag{5.1.11}$$

which are such that $0 < \gamma_1 < \gamma_2 < 1$. We denote the length of the overlap by $\delta := \gamma_2 - \gamma_1$ and assume that there exist constants α and β such that $0 < \alpha < a^\epsilon(x) < \beta$. It is easily concluded that

$$\begin{cases} -\frac{d}{dx}\left[a^\epsilon(x)\frac{d}{dx}u_1(x)\right] = f(x), & x \in \Omega_1, \\ u_1(0) = 0, \\ \\ u_1(\gamma_1) = u_2(\gamma_1), \\ u_1(\gamma_2) = u_2(\gamma_2), \\ \\ -\frac{d}{dx}\left[a^\epsilon(x)\frac{d}{dx}u_2(x)\right] = f(x), & x \in \Omega_2, \\ u_2(1) = 0, \end{cases} \tag{5.1.12}$$

is equivalent to (5.1.1) where $u_i = u^\epsilon|_{\overline{\Omega}_i}$ as before, for $i = 1, 2$. We observe that the *matching conditions*

$$\begin{cases} u_1(\gamma_1) = u_2(\gamma_1), \\ u_1(\gamma_2) = u_2(\gamma_2), \end{cases} \tag{5.1.13}$$

are now both of the same type, but hold at different points in Ω. In order to obtain approximations for the solution of the problem we set up an iterative process that generates a sequence of approximation functions $\{u_i^{(k)}\}_k$ defined on the subdomains $\overline{\Omega}_i$, $i = 1, 2$. One of the matching conditions will be imposed for all the iteration steps and we will iterate in order to obtain the other condition. The iterative process, so-called the *alternating Schwarz method*, can be described in terms of the following algorithm. We denote by $\alpha^{(0)}$ and *Tol* the initial approximation for $u^\epsilon(\gamma_2)$ and the tolerance for the stopping condition, respectively.

Algorithm 5.2

Set $k = 0$. Given: $\alpha^{(0)}$, *Tol*.

1 - Solve

$$\begin{cases} -\frac{d}{dx}\left[a^\epsilon(x)\frac{d}{dx}u_1^{(k+1)}(x)\right] = f(x), & x \in \Omega_1, \\ u_1^{(k+1)}(0) = 0, \\ u_1^{(k+1)}(\gamma_2) = \alpha^{(k)}, \end{cases} \tag{5.1.14}$$

and

$$\begin{cases} -\frac{d}{dx}\left[a^\epsilon(x)\frac{d}{dx}u_2^{(k+1)}(x)\right] = f(x), \qquad x \in \Omega_2, \\ u_2^{(k+1)}(1) = 0, \\ u_2^{(k+1)}(\gamma_1) = u_1^{(k+1)}(\gamma_1). \end{cases} \tag{5.1.15}$$

2 - Update $\alpha^{(k)}$ and increment k

$$\alpha^{(k+1)} = u_2^{(k+1)}(\gamma_2), \tag{5.1.16}$$

$$k \to k+1. \tag{5.1.17}$$

3 - Return to step 1 until

$$|u_1^{(k)}(\gamma_2) - u_2^{(k)}(\gamma_2)| < \mathit{Tol}. \tag{5.1.18}$$

To show the convergence of this iterative process, let us define the error functions $E_i^{(k)} := u_i^{(k)} - u^\epsilon|_{\overline{\Omega}_i}$, for $k \geq 1$. Moreover, let $E_2^{(0)}(x) := \alpha^{(0)} - u_2(x), x \in \overline{\Omega}_2$. Then we have

$$\begin{cases} -\frac{d}{dx}\left[a^\epsilon(x)\frac{d}{dx}E_1^{(k)}(x)\right] = 0, \qquad x \in \Omega_1, \\ E_1^{(k)}(0) = 0, \\ E_1^{(k)}(\gamma_2) = E_2^{(k-1)}(\gamma_2), \end{cases} \tag{5.1.19}$$

and

$$\begin{cases} -\frac{d}{dx}\left[a^\epsilon(x)\frac{d}{dx}E_2^{(k)}(x)\right] = 0, \qquad x \in \Omega_2, \\ E_2^{(k)}(\gamma_1) = E_1^{(k)}(\gamma_1), \\ E_2^{(k)}(1) = 0. \end{cases} \tag{5.1.20}$$

Observe that if the sign of a^ϵ is constant, the functions $E_i^{(k)}$ are strictly monotonous. It is then easy to see that the modulus of the error function defined by

$$E^{(k)}(x) := \begin{cases} E_1^{(k)}(x),\ x \in [0,\ \gamma_1], \\ E_2^{(k)}(x),\ x \in [\gamma_1,\ 1], \end{cases} \tag{5.1.21}$$

decreases as k increases, i.e., $|E^{(k)}(x)| < |E^{(k-1)}(x)|$, for $x \in \overline{\Omega}$. The error behaves as illustrated in Figure 5.1. Note that $E_1^{(k)}(\gamma_1) = E_2^{(k)}(\gamma_1)$ and $E_1^{(k)}(\gamma_2) = E_2^{(k-1)}(\gamma_2)$.

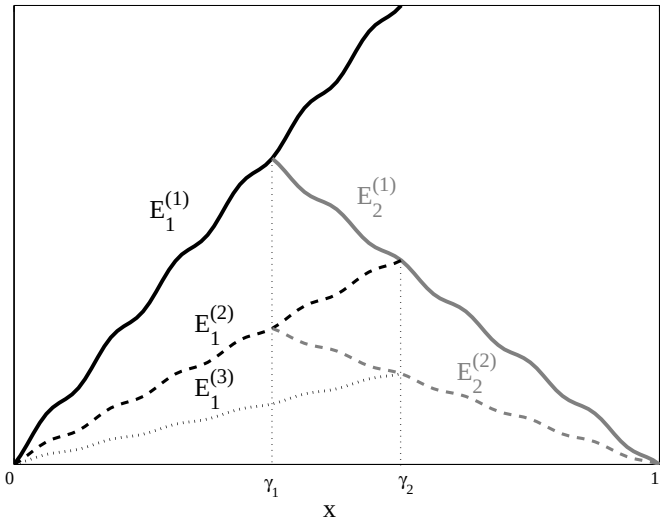

Figure 5.1: Error reduction.

We can now state the following theorem.

Theorem 5.1.1 *Let p be the smallest natural number for which (5.1.18) holds and assume that there exist real constants α and β such that $0 < \alpha < a^\epsilon(x) < \beta$. Then the approximation function*

$$u^{(p)}(x) := \begin{cases} u_1^{(p)}(x), \ x \in [0, \gamma_1], \\ u_2^{(p)}(x), \ x \in [\gamma_1, 1], \end{cases} \tag{5.1.22}$$

for the exact solution u^ϵ of (5.1.1) is such that

$$\|u^{(p)} - u^\epsilon\|_\infty \leq \frac{\int_0^{\gamma_1} 1/a^\epsilon(u)du}{\int_{\gamma_1}^{\gamma_2} 1/a^\epsilon(u)du} Tol. \tag{5.1.23}$$

Proof: The maximum of $|E^{(p)}|$ is attained at $x = \gamma_1$ and so $\|u^{(p)} - u^\epsilon\|_\infty \leq |E_2^{(p)}(\gamma_1)|$. In order to estimate an upper bound for the value of $|E_2^{(p)}(\gamma_1)|$, we note that from (5.1.19) and (5.1.20) it can easily be seen that there exist constants c_i and d_i such that

$$E_1^{(p)}(x) = c_1 \int_0^x \frac{1}{a^\epsilon(u)} du + d_1 \text{ and } E_2^{(p)}(x) = c_2 \int_{\gamma_1}^x \frac{1}{a^\epsilon(u)} du + d_2.$$

These constants can be determined in terms of integrals of the coefficient function a^ϵ. For that we use the boundary conditions for $E_1^{(p)}$ and $E_2^{(p)}$ on $x = 0$ and $x = 1$ respectively, and also the conditions

$$E_1^{(p)}(\gamma_1) = E_2^{(p)}(\gamma_1) \text{ and } |E_1^{(p)}(\gamma_2)| = |E_2^{(p)}(\gamma_2)| + Tol.$$

The result then follows. □

The Schwarz algorithm can be employed to find an approximation to the solution of the problem (5.1.1) with (5.1.2). This yields the results displayed in Tables 5.4 to 5.6 for $\alpha^{(0)} = 0$, $\epsilon = 0.1$ and for various overlapping intervals, centred at $x = 1/2$ and with length δ. The minimum number of iterations k needed to obtain the desired tolerance for each case is displayed in the third columns of the tables. Both (5.1.14) and (5.1.15) are solved employing finite elements. For each of these problems a uniform mesh with width $h = 1E-4$ is used.

Tol	$\|u^{(k)} - u^\epsilon\|_{L^2(\Omega)}$	k
$1E-3$	$1.40E-3$	12
$1E-4$	$1.26E-4$	18
$1E-5$	$1.13E-5$	24

Table 5.4: Error and number of iterations, $\delta = 0.1$.

The L^2 norms of the errors $u^{(k)} - u^\epsilon$ are displayed in the second column of the tables.

Tol	$\|u^{(k)} - u^\epsilon\|_{L^2(\Omega)}$	k
$1E-3$	$3.23E-4$	8
$1E-4$	$6.38E-5$	10
$1E-5$	$5.60E-6$	13

Table 5.5: Error and number of iterations, $\delta = 0.2$.

From these results it appears that larger values of δ yield the stopping condition to be achieved after fewer iterations. The drawback is that the computational effort per

Tol	$\|u^{(k)} - u^{\epsilon}\|_{L^2(\Omega)}$	k
$1E-3$	$1.51E-4$	6
$1E-4$	$4.39E-5$	7
$1E-5$	$3.68E-6$	9

Table 5.6: Error and number of iterations, $\delta = 0.3$.

iteration increases when the problems have to be solved on a larger region. Also, as it would be expected, smaller values of *Tol* imply more accuracy but require a larger number of iterations.

This agrees with the result established in the theorem. In fact, using the upper and lower bounds of a^{ϵ}, it follows from (5.1.23) that

$$\|u^{(k+1)} - u^{\epsilon}\|_{\infty} < \frac{\beta}{\alpha}\frac{\gamma_1}{\delta} Tol. \tag{5.1.24}$$

5.2 The elasticity problem

In the previous chapter, elasticity problems concerning periodically distributed materials were considered. We now look into the more general problem of linear elastic materials that do not necessarily display a periodic behaviour, for which the domain decomposition methods provide suitable numerical techniques.

5.2.1 The Steklov-Poincaré equation

Let us consider the *elasticity problem* given by

$$\begin{cases} -\nabla \cdot \ (\mathbf{A}(\mathbf{x})\boldsymbol{\epsilon}(\mathbf{u})) = \mathbf{f}, & \mathbf{x} \in \Omega, \\ \mathbf{u} = \mathbf{0}, & \mathbf{x} \in \Gamma_D, \\ \boldsymbol{\sigma}(\mathbf{u}) \cdot \mathbf{n} = \boldsymbol{\varphi}_N, & \mathbf{x} \in \Gamma_N. \end{cases} \tag{5.2.1}$$

To partition the computational domain into smaller non-overlapping subdomains Ω_1 and Ω_2, we note that the physics of the problem suggests the continuity of both the displacements and stresses over the interface $\Gamma = \partial\Omega_1 \cap \partial\Omega_2$. Bearing this in mind and

assuming $\mathbf{u}$ to be sufficiently smooth, we may reformulate our original problem in the equivalent form

$$\begin{cases} -\nabla \cdot (\mathbf{A}(\mathbf{x})\boldsymbol{\epsilon}(\mathbf{u_1})) = \mathbf{f}, & \mathbf{x} \in \Omega_1, \\ \\ \mathbf{u_1} = \mathbf{0}, & \mathbf{x} \in \Gamma_D \bigcap \partial\Omega_1, \\ \boldsymbol{\sigma}(\mathbf{u_1}) \cdot \mathbf{n} = \boldsymbol{\varphi}_N, & \mathbf{x} \in \Gamma_N \bigcap \partial\Omega_1, \\ \\ \mathbf{u_1} = \mathbf{u_2}, & \mathbf{x} \in \Gamma, \\ \boldsymbol{\sigma}(\mathbf{u_1}) \cdot \mathbf{n} = \boldsymbol{\sigma}(\mathbf{u_2}) \cdot \mathbf{n}, & \mathbf{x} \in \Gamma, \\ \\ -\nabla \cdot (\mathbf{A}(\mathbf{x})\boldsymbol{\epsilon}(\mathbf{u_2})) = \mathbf{f}, & \mathbf{x} \in \Omega_2, \\ \\ \mathbf{u_2} = \mathbf{0}, & \mathbf{x} \in \Gamma_D \bigcap \partial\Omega_2, \\ \boldsymbol{\sigma}(\mathbf{u_2}) \cdot \mathbf{n} = \boldsymbol{\varphi}_N, & \mathbf{x} \in \Gamma_N \bigcap \partial\Omega_2. \end{cases} \tag{5.2.2}$$

Here $\mathbf{u}_i$ is the restriction of the solution $\mathbf{u}$ of (5.2.1) to $\overline{\Omega}_i$, for $i = 1, 2$. We would like to split the problem (5.2.2) into two separate problems, one defined on $\overline{\Omega}_1$ and the other defined on $\overline{\Omega}_2$. We then start by considering the boundary value problems

$$\begin{cases} -\nabla \cdot (\mathbf{A}(\mathbf{x})\boldsymbol{\epsilon}(\mathbf{w_i})) = \mathbf{f}, & \mathbf{x} \in \Omega_i, \\ \\ \mathbf{w_i} = \mathbf{0}, & \mathbf{x} \in \Gamma_D \bigcap \partial\Omega_i, \\ \boldsymbol{\sigma}(\boldsymbol{w}_i) \cdot \mathbf{n} = \boldsymbol{\varphi}_N, & \mathbf{x} \in \Gamma_N \bigcap \partial\Omega_i, \\ \\ \mathbf{w_i} = \boldsymbol{\lambda}, & \mathbf{x} \in \Gamma, \end{cases} \tag{5.2.3}$$

where $\boldsymbol{\lambda}$ is a given vector function. Clearly, if the value of $\mathbf{u}|_\Gamma$ were known, it would suffice to simply set $\boldsymbol{\lambda} := \mathbf{u}|_\Gamma$ and (5.2.3) would be equivalent to (5.2.2), in the sense that $\mathbf{w}_i = \mathbf{u}_i$. However, since the function $\mathbf{u}|_\Gamma$ is unknown, to ensure this equivalence $\boldsymbol{\lambda}$ must be prescribed so that the solutions of (5.2.3) satisfy the following *matching conditions* on Γ:

$$\mathbf{w}_1 = \mathbf{w}_2, \tag{5.2.4}$$

$$\boldsymbol{\sigma}(\boldsymbol{w}_1) \cdot \mathbf{n} = \boldsymbol{\sigma}(\boldsymbol{w}_2) \cdot \mathbf{n}. \tag{5.2.5}$$

Note that (5.2.4) is trivially verified. As for (5.2.5), this requirement on $\boldsymbol{\lambda}$ can be written in the form of the Steklov-Poincaré equation

$$S\boldsymbol{\lambda} = \boldsymbol{\chi}, \tag{5.2.6}$$

cf. [72]. The *Steklov-Poincaré operator* S plays a central role in the convergence analysis of the domain decomposition methods we will look into. To properly define both S and

χ, let us denote by $H_i\boldsymbol{\lambda}$ the harmonic extension of $\boldsymbol{\lambda}$ into $\overline{\Omega}_i$, that is, the solution of the problem

$$\begin{cases} -\nabla\cdot\ (\mathbf{A}(\mathbf{x})\boldsymbol{\epsilon}(H_i\boldsymbol{\lambda})) = \mathbf{0}, & \mathbf{x}\in\ \Omega_i, \\ \\ H_i\boldsymbol{\lambda} = \mathbf{0}, & \mathbf{x}\in\Gamma_D\bigcap\partial\Omega_i, \\ \boldsymbol{\sigma}(H_i\boldsymbol{\lambda})\cdot\mathbf{n} = \mathbf{0}, & \mathbf{x}\in\Gamma_N\bigcap\partial\Omega_i, \\ \\ H_i\boldsymbol{\lambda} = \boldsymbol{\lambda}, & \mathbf{x}\in\Gamma. \end{cases} \tag{5.2.7}$$

Furthermore, let us denote by $G_i\mathbf{f}$ the solution of

$$\begin{cases} -\nabla\cdot\ (\mathbf{A}(\mathbf{x})\boldsymbol{\epsilon}(G_i\mathbf{f})) = \mathbf{f}, & \mathbf{x}\in\ \Omega_i, \\ \\ G_i\mathbf{f} = \mathbf{0}, & \mathbf{x}\in\Gamma_D\bigcap\partial\Omega_i, \\ \boldsymbol{\sigma}(G_i\mathbf{f})\mathbf{f}\cdot\mathbf{n} = \boldsymbol{\varphi}_N, & \mathbf{x}\in\Gamma_N\bigcap\partial\Omega_i, \\ \\ G_i\mathbf{f} = \mathbf{0}, & \mathbf{x}\in\Gamma. \end{cases} \tag{5.2.8}$$

Then the Steklov-Poincaré operator S is defined by $S := S_1 + S_2$, where

$$S_1\boldsymbol{\lambda} = \boldsymbol{\sigma}(H_1\boldsymbol{\lambda}).\mathbf{n},\ \ S_2\boldsymbol{\lambda} = -\boldsymbol{\sigma}(H_2\boldsymbol{\lambda}).\mathbf{n}, \tag{5.2.9}$$

and $\boldsymbol{\chi}$ is given by

$$\boldsymbol{\chi} = \boldsymbol{\sigma}(G_2\mathbf{f}).\mathbf{n} - \boldsymbol{\sigma}(G_1\mathbf{f}).\mathbf{n}.$$

It can then easily be seen that if $\boldsymbol{\lambda}$ satisfies the Steklov-Poincaré equation the solutions of (5.2.3) satisfy (5.2.5) and so $\mathbf{u}_i = \mathbf{w}_i$. We must then focus on determining the solution of (5.2.6). Several iterative schemes can be employed for that. In particular, the Dirichlet-Neumann method imposes continuity of stresses over Γ for all terms $\mathbf{u}_1^{(k)}$ and $\mathbf{u}_2^{(k)}$ of the sequences of problems that it generates on $\overline{\Omega}_1$ and $\overline{\Omega}_2$ respectively. The quantity $\mathbf{u}_1^{(k)} - \mathbf{u}_2^{(k)}$ should then converge to zero as k tends to infinity. As we will see, this is equivalent to generating a sequence of functions $\boldsymbol{\lambda}^{(k)}$ that converges to the solution of the Steklov-Poincaré interface equation on Γ. The *Dirichlet-Neumann* method can be written as the following algorithm, where θ is a positive acceleration parameter, an initial guess function $\boldsymbol{\lambda}^{(0)}$ must be provided and $\mathbf{Tol} = (Tol_1, Tol_2)$ is the tolerance for the stopping condition.

Algorithm 5.3

Set $k = 0$. Given: θ, $\boldsymbol{\lambda}^{(0)}$, **Tol**.

1 - Solve

$$\begin{cases} -\nabla \cdot \ (\mathbf{A}\boldsymbol{\epsilon}(\mathbf{u}_1^{(k+1)})) = \mathbf{f}, & \mathbf{x} \in \ \Omega_1, \\ \mathbf{u}_1^{(k+1)} = \mathbf{0}, & \mathbf{x} \in \Gamma_D \bigcap \partial\Omega_1, \\ \boldsymbol{\sigma}(\mathbf{u}_1^{(k+1)}) \cdot \mathbf{n} = \boldsymbol{\varphi}_N, & \mathbf{x} \in \Gamma_N \bigcap \partial\Omega_1, \\ \mathbf{u}_1^{(k+1)} = \boldsymbol{\lambda}^{(k)}, & \mathbf{x} \in \Gamma, \end{cases} \tag{5.2.10}$$

and

$$\begin{cases} -\nabla \cdot \ (\mathbf{A}\boldsymbol{\epsilon}(\mathbf{u}_2^{(k+1)})) = \mathbf{f}, & \mathbf{x} \in \ \Omega_2, \\ \mathbf{u}_2^{(k+1)} = \mathbf{0}, & \mathbf{x} \in \Gamma_D \bigcap \partial\Omega_2, \\ \boldsymbol{\sigma}(\mathbf{u}_2^{(k+1)}) \cdot \mathbf{n} = \boldsymbol{\varphi}_N, & \mathbf{x} \in \Gamma_N \bigcap \partial\Omega_2, \\ \boldsymbol{\sigma}(\mathbf{u}_2^{(k+1)}) \cdot \mathbf{n} = \boldsymbol{\sigma}(\mathbf{u}_1^{(k+1)}) \cdot \mathbf{n}, & \mathbf{x} \in \Gamma. \end{cases} \tag{5.2.11}$$

2 - Update $\boldsymbol{\lambda}^{(k)}$ and increment k

$$\boldsymbol{\lambda}^{(k+1)} = \theta \mathbf{u}_2^{(k+1)}|_\Gamma + (1-\theta)\boldsymbol{\lambda}^{(k)}, \tag{5.2.12}$$

$$k \to k+1. \tag{5.2.13}$$

3 - Return to step 1 until

$$\|(\mathbf{u}_1^{(k)}|_\Gamma - \mathbf{u}_2^{(k)}|_\Gamma)_i\|_\infty < Tol_i. \tag{5.2.14}$$

Here, $(\mathbf{u}_1^{(k)}|_\Gamma - \mathbf{u}_2^{(k)}|_\Gamma)_i$ is the i-th component of the vector function $(\mathbf{u}_1^{(k)}|_\Gamma - \mathbf{u}_2^{(k)}|_\Gamma)$, for $i = 1, 2$. Now, the iterative scheme (5.2.10)-(5.2.12) can be reduced to an interface equation given in terms of the components of the Steklov-Poincaré operator. In fact we have

$$\begin{aligned}
\mathbf{u}_2^{(k+1)}|_\Gamma &= (\mathbf{u}_2^{(k+1)} - G_2\mathbf{f})|_\Gamma \\
&= S_2^{-1}S_2(\mathbf{u}_2^{(k+1)} - G_2\mathbf{f})|_\Gamma \\
&= S_2^{-1}\left[-\boldsymbol{\sigma}(\mathbf{u}_1^{(k+1)})\cdot\mathbf{n} + \boldsymbol{\sigma}(G_2\mathbf{f})\cdot\mathbf{n}\right] \\
&= S_2^{-1}\left[-\boldsymbol{\sigma}(H_1\boldsymbol{\lambda}^{(k)} + G_1\mathbf{f})\cdot\mathbf{n} + \boldsymbol{\sigma}(G_2\mathbf{f})\cdot\mathbf{n}\right] \Rightarrow \\
\mathbf{u}_2^{(k+1)}|_\Gamma &= S_2^{-1}\left[-S_1\boldsymbol{\lambda}^{(k)} + \boldsymbol{\chi}\right]. \qquad (5.2.15)
\end{aligned}$$

Inserting (5.2.15) into (5.2.12) we verify that the iterative scheme on $\boldsymbol{\lambda}^{(k)}$ described in the previous algorithm reduces to the *preconditioned Richardson method*

$$S_2(\boldsymbol{\lambda}^{(k+1)} - \boldsymbol{\lambda}^{(k)}) = \theta(\boldsymbol{\chi} - S\boldsymbol{\lambda}^{(k)}), \quad k \geq 0, \qquad (5.2.16)$$

for the Steklov-Poincaré equation with the preconditioner S_2.

Several alternatives of domain decomposition methods exist that approximate the solution of the elasticity problem (5.2.1). Among these we distinguish *substructuring methods* such as the Neumann-Neumann, the Robin method, or the Dirichlet-Neumann scheme we have described earlier, cf. [72]. All of these partition the computational domain in non-overlapping subdomains. Sometimes however it is more appropriate to have overlap. In particular, the *Schwarz* scheme for (5.2.1) with overlapping subdomains $\overline{\Omega}_1$ and $\overline{\Omega}_2$ is given by Algorithm 5.4.

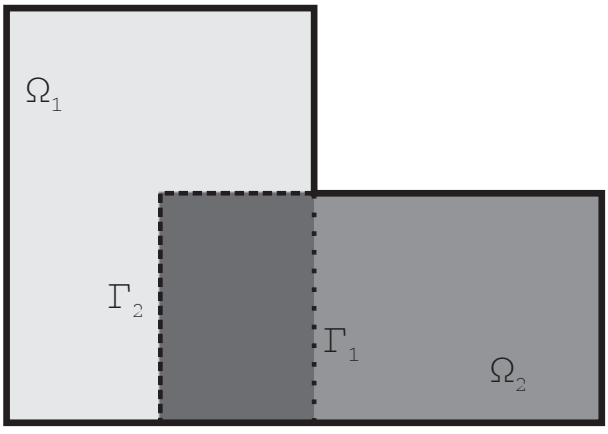

Figure 5.2: Overlapping subdomains.

Let once again θ be a positive acceleration parameter, $\boldsymbol{\lambda}^{(0)}$ an initial guess function and $\mathbf{Tol} = (Tol_1, Tol_2)$ the tolerance for the stopping condition. Moreover, let Γ_1 and Γ_2 be the

portions of $\partial\Omega_1$ and $\partial\Omega_2$ that are not in $\partial\Omega$, respectively, see Figure 5.2. The algorithm reads

Algorithm 5.4

Set $k = 0$. Given: $\boldsymbol{\lambda}^{(0)}$, **Tol**.

1 - Solve

$$\begin{cases} -\nabla \cdot \ (\mathbf{A}\boldsymbol{\epsilon}(\mathbf{u}_1^{(k+1)})) = \mathbf{f}, & \mathbf{x} \in \ \Omega_1, \\ \mathbf{u}_1^{(k+1)} = \mathbf{0}, & \mathbf{x} \in \Gamma_D \bigcap \partial\Omega_1, \\ \boldsymbol{\sigma}(\mathbf{u}_1^{(k+1)}) \cdot \mathbf{n} = \boldsymbol{\varphi}_N, & \mathbf{x} \in \Gamma_N \bigcap \partial\Omega_1, \\ \mathbf{u}_1^{(k+1)} = \boldsymbol{\lambda}^{(k)}, & \mathbf{x} \in \Gamma_1, \end{cases} \tag{5.2.17}$$

and

$$\begin{cases} -\nabla \cdot \ (\mathbf{A}\boldsymbol{\epsilon}(\mathbf{u}_2^{(k+1)})) = \mathbf{f}, & \mathbf{x} \in \ \Omega_2, \\ \mathbf{u}_2^{(k+1)} = \mathbf{0}, & \mathbf{x} \in \Gamma_D \bigcap \partial\Omega_2, \\ \boldsymbol{\sigma}(\mathbf{u}_2^{(k+1)}) \cdot \mathbf{n} = \boldsymbol{\varphi}_N, & \mathbf{x} \in \Gamma_N \bigcap \partial\Omega_2, \\ \mathbf{u}_2^{(k+1)} = \mathbf{u}_1^{(k+1)}, & \mathbf{x} \in \Gamma_2. \end{cases} \tag{5.2.18}$$

2 - Update $\boldsymbol{\lambda}^{(k)}$ and increment k

$$\boldsymbol{\lambda}^{(k+1)} = \mathbf{u}_2^{(k+1)}|_{\Gamma_1}, \tag{5.2.19}$$

$$k \rightarrow k + 1. \tag{5.2.20}$$

3 - Return to step 1 until

$$\|(\mathbf{u}_1^{(k)}|_{\Gamma_1} - \mathbf{u}_2^{(k)}|_{\Gamma_1})_i\|_\infty < Tol_i. \tag{5.2.21}$$

We note that both iterative schemes included in Algorithms 5.3 and 5.4 can be generalised to the case of having more subdomains. The idea is to perform each iteration step on all subdomains, with exchange of information occurring only over the interfaces of neighbouring subdomains. This can be implemented using parallel computing, cf. [35, 80].

5.2.2 Convergence analysis

Earlier the Dirichlet-Neumann iterative scheme expressed by (5.2.10)-(5.2.12) was proposed to solve (5.2.1). Following [72] we will establish the convergence of this scheme. We begin by rewriting (5.2.1) in a variational formulation

$$a(\mathbf{u},\mathbf{v}) = \langle \mathbf{l},\mathbf{v}\rangle, \forall\, \mathbf{v} \in \mathcal{V}, \tag{5.2.22}$$

where, as we have already introduced in Chapter 2,

$$a(\mathbf{u},\mathbf{v}) = \int_\Omega \sum_{i,j=1}^{2} \sigma_{ij}(\mathbf{u})\epsilon_{ij}(\mathbf{v})dV, \tag{5.2.23}$$

$$\langle \mathbf{l},\mathbf{v}\rangle = \int_\Omega \sum_{i=1}^{2} f_i v_i dV + \oint_{\Gamma_D} \sum_{i=1}^{2} \boldsymbol{\varphi}_{N,i} v_i dS. \tag{5.2.24}$$

We assume that $\mathbf{f} \in (L^2(\Omega))^2$, $\boldsymbol{\varphi}_N \in (L^2(\Gamma_N))^2$ and

$$\mathcal{V} = \{\mathbf{v} \mid \mathbf{v} \in (H^1(\Omega))^2,\ \boldsymbol{\gamma}(\mathbf{v}) = 0 \text{ on } \Gamma_D\}. \tag{5.2.25}$$

Recall that (5.2.1) can be rewritten as (5.2.2). This can in turn be written in a variational formulation as follows

$$\begin{cases} a_1(\mathbf{u}_1,\mathbf{v}_1) = \langle \mathbf{l}_1,\mathbf{v}_1\rangle, & \forall\, \mathbf{v}_1 \in \mathcal{V}_1^0, \\ \mathbf{u}_1 = \mathbf{u}_2, & \mathbf{x} \in \Gamma, \\ a_2(\mathbf{u}_2,\mathbf{v}_2) = \langle \mathbf{l}_2,\mathbf{v}_2\rangle, & \forall\, \mathbf{v}_2 \in \mathcal{V}_2^0, \\ a_2(\mathbf{u}_2,\boldsymbol{\mathcal{R}}_2\mu) = \langle \mathbf{l}_2,\boldsymbol{\mathcal{R}}_2\mu\rangle + \langle \mathbf{l}_1,\boldsymbol{\mathcal{R}}_1\mu\rangle - a_1(\mathbf{u}_1,\boldsymbol{\mathcal{R}}_1\mu), & \forall\, \mu \in \Lambda, \end{cases} \tag{5.2.26}$$

where $\mathbf{u}_i$ and $\mathbf{v}_i$ denote the restrictions of $\mathbf{u} = (u_1,u_2)$ and $\mathbf{v} = (v_1,v_2)$ to $\overline{\Omega}_i$, for $i = 1,2$. Moreover, $\boldsymbol{\mathcal{R}}_i$ denotes any possible extension operator from Λ to $\mathcal{V}_i$ and

$$\mathcal{V}_i := \{\mathbf{v}_i \in (H^1(\Omega_i))^2 |\ \mathbf{v}_i|_{(\partial\Omega\cap\partial\Omega_i)} = 0\},$$
$$\mathcal{V}_i^0 := (H_0^1(\Omega_i))^2,$$
$$\Lambda := \{\boldsymbol{\eta} \in (H^{1/2}(\Gamma))^2 |\ \exists\, \mathbf{v} \in \mathcal{V} :\ \boldsymbol{\eta} = \mathbf{v}|_\Gamma\},$$
$$a_i(\mathbf{u}_i,\mathbf{v}_i) := \textstyle\int_{\Omega_i} \sum_{j,k=1}^{2} \sigma_{jk}(\mathbf{u}_i)\epsilon_{jk}(\mathbf{v}_i)dV,$$
$$\langle \mathbf{l}_i,\mathbf{v}_i\rangle := \textstyle\int_{\Omega_i} \sum_{j=1}^{2} [f_j v_j]|_{\Omega_i} dV + \oint_{\Gamma_D\cap\partial\Omega_i} \sum_{j=1}^{2} [\boldsymbol{\varphi}_{N,j} v_j]|_{\Omega_i} dS.$$

Next we want to write the *Steklov-Poincaré equation* in a variational formulation. For that we first introduce for each $\boldsymbol{\eta} \in \Lambda$ the solution $\boldsymbol{\mathcal{H}}_i\boldsymbol{\eta} \in \mathcal{V}_i$ of the Dirichlet boundary value problem

$$\begin{cases} a_i(\boldsymbol{\mathcal{H}}_i\boldsymbol{\eta}, \mathbf{v}_i) = 0, & \forall\, \mathbf{v}_i \in \mathcal{V}_i^0, \\ \boldsymbol{\mathcal{H}}_i\boldsymbol{\eta} = \boldsymbol{\eta}, & \mathbf{x} \in \Gamma, \end{cases} \tag{5.2.27}$$

and the solution $\boldsymbol{\mathcal{G}}_i\mathbf{f} \in \mathcal{V}_i^0$ of

$$a_i(\boldsymbol{\mathcal{G}}_i\mathbf{f}, \mathbf{v}_i) = \langle \mathbf{l}_i, \mathbf{v}_i \rangle, \ \ \forall\, \mathbf{v}_i \in \mathcal{V}_i^0. \tag{5.2.28}$$

We are now able to define the symmetric and coercive *Steklov-Poincaré operators*. For each $\boldsymbol{\eta}, \boldsymbol{\mu} \in \Lambda$, let

$$\langle S_i\boldsymbol{\eta}, \boldsymbol{\mu} \rangle := a_i(\boldsymbol{\mathcal{H}}_i\boldsymbol{\eta}, \boldsymbol{\mathcal{H}}_i\boldsymbol{\mu}).$$

Finally, let $\boldsymbol{\lambda} = \mathbf{u}|_\Gamma$, $S := S_1 + S_2$ and $\chi := \chi_1 + \chi_2$, with

$$\langle \chi_i, \boldsymbol{\mu} \rangle := \langle \mathbf{l}_i, \boldsymbol{\mathcal{H}}_i\boldsymbol{\mu} \rangle - a_i(\boldsymbol{\mathcal{G}}_i\mathbf{f}, \boldsymbol{\mathcal{H}}_i\boldsymbol{\mu}), \ \ \forall\, \boldsymbol{\mu} \in \Lambda.$$

The stress continuity condition (5.2.5) then translates into the following interface equation on Γ:

$$S\boldsymbol{\lambda} = \chi. \tag{5.2.29}$$

We now turn our attention to the *Dirichlet-Neumann* scheme (5.2.10)-(5.2.12). In a weak form, this is given by the following algorithm, where θ is an acceleration parameter, $\boldsymbol{\lambda}^{(0)}$ is the initial approximation for $\mathbf{u}|_\Gamma$ and $\mathbf{Tol} = (\mathrm{Tol}_1, \mathrm{Tol}_2)$ is the tolerance for the stopping condition.

Algorithm 5.5

Set $k = 0$. Given: $\boldsymbol{\lambda}^{(0)}$, **Tol**.

1 - Find $\mathbf{u}_1^{(k+1)} \in \mathcal{V}_1$ and $\mathbf{u}_2^{(k+1)} \in \mathcal{V}_2$ such that

$$\begin{cases} a_1(\mathbf{u}_1^{(k+1)}, \mathbf{v}_1) = \langle \mathbf{l}_1, \mathbf{v}_1 \rangle, & \forall\, \mathbf{v}_1 \in \mathcal{V}_1^0, \\ \mathbf{u}_1^{(k+1)} = \boldsymbol{\lambda}^{(k)}, & \mathbf{x} \in \Gamma, \end{cases} \tag{5.2.30}$$

and

$$\begin{cases} a_2(\mathbf{u}_2^{(k+1)}, \mathbf{v}_2) = \langle \mathbf{l}_2, \mathbf{v}_2 \rangle, & \forall\, \mathbf{v}_2 \in \mathcal{V}_2^0, \\ a_2(\mathbf{u}_2^{(k+1)}, \boldsymbol{\mathcal{R}}_2\boldsymbol{\mu}) = \langle \mathbf{l}_2, \boldsymbol{\mathcal{R}}_2\boldsymbol{\mu} \rangle + \langle \mathbf{l}_1, \boldsymbol{\mathcal{R}}_1\boldsymbol{\mu} \rangle & \\ \qquad\qquad - a_1(\mathbf{u}_1^{(k+1)}, \boldsymbol{\mathcal{R}}_1\boldsymbol{\mu}), & \forall\, \boldsymbol{\mu} \in \Lambda. \end{cases} \tag{5.2.31}$$

2 - Update $\boldsymbol{\lambda}^{(k)}$ and increment k

$$\boldsymbol{\lambda}^{(k+1)} = \theta \mathbf{u}_2^{(k+1)}|_\Gamma + (1-\theta)\boldsymbol{\lambda}^{(k)}, \tag{5.2.32}$$

$$k \to k+1. \tag{5.2.33}$$

3 - Return to step 1 until

$$\|(\mathbf{u}_1^{(k)}|_\Gamma - \mathbf{u}_2^{(k)}|_\Gamma)_i\|_{H^{1/2}(\Gamma)} < Tol_i. \tag{5.2.34}$$

We observe that this iterative scheme reduces to the *preconditioned Richardson method*

$$S_2(\boldsymbol{\lambda}^{(k+1)} - \boldsymbol{\lambda}^{(k)}) = \theta(\boldsymbol{\chi} - S\boldsymbol{\lambda}^{(k)}), \quad k \geq 0, \tag{5.2.35}$$

for (5.2.29), where S_2 is employed as a preconditioner for S. The convergence of $\{\boldsymbol{\lambda}^{(k)}\}_k$ to the unique solution $\boldsymbol{\lambda}$ of the Steklov-Poincaré equation is established in the following general theorem, cf. [72].

Theorem: Let X be a real Hilbert space, X' its dual space, $Q : X \to X'$ a linear invertible continuous operator and $G \in X'$. Assume that $Q = Q_1 + Q_2$, where Q_1 and Q_2 are continuous linear operators, Q_2 is also coercive and there exist positive constants α, k^* and β_i such that

$$\begin{gathered} \langle Q_i\eta, \mu \rangle \leq \beta_i \|\eta\|_X \|\mu\|_X, \ \forall\, \eta, \mu \in X, \\ \langle Q_2\eta, \eta \rangle \geq \alpha \|\eta\|_X^2, \ \forall\, \eta \in X, \\ \langle Q_2\eta, Q_2^{-1}Q\eta \rangle + \langle Q\eta, \eta \rangle \geq k^* \|\eta\|_X^2, \ \forall\, \eta \in X. \end{gathered}$$

for $i = 1, 2$. Then, for any given $\lambda^{(0)} \in X$ and for any θ satisfying $0 < \theta < \theta_{max}$, with

$$\theta_{max} := \frac{k^* \alpha^2}{\beta_2(\beta_1 + \beta_2)^2},$$

the sequence $\{\lambda^{(k)}\}_k$ given by

$$Q_2(\lambda^{(k+1)} - \lambda^{(k)}) = \theta(G - Q\lambda^{(k)}), \tag{5.2.36}$$

converges in X to the solution $\lambda \in X$ of $Q\lambda = G$.

5.3 Discrete solution

Domain decomposition algorithms are often perceived to be quite complex. They are more easily understood when presented in the discrete form, using matrix notation. In this section the Dirichlet-Neumann method is studied at a discrete level for the solution of the elasticity problem that in the variational formulation is given by (5.2.22). A convergence analysis is carried out and an optimal value for the acceleration parameter θ is discussed.

As we have seen in Chapter 2, a *finite element* approximation $\mathbf{u}_h$ to the solution $\mathbf{u}$ of (5.2.22) consists of a linear combination of the form

$$\mathbf{u}_h = \sum_{j=1}^{N} y_j \boldsymbol{\phi}_j. \tag{5.3.1}$$

Here, $\{\boldsymbol{\phi}_j\}_{j=1,\ldots,N}$ is a base of a finite dimensional subspace $\mathcal{V}_h$ of $\mathcal{V}$, with $\dim \mathcal{V}_h = N$. We denote the finite element nodes by $\mathbf{a}_j$ so that we have

$$\boldsymbol{\phi}_i(\mathbf{a}_j) = \delta_{ij}. \tag{5.3.2}$$

To determine the vector $\mathbf{y} = (y_i)_{i=1,\ldots,N}$, we insert (5.3.1) into the variational problem (5.2.22), which yields

$$a(\sum_{j=1}^{N} y_j \boldsymbol{\phi}_j, \boldsymbol{\phi}_k) = \langle \mathbf{l}, \boldsymbol{\phi}_k \rangle, \quad k = 1, \ldots, N. \tag{5.3.3}$$

This leads to the linear system

$$\mathbf{D}\mathbf{y} = \mathbf{b}, \tag{5.3.4}$$

where the components of $\mathbf{b} = (b_i)_{i=1,\dots,N}$ and the components of the finite element *stiffness matrix* $\mathbf{D} = [d_{ij}]_{i,j=1,\ \dots,\ N}$ are given by

$$b_i := \langle \mathbf{l}, \boldsymbol{\phi}_i \rangle \ \text{ and } \ d_{ij} := a(\boldsymbol{\phi}_i, \boldsymbol{\phi}_j), \tag{5.3.5}$$

respectively. Before we proceed, we would like to draw a parallel to section 5.2. Like there we will rewrite the problem at hand, expressed by (5.3.4), in a form that suggests it may be split into smaller problems. For that we decompose the vector of unknowns $\mathbf{y}$ into three vectors $\mathbf{y}_1$, $\mathbf{y}_2$ and $\mathbf{y}_\Gamma$ of length N_1, N_2 and N_Γ respectively. The components of these vectors are the components of $\mathbf{y}$ corresponding to the nodes belonging to $\overline{\Omega}_1 \setminus \Gamma$, $\overline{\Omega}_2 \setminus \Gamma$ and Γ, respectively. Likewise, $\mathbf{b}$ is decomposed into $\mathbf{b}_1$, $\mathbf{b}_2$ and $\mathbf{b}_\Gamma$. The equation (5.3.4) can then be rewritten in the form

$$\begin{bmatrix} \mathbf{D}_{11} & \mathbf{0} & \mathbf{D}_{1\Gamma} \\ \mathbf{0} & \mathbf{D}_{22} & \mathbf{D}_{2\Gamma} \\ \mathbf{D}_{\Gamma 1} & \mathbf{D}_{\Gamma 2} & \mathbf{D}_{\Gamma\Gamma} \end{bmatrix} \begin{bmatrix} \mathbf{y}_1 \\ \mathbf{y}_2 \\ \mathbf{y}_\Gamma \end{bmatrix} = \begin{bmatrix} \mathbf{b}_1 \\ \mathbf{b}_2 \\ \mathbf{b}_\Gamma \end{bmatrix}. \tag{5.3.6}$$

Here the j^{th} line and k^{th} column of the matrices $\mathbf{D}_{ii}$ and $\mathbf{D}_{i\Gamma}$ are given by

$$a_i(\boldsymbol{\phi}_j^{(i)}, \boldsymbol{\phi}_k^{(i)}), \text{ for } j,k = 1,\dots,N_i \quad \text{and}$$
$$a_i(\boldsymbol{\phi}_j^{(\Gamma)}, \boldsymbol{\phi}_k^{(i)}), \text{ for } j = 1,\dots,N_\Gamma,\ k = 1,\dots,N_i,$$

respectively. The basis functions denoted by $\boldsymbol{\phi}_j^{(i)}$ correspond to the nodes lying in $\overline{\Omega}_i \setminus \Gamma$, while $\boldsymbol{\phi}_j^{(\Gamma)}$ are associated with the nodes lying on Γ. As for $\mathbf{D}_{\Gamma\Gamma}$, its components read

$$a_1(\boldsymbol{\phi}_j^{(\Gamma)}, \boldsymbol{\phi}_k^{(\Gamma)}) + a_2(\boldsymbol{\phi}_j^{(\Gamma)}, \boldsymbol{\phi}_k^{(\Gamma)}), \text{ for } j,k = 1,\dots,N_\Gamma.$$

We denote the contribution to $\mathbf{D}_{\Gamma\Gamma}$ coming from a_i by $\mathbf{D}_{\Gamma\Gamma}^{(i)}$. Eliminating $\mathbf{y}_1$ and $\mathbf{y}_2$ from (5.3.6) we obtain

$$\boldsymbol{\Sigma}_h \mathbf{y}_\Gamma = \boldsymbol{\chi}_h, \tag{5.3.7}$$

with

$$\boldsymbol{\Sigma}_h := \mathbf{D}_{\Gamma\Gamma} - \mathbf{D}_{\Gamma 1}\mathbf{D}_{11}^{-1}\mathbf{D}_{1\Gamma} - \mathbf{D}_{\Gamma 2}\mathbf{D}_{22}^{-1}\mathbf{D}_{2\Gamma}, \tag{5.3.8}$$

$$\boldsymbol{\chi}_h := \mathbf{b}_\Gamma - \mathbf{D}_{\Gamma 1}\mathbf{D}_{11}^{-1}\mathbf{b}_1 - \mathbf{D}_{\Gamma 2}\mathbf{D}_{22}^{-1}\mathbf{b}_2. \tag{5.3.9}$$

The matrix $\mathbf{\Sigma}_h$ is the *Schur complement matrix*, the algebraic counterpart of the Steklov-Poincaré operator on the discrete level. The solution of (5.3.7) can be determined easily because $\mathbf{\Sigma}_h$ is symmetric and positive definite. However, it is also ill-conditioned, cf. [72]. To deal with that, we note that like $\mathbf{D}_{\Gamma\Gamma}$, $\mathbf{\Sigma}_h$ can also be split to two components

$$\mathbf{\Sigma}_h = \mathbf{\Sigma}_{1,h} + \mathbf{\Sigma}_{2,h}, \tag{5.3.10}$$

where

$$\mathbf{\Sigma}_{i,h} = \mathbf{D}_{\Gamma\Gamma}^{(i)} - \mathbf{D}_{\Gamma i}\mathbf{D}_{ii}^{-1}\mathbf{D}_{i\Gamma}. \tag{5.3.11}$$

The idea is to employ any of the matrices $\mathbf{\Sigma}_{1,h}$ and $\mathbf{\Sigma}_{2,h}$ as a preconditioner for $\mathbf{\Sigma}_h$. We can then determine $\mathbf{y}_\Gamma$ without having to solve (5.3.7) directly. As we will see, the discrete version of the *Dirichlet-Neumann method* uses $\mathbf{\Sigma}_{2,h}$ as a preconditioner for $\mathbf{\Sigma}_h$. Before we introduce the corresponding algorithm, let us define

$$\begin{aligned}
&\mathcal{V}_{i,h} := \{\mathbf{v}_h|_{\overline{\Omega}_i} \mid \mathbf{v}_h \in \mathcal{V}_h\},\\
&\mathcal{V}_{i,h}^0 := \{\mathbf{w}_h \in \mathcal{V}_{i,h} \mid \mathbf{w}_h|_\Gamma = 0\},\\
&\Lambda_h := \{\mathbf{v}_h|_\Gamma \mid \mathbf{v}_h \in \mathcal{V}_h\},
\end{aligned}$$

and denote by $\mathcal{R}_{i,h}$ any extension operator from Λ_h to $\mathcal{V}_{i,h}$, i=1,2. Let $\boldsymbol{\lambda}_h^{(0)}$ be an initial approximation for $\mathbf{u}_h|_\Gamma$ and **Tol** the tolerance for the stopping condition. The algorithm then reads

Algorithm 5.6

Set $k = 0$. Given: $\boldsymbol{\lambda}_h^{(0)}$, **Tol**.

1 - Find $\mathbf{u}_{1,h}^{(k+1)} \in \mathcal{V}_{1,h}$ and $\mathbf{u}_{2,h}^{(k+1)} \in \mathcal{V}_{2,h}$ satisfying

$$\begin{cases} a_1(\mathbf{u}_{1,h}^{(k+1)}, \mathbf{v}_{1,h}) = \langle \mathbf{l}_1, \mathbf{v}_{1,h}\rangle, & \forall\, \mathbf{v}_{1,h} \in \mathcal{V}_{1,h}^0,\\ \mathbf{u}_{1,h}^{(k+1)} = \boldsymbol{\lambda}_h^{(k)}, & \mathbf{x} \in \Gamma, \end{cases} \tag{5.3.12}$$

and

$$\begin{cases} a_2(\mathbf{u}_{2,h}^{(k+1)}, \mathbf{v}_{2,h}) = \langle \mathbf{l}_2, \mathbf{v}_{2,h} \rangle, & \forall\, \mathbf{v}_{2,h} \in \mathcal{V}_{2,h}^0, \\ a_2(\mathbf{u}_{2,h}^{(k+1)}, \boldsymbol{\mathcal{R}}_{2,h}\boldsymbol{\mu}_h) = \langle \mathbf{l}_2, \boldsymbol{\mathcal{R}}_{2,h}\boldsymbol{\mu}_h \rangle + \langle \mathbf{l}_1, \boldsymbol{\mathcal{R}}_{1,h}\boldsymbol{\mu}_h \rangle & \\ \qquad\qquad -a_1(\mathbf{u}_{1,h}^{(k+1)}, \boldsymbol{\mathcal{R}}_{1,h}\boldsymbol{\mu}_h), & \forall\, \boldsymbol{\mu}_h \in \Lambda_h. \end{cases} \tag{5.3.13}$$

2 - Update $\boldsymbol{\lambda}_h^{(k)}$ and increment k

$$\boldsymbol{\lambda}_h^{(k+1)} = \theta \mathbf{u}_{2,h}^{(k+1)}|_\Gamma + (1-\theta)\boldsymbol{\lambda}_h^{(k)}, \tag{5.3.14}$$

$$k \to k+1. \tag{5.3.15}$$

3 - Return to step 1 until

$$\|(\mathbf{u}_{1,h}^{(k)}|_\Gamma - \mathbf{u}_{2,h}^{(k)}|_\Gamma)_i\|_{H^{1/2}(\Gamma)} < Tol_i. \tag{5.3.16}$$

It is convenient to interpret the scheme described in the previous algorithm in an algebraic form. For that we introduce the vectors $\mathbf{y}_1^{(k)} = (y_{1,j}^{(k)})_{j=1,\dots,N_1}$, $\mathbf{y}_2^{(k)} = (y_{2,j}^{(k)})_{j=1,\dots,N_2}$ and $\mathbf{y}_\Gamma^{(k)} = (y_{\Gamma,j}^{(k)})_{j=1,\dots,N_\Gamma}$, which are such that

$$\mathbf{u}_{1,h}^{(k)} = \sum_{j=1}^{N_1} y_{1,j}^{(k)} \boldsymbol{\phi}_j^{(1)},$$

$$\mathbf{u}_{2,h}^{(k)} = \sum_{j=1}^{N_2} y_{2,j}^{(k)} \boldsymbol{\phi}_j^{(2)},$$

$$\boldsymbol{\lambda}_h^{(k)} = \sum_{j=1}^{N_\Gamma} y_{\Gamma,j}^{(k)} \boldsymbol{\phi}_j^{(\Gamma)}.$$

Now (5.3.12) corresponds to the Dirichlet problem

$$\mathbf{D}_{11}\mathbf{y}_1^{(k+1)} = \mathbf{b}_1 - \mathbf{D}_{1\Gamma}\mathbf{y}_\Gamma^{(k)}. \tag{5.3.17}$$

Solving (5.3.17) for $\mathbf{y}_1^{(k+1)}$ yields

$$\mathbf{y}_1^{(k+1)} = \mathbf{D}_{11}^{-1}\mathbf{b}_1 - \mathbf{D}_{11}^{-1}\mathbf{D}_{1\Gamma}\mathbf{y}_\Gamma^{(k)}. \tag{5.3.18}$$

We can rewrite (5.3.13) as

$$\begin{bmatrix} \mathbf{D}_{22} & \mathbf{D}_{2\Gamma} \\ \mathbf{D}_{\Gamma 2} & \mathbf{D}_{\Gamma\Gamma}^{(2)} \end{bmatrix} \begin{bmatrix} \mathbf{y}_2^{(k+1)} \\ \mathbf{y}_\Gamma^{(k+1/2)} \end{bmatrix} = \begin{bmatrix} \mathbf{b}_2 \\ \mathbf{b}_\Gamma - \mathbf{D}_{\Gamma 1}\mathbf{y}_1^{(k+1)} - \mathbf{D}_{\Gamma\Gamma}^{(1)}\mathbf{y}_\Gamma^{(k)} \end{bmatrix}. \tag{5.3.19}$$

From (5.3.18) and (5.3.19) we conclude

$$\begin{aligned} (\mathbf{D}_{\Gamma\Gamma}^{(2)} - \mathbf{D}_{\Gamma 2}\mathbf{D}_{22}^{-1}\mathbf{D}_{2\Gamma})\mathbf{y}_\Gamma^{(k+1/2)} &= (-\mathbf{D}_{\Gamma\Gamma}^{(1)} + \mathbf{D}_{\Gamma 1}\mathbf{D}_{11}^{-1}\mathbf{D}_{1\Gamma})\mathbf{y}_\Gamma^{(k)} \\ &\quad + \mathbf{b}_\Gamma - \mathbf{D}_{\Gamma 1}\mathbf{D}_{11}^{-1}\mathbf{b}_1 - \mathbf{D}_{\Gamma 2}\mathbf{D}_{22}^{-1}\mathbf{b}_2, \end{aligned} \tag{5.3.20}$$

which is equivalent to

$$\mathbf{\Sigma}_{2,h}\mathbf{y}_\Gamma^{(k+1/2)} = \chi_\Gamma - \mathbf{\Sigma}_{1,h}\mathbf{y}_\Gamma^{(k)}. \tag{5.3.21}$$

Finally, (5.3.14) leads to

$$\mathbf{y}_\Gamma^{(k+1)} = \theta\mathbf{\Sigma}_{2,h}^{-1}(\chi_h - \mathbf{\Sigma}_{1,h}\mathbf{y}_\Gamma^{(k)}) + (1-\theta)\mathbf{y}_\Gamma^{(k)}, \tag{5.3.22}$$

which can be recognised as a Richardson iteration

$$\mathbf{P}_h(\mathbf{y}_\Gamma^{(k+1)} - \mathbf{y}_\Gamma^{(k)}) = \theta(\chi_h - \mathbf{\Sigma}_h\mathbf{y}_\Gamma^{(k)}), \quad \text{for } k \geq 0 \tag{5.3.23}$$

for (5.3.7), where $\mathbf{P}_h = \mathbf{\Sigma}_{2,h}$ is being used as a preconditioner for $\mathbf{\Sigma}_h$.

The convergence of the Dirichlet-Neumann scheme is stated in the following theorem, cf. [72].

Theorem 5.3.1 *: The sequence $(\mathbf{y}_\Gamma^{(k)})_k$ generated by the preconditioned Richardson iterations (5.3.23) converges to the unique solution $\mathbf{y}_\Gamma$ of (5.3.7) if and only if θ satisfies*

$$0 < \theta < \frac{2}{\nu_{max}}, \tag{5.3.24}$$

where we denote by ν_{max} and ν_{min} the maximum and minimum eigenvalues of the matrix $\mathbf{\Sigma}_{2,h}^{-1}\mathbf{\Sigma}_h$. Moreover, the optimal value θ_{opt} which minimises the spectral radius of the iteration matrix is

$$\theta = \theta_{opt} := \frac{2}{\nu_{min} + \nu_{max}}. \tag{5.3.25}$$

This result allows us to find the optimal value for the acceleration parameter θ in terms of the two components of the Schur complement matrix.

Chapter 6

Hybrid approach

Up to now, two distinct techniques were analysed for solving boundary value problems with oscillating coefficients that express the behaviour of materials with complex microstructures. These techniques share the feature of reducing the computational complexity of the problem at hand. In general terms, homogenisation was presented for periodic structures, whilst domain decomposition is applicable to more complex structures but requires the resolution of the heterogeneous scale.

In this chapter boundary value problems related to periodic materials with localised imperfections are considered. Algorithms that borrow concepts from the theory of homogenisation and also from the domain decomposition methods, making use of the periodic structure of the material as much of possible, are introduced and studied.

6.1 One-dimensional problem

Let us begin by considering a modification of the boundary value problem (4.1.2) studied earlier given by

$$\begin{cases} -\frac{d}{dx}\left[a(x)\frac{d}{dx}u(x)\right] = f(x), & x \in (0,1), \\ u(0) = 0, \\ u(1) = 0. \end{cases} \tag{6.1.1}$$

The coefficient of the differential equation is now the more general piecewise function

$$a(x) = \begin{cases} a_1(x), \ x \in [0, \ \gamma_1], \\ a_2^\epsilon(x), \ x \in (\gamma_1, \ 1], \end{cases} \tag{6.1.2}$$

where a_2^ϵ is an ϵ-periodic function, $\epsilon \ll 1$ and

$$0 < \alpha < a(x) < \beta, \ \text{for } x \in [0, 1]. \tag{6.1.3}$$

We like to think of $\gamma_1 < 1/2$, so that $a = a(x)$ is periodic everywhere except on the smaller interval $[0, \gamma_1]$. In a broader setting, there are many examples of problems for which the material's microstructure is only really relevant on a localised subdomain. This may happen either because the composition of the material differs in this local region or the phenomenon that is being modelled is occurring there. In the remainder of the computational domain, the material may be replaced by an equivalent homogenised medium. The one-dimensional example we now consider should serve as illustration for this type of problems.

6.1.1 The algorithm

As we have seen in the previous chapter, approximations for (6.1.1) can be found employing domain decomposition, either using substructuring or overlapping algorithms. The latter produce some advantages, namely they are more generally applicable and robust [17, 40]. Furthermore, they involve computing u and not its derivative du/dx at the interfaces. Note that when the function $a = a(x)$ oscillates rapidly, expressing a complex microstructure, the derivative of u will change more abruptly than u itself. Moreover, the function u is the primary unknown that we approximate using finite elements and there is a natural loss of accuracy when du/dx is determined numerically. Finally, there is another advantage in employing Schwarz methods to deal with problems with a localised relevant microstructure if in the remainder of the computational domain a macroscopic approach is to be adopted. In that case we expect the overlapping region to smooth out the effect of prescribing macroscopic boundary conditions to the smaller microscopic regions.

In order to consider an overlapping scheme for (6.1.1) we introduce $\gamma_2 \in (0, 1)$ that is such that $\gamma_1 < \gamma_2$. As we have seen, the Schwarz procedure described in Algorithm 5.2 iterates over $[\gamma_1, \gamma_2]$ such that sequences of functions $\{u_1^{(k)}\}_k$ and $\{u_2^{(k)}\}_k$ are generated. These converge to $u|_{[0,\gamma_2]}$ and $u|_{[\gamma_1,1]}$, respectively.

Naturally, the periodic behaviour of the coefficients of the differential equation over $[\gamma_1, 1]$ suggest that homogenisation can and should be employed over this interval. Doing so prevents resolving the microscale unnecessarily, thus reducing the complexity of the problem. The idea now is to decouple the problem into two smaller problems and using homogenisation on the subproblem that allows it. This results in the hybrid

approach expressed in the following algorithm, where we denote by $\widehat{\lambda}^{(0)}$ the initial approximation for $u(\gamma_2)$ and *Tol* is the tolerance for the stopping condition. Moreover, $\overline{a}$ is the effective coefficient associated to a_2^ϵ and χ is the solution of the respective cell problem, as described in Chapter 4.

Algorithm 6.1

Set $k = 0$. Given: $\widehat{\lambda}^{(0)}$, *Tol*.

1 - Solve

$$\begin{cases} -\frac{d}{dx}\left[a(x)\frac{d}{dx}\widehat{u}_1^{(k+1)}(x)\right] = f(x), & x \in (0,\gamma_2), \\ \widehat{u}_1^{(k+1)}(0) = 0, \\ \widehat{u}_1^{(k+1)}(\gamma_2) = \widehat{\lambda}^{(k)}, \end{cases} \tag{6.1.4}$$

and

$$\begin{cases} -\frac{d}{dx}\left[\overline{a}(x)\frac{d}{dx}\overline{w}^{(k+1)}(x)\right] = f(x), & x \in (\gamma_1,1), \\ \overline{w}^{(k+1)}(\gamma_1) = \widehat{u}_1^{(k+1)}(\gamma_1), \\ \overline{w}^{(k+1)}(1) = 0. \end{cases} \tag{6.1.5}$$

2- Set

$$w_1^{(k+1)}(x) := \chi(x/\epsilon)\frac{d\overline{w}^{(k+1)}}{dx}(x). \tag{6.1.6}$$

3- Solve

$$\begin{cases} -\frac{d}{dx}\left[\overline{a}(x)\frac{d}{dx}C^{(k+1)}(x)\right] = 0, & x \in (\gamma_1,1), \\ C^{(k+1)}(\gamma_1) = -\epsilon w_1^{(k+1)}(\gamma_1), \\ C^{(k+1)}(1) = -\epsilon w_1^{(k+1)}(1). \end{cases} \tag{6.1.7}$$

4- Set $\widehat{u}_2^{(k+1)} := \overline{w}^{(k+1)} + \epsilon w_1^{(k+1)} + C^{(k+1)}$.

5 - Update $\widehat{\lambda}^{(k)}$ and increment k

$$\widehat{\lambda}^{(k+1)} = \widehat{u}_2^{(k+1)}(\gamma_2). \tag{6.1.8}$$
$$k \to k+1. \tag{6.1.9}$$

6 - Return to step 1 until $|\widehat{u}_1^{(k)}(\gamma_2) - \widehat{u}_2^{(k)}(\gamma_2)| < Tol$.

This algorithm generates sequences of approximation functions $\{\widehat{u}_1^{(k)}\}_k$ and $\{\widehat{u}_2^{(k)}\}_k$ to $u|_{[0,\gamma_2]}$ and $u|_{[\gamma_1,1]}$, respectively. Note that $\widehat{u}_2^{(k)}$ is the homogenised corrected solution corresponding to the problem that reads

$$\begin{cases} -\frac{d}{dx}\left[a_2^\varepsilon(x)\frac{d}{dx}w^{(k)}(x)\right] = f(x), & x \in (\gamma_1, 1), \\ w^{(k)}(\gamma_1) = \widehat{u}_1^{(k)}(\gamma_1), \\ w^{(k)}(1) = 0. \end{cases} \tag{6.1.10}$$

It is possible to skip steps 2 and 3 of the algorithm and avoid computing the correctors. In that case, step 4 should be replaced by setting $\widehat{u}_2^{(k+1)} := \overline{w}^{(k+1)}$. This approach will then become less complex, but also less accurate.

6.1.2 Behaviour of the error

We can now analyse the behaviour of the error associated to the previous iterative scheme. Let us denote the error of the approximations $\widehat{u}_1^{(k)}$ and $\widehat{u}_2^{(k)}$ by $\widehat{E}_1^{(k)} := \widehat{u}_1^{(k)} - u|_{[0,\gamma_2]}$ and $\widehat{E}_2^{(k)} := \widehat{u}_2^{(k)} - u|_{[\gamma_1,1]}$, respectively. Clearly for $k \geq 1$ the function $\widehat{E}_1^{(k)}$ satisfies

$$\begin{cases} -\frac{d}{dx}\left[a(x)\frac{d}{dx}\widehat{E}_1^{(k)}(x)\right] = 0, & x \in (0, \gamma_2), \\ \widehat{E}_1^{(k)}(0) = 0, \\ \widehat{E}_1^{(k)}(\gamma_2) = \widehat{E}_2^{(k-1)}(\gamma_2), \end{cases} \tag{6.1.11}$$

where we define $\widehat{E}_2^{(0)}(\gamma_2)$ as the error of the initial guess at $x = \gamma_2$. As for the function $\widehat{E}_2^{(k)}$, it can be written as the sum of $E_2^{(k)}$ with $e_H^{(k)}$, where

$$\begin{cases} -\frac{d}{dx}\left[a_2^\varepsilon(x)\frac{d}{dx}E_2^{(k)}(x)\right] = 0, & x \in (\gamma_1, 1), \\ E_2^{(k)}(\gamma_1) = \widehat{E}_1^{(k)}(\gamma_1), \\ E_2^{(k)}(1) = 0, \end{cases} \tag{6.1.12}$$

and $e_H^{(k)} := \hat{u}_2^{(k)} - w^{(k)}$ is the homogenisation error at step k. Recall that $w^{(k)}$ is the solution of (6.1.10). Now take a fixed value for k. Assume for the sake of simplicity that $\widehat{E}_2^{(k-1)}(\gamma_2)$, the error arising of the previous iteration, is positive. The more general case follows a similar proof. From the differential equations in (6.1.11) and (6.1.12) it can be seen that both $\widehat{E}_1^{(k)}$ and $E_2^{(k)}$ are strictly monotonous functions. They are illustrated in Figure 6.1. Note that $\widehat{E}_1^{(k)}(\gamma_1) = E_2^{(k)}(\gamma_1)$ and $\widehat{E}_1^{(k)}(\gamma_2) = \widehat{E}_2^{(k-1)}(\gamma_2)$.

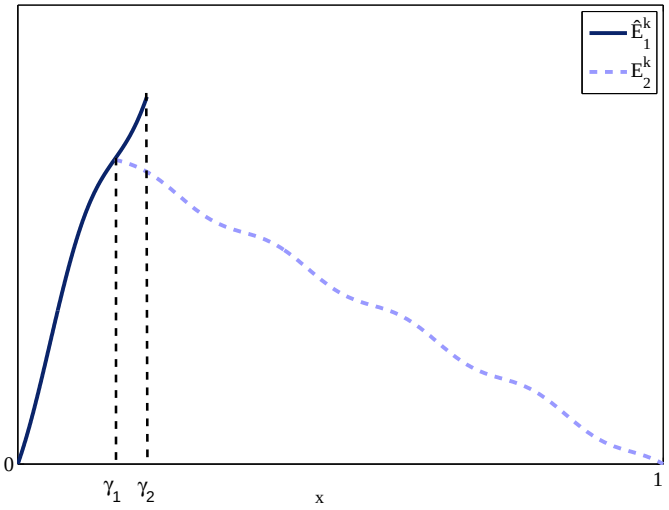

Figure 6.1: Errors.

It is now easy to see that

$$E_2^{(k)}(\gamma_2) < \widehat{E}_1^{(k)}(\gamma_2).$$

Also, as long as $\widehat{E}_1^{(k)}(\gamma_2) - E_2^{(k)}(\gamma_2) > |e_H^{(k)}(\gamma_2)|$, we have

$$\widehat{E}_1^{(k+1)}(\gamma_2) = \widehat{E}_2^{(k)}(\gamma_2) = E_2^{(k)}(\gamma_2) + e_H^{(k)}(\gamma_2) < \widehat{E}_1^{(k)}(\gamma_2).$$

In other words, at the end of the iteration step, the maximum of the approximation error coming from the previous iteration, $\widehat{E}_1^{(k)}(\gamma_2)$, will be reduced to $\widehat{E}_1^{(k+1)}(\gamma_2)$.

A natural stopping criterion for the hybrid approach algorithm would then be given by

$$|\widehat{E}_1^{(k)}(\gamma_2) - E_2^{(k)}(\gamma_2)| \leq e_H, \tag{6.1.13}$$

where e_H is the maximum of the error, in modulus, of the approximation yielded by the homogenisation procedure. Indeed, until this condition is satisfied the error decreases at each iteration step. Note, however, that $\widehat{E}_1^{(k)}(\gamma_2)$ and $E_2^{(k)}(\gamma_2)$ are not known. Therefore, instead of (6.1.13) we will adopt the following stopping criterion

$$|\widehat{E}_1^{(k)}(\gamma_2) - \widehat{E}_2^{(k)}(\gamma_2)| \leq Tol, \tag{6.1.14}$$

which can also be written as

$$|\widehat{u}_1^{(k)}(\gamma_2) - \widehat{u}_2^{(k)}(\gamma_2)| \leq Tol. \tag{6.1.15}$$

We can now establish the following theorem that gives the error of the approximation obtained when the quantities $|\widehat{E}_1^{(k)}(\gamma_2) - \widehat{E}_2^{(k)}(\gamma_2)|$ decrease with k until (6.1.15) holds, for a given *Tol*.

Theorem 6.1.1 *Let* p *be the smallest natural number such that (6.1.15) holds. Then the approximation*

$$\widehat{u}^{(p)}(x) := \begin{cases} \widehat{u}_1^{(p)}(x), \ x \in [0, \gamma_1], \\ \widehat{u}_2^{(p)}(x), \ x \in (\gamma_1, 1], \end{cases} \tag{6.1.16}$$

for the exact solution u *of (6.1.1) with (6.1.2) is such that*

$$\|\widehat{u}^{(p)} - u\|_\infty \leq \frac{\int_0^{\gamma_1} 1/a(u)du}{\int_{\gamma_1}^{\gamma_2} 1/a(u)du}(e_H + Tol) + e_H. \tag{6.1.17}$$

Proof: For each iteration, the maximum of the function

$$E^{(p)}(x) := \begin{cases} \widehat{E}_1^{(p)}(x), \ x \in [0, \gamma_1], \\ E_2^{(p)}(x), \ x \in [\gamma_1, 1], \end{cases} \tag{6.1.18}$$

is attained for $x = \gamma_1$. Now, since

$$\widehat{E}_2^{(p)}(x) = E_2^{(p)}(x) + e_H^{(p)}(x) \leq E_2^{(p)}(x) + e_H,$$

the maximum of $E^{(p)}$ added to e_H gives an upper bound for the error function

$$\widehat{E}^{(p)}(x) := \begin{cases} \widehat{E}_1^{(p)}(x),\ x \in [0,\ \gamma_1], \\ \widehat{E}_2^{(p)}(x),\ x \in (\gamma_1,\ 1]. \end{cases} \tag{6.1.19}$$

Consequently,

$$\|\widehat{u}^{(p)} - u\|_\infty \leq E_2^{(p)}(\gamma_1) + e_H. \tag{6.1.20}$$

In order to estimate the value of $E_2^{(p)}(\gamma_1)$, we proceed like in Theorem 5.1.1. From (6.1.11) and (6.1.12) it can be easily seen that there exist constants c_i and d_i such that we have

$$\widehat{E}_1^{(p)}(x) = c_1 \int_0^x \frac{1}{a(u)} du + d_1 \ \text{ and } \ E_2^{(p)}(x) = c_2 \int_{\gamma_1}^x \frac{1}{a(u)} du + d_2.$$

To determine these constants we use the boundary conditions for $\widehat{E}_1^{(p)}$ and $E_2^{(p)}$ on $x = 0$ and $x = 1$ respectively, and also the conditions

$$\widehat{E}_1^{(p)}(\gamma_1) = E_2^{(p)}(\gamma_1) \ \text{ and } \ \widehat{E}_1^{(p)}(\gamma_2) = E_2^{(p)}(\gamma_2) + e_H + \mathit{Tol}.$$

The latter equality ensures that we compute an upper bound for $E_2^{(p)}(\gamma_1)$. The result then follows from (6.1.20). □

An estimate for the error in which the size of the overlapping region plays an explicit role is given in the following result.

Corollary 6.1.2 *Under the conditions of the previous theorem, an upper bound for the error is*

$$\|\widehat{u}^{(k)} - u\|_\infty \leq \frac{\beta \int_0^{\gamma_1} 1/a(u) du}{\gamma_2 - \gamma_1} (e_H + \mathit{Tol}) + e_H.$$

Proof: It follows from (6.1.17) and (6.1.3). □

The latter inequality tells us that the size $\delta := \gamma_2 - \gamma_1$ of the overlapping region should be chosen as large as possible in order to minimise the error at the end of the iterative process. The drawback is that choosing a bigger value for δ implies at each iteration step a bigger computational effort.

On the other hand producing a good choice for the value of *Tol* is not trivial. The quantity $|\widehat{u}_1^{(k)}(\gamma_2) - \widehat{u}_2^{(k)}(\gamma_2)|$ will initially decrease as k increases, but at a certain point the homogenisation error may prevent it from decreasing further and it might even increase. The iterative process can then be stopped after $|\widehat{u}_1^{(k)}(\gamma_2) - \widehat{u}_2^{(k)}(\gamma_2)|$ starts increasing and the approximation we seek taken from the previous iteration. Alternatively, a value for *Tol* may be prescribed, which might be useful to avoid having too many iteration steps. In any case, the result from the previous theorem will then give an upper bound for the error. In Section 6.3 we will present a couple of examples where we estimate e_H and simply take $Tol = e_H/2$.

Finally, we note that the error of this iterative process depends a great deal on the accuracy of the homogenisation procedure. It may then be wise to improve the quality of the homogeneous solution by employing correctors, though this is likely unnecessary when ϵ is very small.

6.2 The elasticity problem

Let us consider a composite plate with linear elastic constituents. When these are finely mixed, computing the displacement vector field for this plate is rather complex, requiring the adoption of appropriate numerical techniques. In particular, if the material is periodically distributed, this problem is expressed by (4.2.2) and so the theory of Chapter 4 may be employed. For the more general case, one may recur to domain decomposition methods that cut up the original problem into smaller and more manageable problems. In what follows we adapt and extend the results of the previous section to the problem of linear *elasticity* given by

$$\begin{cases} -\nabla \cdot \ (\mathbf{A}(\mathbf{x})\boldsymbol{\epsilon}(\mathbf{u})) = \mathbf{f}, & \mathbf{x} \in \ \Omega, \\ \\ \mathbf{u} = \mathbf{0}, & \mathbf{x} \in \Gamma_D, \\ \boldsymbol{\sigma}(\mathbf{u}) \cdot \mathbf{n} = \boldsymbol{\varphi}_N, & \mathbf{x} \in \Gamma_N, \end{cases} \tag{6.2.1}$$

where the domain Ω is partitioned into non-overlapping subdomains Ω_1 and Ω_2 such that $\Omega = \Omega_1 \cup \Omega_2$ and

$$\mathbf{A}(\mathbf{x}) := \begin{cases} \mathbf{A}_1(\mathbf{x}), \ \mathbf{x} \in \Omega_1, \\ \mathbf{A}_2^\epsilon(\mathbf{x}), \ \mathbf{x} \in \Omega_2. \end{cases} \tag{6.2.2}$$

Here $\mathbf{A}_2^\epsilon$ is an ϵ-periodic tensor and it is assumed that $|\Omega_1| < |\Omega_2|$. Note that the homogenisation method described earlier may not be employed to solve (6.2.1) with (6.2.2) as $\mathbf{A}$ is not periodic everywhere. On the other hand, using domain decomposition techniques has the drawback of not making use of the periodicity of the elasticity tensor over

Ω_2. We then proceed as in Section 6.1 and establish a hybrid approach for this problem where again we combine homogenisation and domain decomposition techniques.

We will introduce a sequence of problems defined on the two overlapping subdomains $\widehat{\Omega}_1$ and Ω_2, where $\Omega_1 \subset \widehat{\Omega}_1 \subset \Omega$. Let $\Gamma_1 = \partial\Omega_1 \cap \partial\Omega_2$ and $\Gamma_2 = \partial\widehat{\Omega}_1 \cap \overline{\Omega}_2$, as illustrated in Figure 6.2.

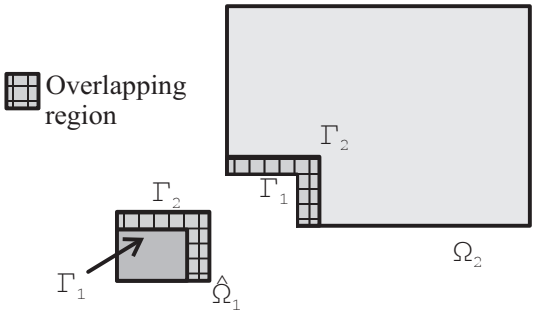

Figure 6.2: Computational domain Ω, the union of the overlapping subdomains $\widehat{\Omega}_1$ and Ω_2.

The algorithm expressing the hybrid approach for elasticity is as follows. Let $\widehat{\boldsymbol{\lambda}}^{(0)}$ be the initial guess for $\mathbf{u}|_{\Gamma_2}$ and $\mathbf{Tol} = (\mathtt{Tol}_1, \mathtt{Tol}_2)$ the tolerance for the stopping condition.

Algorithm 6.2

Set $k = 0$. Given: $\widehat{\boldsymbol{\lambda}}^{(0)}$, **Tol**.

1 - Solve

$$\begin{cases} -\nabla \cdot \ (\mathbf{A}\boldsymbol{\epsilon}(\widehat{\mathbf{u}}_1^{(k+1)})) = \mathbf{f}, & \mathbf{x} \in \widehat{\Omega}_1, \\ \widehat{\mathbf{u}}_1^{(k+1)} = \mathbf{0}, & \mathbf{x} \in \Gamma_D \bigcap \partial\widehat{\Omega}_1, \\ \boldsymbol{\sigma}(\widehat{\mathbf{u}}_1^{(k+1)}) \cdot \mathbf{n} = \boldsymbol{\varphi}_N, & \mathbf{x} \in \Gamma_N \bigcap \partial\widehat{\Omega}_1, \\ \\ \widehat{\mathbf{u}}_1^{(k+1)} = \widehat{\boldsymbol{\lambda}}^{(k)}, & \mathbf{x} \in \Gamma_2, \end{cases} \tag{6.2.3}$$

and

$$\begin{cases} -\nabla\cdot\ (\overline{\mathbf{A}}\boldsymbol{\epsilon}(\overline{\boldsymbol{w}}^{(k+1)})) = \mathbf{f}, & \mathbf{x}\ \in\ \Omega_2, \\ \overline{\boldsymbol{w}}^{(k+1)} = \mathbf{0}, & \mathbf{x}\in\Gamma_D\bigcap\partial\Omega_2, \\ \boldsymbol{\sigma}(\overline{\boldsymbol{w}}^{(k+1)})\cdot\mathbf{n} = \boldsymbol{\varphi}_N, & \mathbf{x}\in\Gamma_N\bigcap\partial\Omega_2, \\ \overline{\boldsymbol{w}}^{(k+1)} = \widehat{\mathbf{u}}_1^{(k+1)}, & \mathbf{x}\in\Gamma_1. \end{cases} \tag{6.2.4}$$

2- Set

$$\mathbf{w}_1(\mathbf{x}) = \frac{1}{2}\sum_{i,j=1,2}\left(\frac{\partial\overline{w}_i}{\partial x_j}+\frac{\partial\overline{w}_j}{\partial x_i}\right)\chi^{ij}(\frac{\mathbf{x}}{\epsilon}). \tag{6.2.5}$$

3- Solve

$$\begin{cases} -\nabla\cdot\ (\overline{\mathbf{A}}\boldsymbol{\epsilon}(\mathbf{C}^{(k+1)})) = \mathbf{0}, & \mathbf{x}\ \in\ \Omega_2, \\ \mathbf{C}^{(k+1)} = -\epsilon\mathbf{w}_1, & \mathbf{x}\in\Gamma_D\cap\partial\Omega_2, \\ \boldsymbol{\sigma}(\mathbf{C}^{(k+1)})\cdot\mathbf{n} = \mathbf{0}, & \mathbf{x}\in\Gamma_N\cap\partial\Omega_2. \end{cases} \tag{6.2.6}$$

4- Set $\widehat{\mathbf{u}}_2^{(k+1)} := \overline{\boldsymbol{w}}^{(k+1)} + \epsilon\mathbf{w}_1^{(k+1)} + \mathbf{C}^{(k+1)}$.

5 - Update $\widehat{\boldsymbol{\lambda}}^{(k)}$ and increment k

$$\widehat{\boldsymbol{\lambda}}^{(k+1)} = \widehat{\mathbf{u}}_2^{(k+1)}|_{\Gamma_2}, \tag{6.2.7}$$

$$k \to k+1. \tag{6.2.8}$$

6 - Return to step 1 until

$$\|(\widehat{\mathbf{u}}_1^{(k)}|_{\Gamma_2} - \widehat{\mathbf{u}}_2^{(k)}|_{\Gamma_2})_i\|_\infty < \mathrm{Tol}_i,\ \text{for } i = 1,2. \tag{6.2.9}$$

Here, $(\widehat{\mathbf{u}}_1^{(k)}|_{\Gamma_2} - \widehat{\mathbf{u}}_2^{(k)}|_{\Gamma_2})_i$ represents the i^{th} component of the vector function $(\widehat{\mathbf{u}}_1^{(k)}|_{\Gamma_2} - \widehat{\mathbf{u}}_2^{(k)}|_{\Gamma_2})$.

We note that this algorithm may be significantly simplified if the accuracy requirements are not too demanding. The iteration steps 2 to 4, where correctors are employed to improve the accuracy of the overall procedure, may be replaced by simply having

$\widehat{\mathbf{u}}_2^{(k+1)} := \overline{\boldsymbol{w}}^{(k+1)}$. In any case the error originating from this procedure will depend on the accuracy of the homogenised solution, which improves for smaller values of ϵ.

6.3 Numerical results

We conclude this chapter with a discussion of the implementation of the algorithms presented earlier. A one-dimensional example related to Algorithm 6.1 is included. The underlying differential equation has periodic coefficients everywhere except for a small portion of the computational domain. A layered material with localised inclusions is also analysed, for which Algorithm 6.2 is employed.

6.3.1 One-dimensional example

Let us consider the problem (6.1.1) with

$$a(x) = \begin{cases} 2 + 1.9\cos(2\pi x/0.03), \ x \in [0,\ \gamma_1) \\ \left[2 + \sin(\frac{2\pi x}{\epsilon})\right]^{-1}, \ x \in [\gamma_1,\ 1] \end{cases}, \ f(x) = 1, \ \epsilon = 0.1, \ \gamma_1 = 0.1. \qquad (6.3.1)$$

For future convenience we start by computing a reference solution u for this problem, using quadratic finite elements on a very fine mesh.

An approximation for u can be determined using the hybrid approach described in Algorithm 6.1 that takes the ϵ-periodic behaviour of $a|_{[\gamma_1,1]}$ into account. This will generate the sequence of approximations $\{\widehat{u}^{(k)}\}_k$ defined in (6.1.16), as we iterate over the overlapping region $[\gamma_1,\ \gamma_2]$, for some given γ_2 that satisfies $0 < \gamma_1 < \gamma_2 < 1$. In order to start the iterative process, an initial approximation $\widehat{\lambda}^{(0)}$ for $u(\gamma_2)$ must be provided. For this we consider the auxiliary problem (6.1.1) with

$$a(x) := a^\epsilon(x) = \frac{1}{2 + \sin(\frac{2\pi x}{\epsilon})}, \quad \text{for } x \in [0,1], \ \ f(x) = 1, \ \ \epsilon = 0.1. \qquad (6.3.2)$$

This is a modification of the original problem (6.1.1) with (6.3.1) obtained by disregarding the behaviour of the coefficients $a = a(x)$ in (6.3.1) over the smaller interval $[0,\gamma_1]$. Instead, ϵ-periodic coefficients are considered throughout Ω. This periodic problem had already been considered in Chapter 4. There we used the homogenised solution $\overline{u}$ and the homogenised corrected solution $\overline{u} + u_1 + C$ as approximations for u^ϵ, cf. Table 4.1. In this setting, we may use either $\overline{u}$ or $\overline{u} + u_1 + C$ as cheap initial guesses for the solution u of (6.1.1) with (6.3.1). The L^2 and maximum norms of the errors $E := \overline{u} - u$ and $E_C := (\overline{u} + u_1 + C) - u$ are displayed in Table 6.1.

	$\|\cdot\|_\infty$	$\|\cdot\|_{L^2(0,1)}$
$\overline{E}$	$2.2E-2$	$1.2E-2$
E_C	$2.7E-2$	$1.3E-2$

Table 6.1: Error of the approximations.

We now turn our attention again to (6.1.1) with (6.3.1) and employ Algorithm 6.1, taking $\widehat{\lambda}^{(0)} = \overline{u}(\gamma_2)$. Approximations for the solutions of the problems (6.1.4), (6.1.5) and (6.1.7), as well as the cell problem, are computed using quadratic finite elements. A finer uniform grid with grid size $h = 1E-4$ is required to solve the problem on $[0,\ \gamma_1]$. As for the other problems, the grid size is taken to be $h = 1E-1$. Finally, note that w_1 depends on components of the cell function and on derivatives of components of the homogenised function $\overline{w}$. The latter are determined by numerical differentiation.

	$\|\cdot\|_\infty$	$\|\cdot\|_{L^2(0,1)}$	k	Upper bound
$\overline{E}$	$1.5E-2$	$5.7E-3$	2	$5.0E-2$
E_C	$7.9E-4$	$3.9E-4$	6	$1.4E-3$

Table 6.2: Error arising from the hybrid procedure for $\gamma_2 = 0.15$.

	$\|\cdot\|_\infty$	$\|\cdot\|_{L^2(0,1)}$	k	Upper bound
$\overline{E}$	$1.4E-2$	$5.2E-3$	2	$2.9E-2$
E_C	$5.6E-4$	$2.8E-4$	4	$9.7E-4$

Table 6.3: Error arising from the hybrid procedure for $\gamma_2 = 0.25$.

	$\|\cdot\|_\infty$	$\|\cdot\|_{L^2(0,1)}$	k	Upper bound
$\overline{E}$	$1.4E-2$	$4.7E-3$	2	$2.2E-2$
E_C	$4.8E-4$	$2.5E-4$	4	$8.0E-4$

Table 6.4: Error arising from the hybrid procedure for $\gamma_2 = 0.35$.

Tables 6.2 to 6.4 display the errors obtained by employing the procedure above for various sizes of the overlapping region, with the parameter γ_2 taking the values 0.15, 0.25 and 0.35, respectively. On the second lines of the tables, $\overline{E}$ gives the error when simple homogenisation is applied on the domain $[\gamma_1, 1]$, i.e., when steps 2 and 3 of the algorithm are skipped. As for E_C, it corresponds to the error obtained by improving the

homogenised solution with the first order corrector and the boundary corrector. The fourth column of the tables displays the number of iterations k required to satisfy the stopping condition (6.1.15) with $Tol = e_H/2$, and the last column the theoretical upper bound given by (6.1.17). Estimates for the maximum error e_H of the homogenisation procedure were taken from Table 4.1. In Figure 6.3 we show the exact solution of (6.1.1) with (6.3.1) in black dots, the initial approximation $\overline{u}$ as a dotted line and the hybrid solution given by Algorithm 6.1, employing the correctors, as the full gray line that nearly coincides with the exact solution.

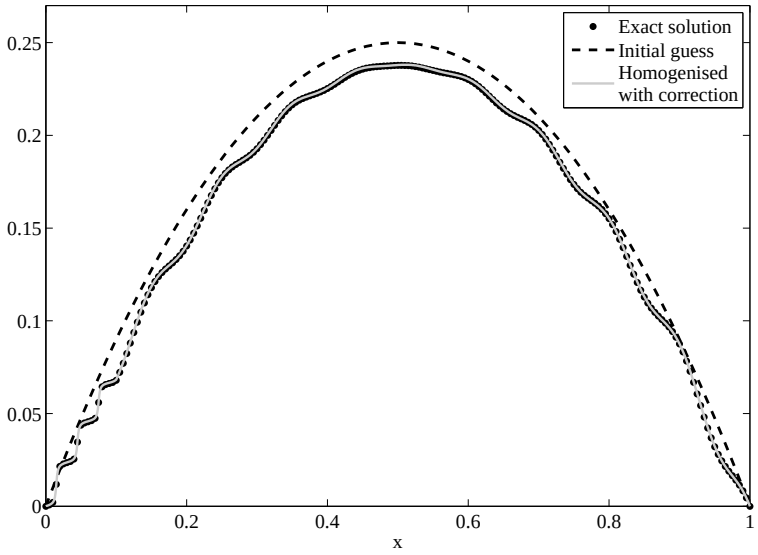

Figure 6.3: Exact and approximated solutions.

As one can see, the accuracy of the results depends on that of the homogenisation procedure. In practice, ϵ should be much smaller than 0.1, the value that we took for this example. This will lower the homogenisation error and improve the overall results further.

6.3.2 Layered elastic materials

In what follows we present an example related to the elasticity problems introduced in Section 6.2. This demonstrates the capability of the hybrid approach to deal with materials with localised imperfections. We will consider a problem in which the material is periodic everywhere except for a small portion of the domain, where some inclusions are added. As a first step, we disregard the inclusions.

Let us then begin by considering the problem (6.2.1) with $\Omega = [0,1] \times [0,1]$ and assume that the underlying material is isotropic. This means that the components of the elasticity tensor $\widetilde{\mathbf{A}}$ can be written as

$$\widetilde{a}_{2222}(\mathbf{y}) = \widetilde{a}_{1111}(\mathbf{y}) = \frac{E(\mathbf{y})}{1-\nu^2(\mathbf{y})}; \qquad \widetilde{a}_{2211}(\mathbf{y}) = \frac{E(\mathbf{y})\nu(\mathbf{y})}{1-\nu^2(\mathbf{y})}; \tag{6.3.3}$$

$$\widetilde{a}_{2121}(\mathbf{y}) = \frac{E(\mathbf{y})}{2(1+\nu(\mathbf{y}))}; \qquad \widetilde{a}_{2111}(\mathbf{y}) = \widetilde{a}_{2221}(\mathbf{y}) = 0, \tag{6.3.4}$$

see Chapter 4. We further assume that the material is also layered and that its reference cell $Y = [0,1] \times [0,1]$ can be decomposed into two subdomains $Y_1 = [0,\ \frac{1}{2}] \times [0,\ 1]$, $Y_2 = [\frac{1}{2},\ 1] \times [0,\ 1]$, see Figure 6.4. These are such that Y_i is occupied by a linear elastic material with Young's modulus $E_i = E_i(y_1)$ and Poisson's ratio $\nu_i = \nu_i(y_1)$, where $\mathbf{y} = (y_1,\ y_2)$ and $i = 1, 2$. We can then write

$$E(\mathbf{y}) = E_1\chi_1(y_1) + E_2\chi_2(y_1), \tag{6.3.5}$$

$$\nu(\mathbf{y}) = \nu_1\chi_1(y_1) + \nu_2\chi_2(y_1), \tag{6.3.6}$$

where χ_1 and χ_2 are the characteristic functions of the sets Y_1 and Y_2.

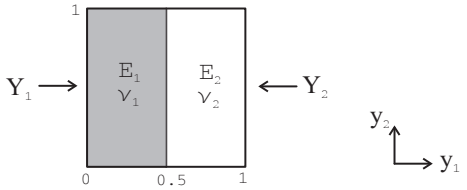

Figure 6.4: Reference cell Y, composed of two different materials.

Finally let

$$\nu_1 = \nu_2 = 0.3, \ \ E_1 = 1, \ \ E_2 = 3, \ \ \epsilon = 0.02, \ \ \mathbf{f} = \mathbf{0}, \tag{6.3.7}$$

and the boundary conditions be such that

$$\Gamma_D = \{0\} \times [0,1], \ \boldsymbol{\varphi}_N(\mathbf{x}) = \begin{cases} (0,1), & x_2 = 1, \\ (0,0), & x_2 = 0, \\ (1,0), & x_1 = 1. \end{cases} \tag{6.3.8}$$

A reference solution $\mathbf{u}^\epsilon$ for (6.2.1) with (6.3.3)-(6.3.8) can be determined using finite elements with a very fine mesh. What we want to do now is to approximate the solution of this problem using homogenisation to obtain a cheap initial guess for the problem we will consider next, where inclusions are present. Recall that the homogenised medium corresponding to the isotropic layered material we have mentioned is orthotropic with material constants given by

$$E_x = \frac{\overline{E}}{\overline{\nu}^2 + A\overline{E}},\ E_y = \overline{E}, \tag{6.3.9}$$

$$\nu_{xy} = \frac{\overline{\nu}}{\overline{\nu}^2 + A\overline{E}},\ \nu_{yx} = \overline{\nu}, \tag{6.3.10}$$

$$G = \frac{1}{(1+\nu_1)/E_1 + (1+\nu_2)/E_2}, \tag{6.3.11}$$

where

$$\overline{E} = \frac{1}{2}(E_1 + E_2),\ \ \overline{\nu} = \frac{1}{2}(\nu_1 + \nu_2),\ \ A = \frac{1}{2}(\frac{1-\nu_1^2}{E_1} + \frac{1-\nu_2^2}{E_2}). \tag{6.3.12}$$

We use quadratic finite elements to compute the homogenised solution $\overline{\mathbf{u}}$. A uniform square grid with 50×50 elements is employed. The norms of the horizontal and vertical components of the error $\overline{\mathbf{E}} := \overline{\mathbf{u}} - \mathbf{u}^\epsilon$ of this approximation are displayed in the third line of Table 6.5.

	Horizontal component		Vertical component	
	$\|\cdot\|_\infty$	$\|\cdot\|_{L^2(0,1)}$	$\|\cdot\|_\infty$	$\|\cdot\|_{L^2(0,1)}$
$\overline{\mathbf{E}}$	$1.2E-1$	$2.2E-2$	$1.9E-1$	$6.2E-2$
$\mathbf{E}_C$	$3.3E-2$	$3.5E-3$	$3.0E-2$	$3.6E-3$

Table 6.5: Error arising from the homogenisation procedure.

In order to obtain a better approximation for $\mathbf{u}^\epsilon$, we will make use of the *first order corrector* $\mathbf{u}_1$ and the *boundary corrector* $\mathbf{C}$. The former is given by

$$\mathbf{u}_1(\mathbf{x}) = \frac{1}{2}\sum_{i,j=1,2}\left(\frac{\partial \overline{u}_i}{\partial x_j} + \frac{\partial \overline{u}_j}{\partial x_i}\right)\chi^{ij}(\frac{\mathbf{x}}{\epsilon}), \tag{6.3.13}$$

where χ^{ij} is the solution of the cell problem (4.2.7). The boundary corrector $\mathbf{C}$ can be approximated by the solution of the following problem

$$\begin{cases} -\nabla \cdot (\overline{\mathbf{A}}\boldsymbol{\epsilon}(\mathbf{C})) = \mathbf{0}, & \mathbf{x} \in \Omega, \\ \mathbf{C} = -\epsilon \mathbf{u}_1, & \mathbf{x} \in \Gamma_D, \\ \boldsymbol{\sigma}(\mathbf{C}) \cdot \mathbf{n} = 0, & \mathbf{x} \in \Gamma_N. \end{cases} \tag{6.3.14}$$

Now, to compute $\mathbf{u}_1$ we first have to solve the cell problem. We do so by approximating the piecewise constant function E by a continuous smooth function as in Chapter 4. As before, we employ square quadratic finite elements. The derivatives of components of the homogenised function $\overline{\mathbf{u}}$ in (6.3.13) are determined by numerical differentiation. As for the boundary corrector, it can be computed from (6.3.14) again by using finite elements.

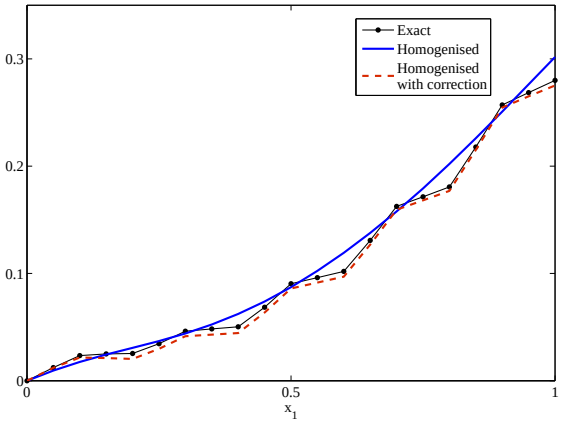

Figure 6.5: Exact and approximated solutions for the horizontal component of the displacement along $x_2 = 0.7$.

The norms of the horizontal and vertical components of the error function $\mathbf{E}_C := (\overline{\mathbf{u}} + \epsilon\mathbf{u}_1 + \mathbf{C}) - \mathbf{u}^\epsilon$ are displayed in the last line of Table 6.5. As expected, the use of correctors gives better results than using the homogenised solution $\overline{\mathbf{u}}$ as an approximation. In Figure 6.5 we plot the horizontal components of the exact solution of the problem $\mathbf{u}^\epsilon$, the homogenised function $\overline{\mathbf{u}}$ and the homogenised corrected approximation $\overline{\mathbf{u}} + \epsilon\mathbf{u}_1 + \mathbf{C}$, along $x_2 = 0.7$.

Up to this point we considered a problem concerning an ϵ-periodic material plate. We will now look into a modification of this problem where inclusions are present, as originally intended. Consider (6.2.1) with (6.2.2), where the computational domain $\Omega = [0,1] \times [0,1]$ is split into the non-overlapping subdomains $\Omega_1 = [0, 0.1] \times [0, 0.1]$ and $\Omega_2 = \Omega - \Omega_1$. The components of the elasticity tensor are assumed to satisfy (6.3.3)-(6.3.6) with (6.3.7) throughout Ω except for some circular inclusions on Ω_1, see Figure 6.6. Furthermore, we assume that (6.3.8) holds.

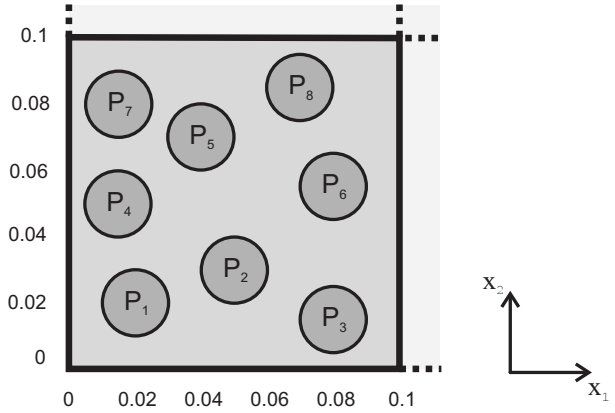

Figure 6.6: Inclusions present on the subdomain Ω_1.

The inclusions consist of a linear elastic material characterised by Young's modulus $E_3 = 4$ and Poisson's ratio $\nu_3 = 0.1$. The radius of each inclusion is $r = 0.01$. They are centred at the points

$$P_1 = (0.02,\ 0.02),\ P_2 = (0.05,\ 0.03),\ P_3 = (0.08,\ 0.015),$$
$$P_4 = (0.015,\ 0.05),\ P_5 = (0.04,\ 0.07),\ P_6 = (0.08,\ 0.055),$$
$$P_7 = (0.015,\ 0.08),\ P_8 = (0.07,\ 0.085).$$

We thus deal with a problem related to a periodic structure with localised imperfections. A reference solution $\mathbf{u}$ for this problem can be determined using finite elements with a very fine mesh.

To find an approximation for $\mathbf{u}$, we employ the hybrid approach for elasticity expressed by Algorithm 6.2. Let $\widehat{\Omega}_1 = [0,\ 0.15] \times [0,\ 0.15]$, cf. Figure 6.2. The algorithm iterates over the overlapping region $[0.10,\ 0.15] \times [0.10,\ 0.15]$, generating a sequence of approximations

$$\widehat{\mathbf{u}}^{(k)}(\mathbf{x}) := \begin{cases} \widehat{\mathbf{u}}_1^{(k)}(\mathbf{x}),\ \mathbf{x} \in \Omega_1, \\ \widehat{\mathbf{u}}_2^{(k)}(\mathbf{x}),\ \mathbf{x} \in \Omega_2. \end{cases} \tag{6.3.15}$$

We take $\widehat{\boldsymbol{\lambda}}^{(0)} := \overline{\mathbf{u}}|_{\Gamma_2}$, where $\overline{\mathbf{u}}$ is the homogenised solution computed previously. At each iteration step, finite elements and numerical differentiation are used, adapting the procedure described for the one-dimensional example.

The third line of Table 6.6 displays the norms of the error $\mathbf{E}^0 := \mathbf{u} - \overline{\mathbf{u}}$ of the approximation which we give as an initial guess. On the fifth line of the table we show the norms of

	Horizontal component		Vertical component		Iterations
	$\|\cdot\|_\infty$	$\|\cdot\|_{L^2(0,1)}$	$\|\cdot\|_\infty$	$\|\cdot\|_{L^2(0,1)}$	k
$\mathbf{E}^0$	$1.7E-1$	$2.8E-2$	$2.3E-1$	$7.5E-2$	–
$\overline{\mathbf{E}}$	$8.2E-2$	$8.5E-3$	$1.0E-1$	$2.7E-2$	5
$\mathbf{E}_C$	$3.8E-2$	$5.4E-3$	$3.9E-2$	$5.8E-3$	7

Table 6.6: Error arising from the hybrid procedure.

the approximations obtained by using the hybrid approach as described. Alternatively, steps 2 to 3 of Algorithm 6.2 may be skipped, avoiding having to compute correctors. We then obtain the results shown in the fourth line of Table 6.6.

Chapter 7

Fracture of composites

In a linear elastic, homogeneous and isotropic material, the stress and displacement fields around a crack tip are characterised by the SIFs, as was seen in Chapter 3. Once these parameters have been determined, it is possible to predict the future behaviour of a crack, namely whether it will propagate and if so in what direction.

For composite materials finding the path of a pre-existent crack is a very challenging problem. Not only the interaction of the crack with the heterogeneities has to be accounted for, but already solving the underlying elasticity problems is computationally very complex. It requires appropriate numerical techniques such as those introduced in Chapters 4 to 6.

In this chapter the effect of the local structure on the process of crack propagation occurring on a highly heterogeneous composite plate is analysed. The evaluation of stress intensity factors using the hybrid approach, which leads to accurate and computationally feasible solutions of the elasticity problems, is discussed. Finally, an algorithm to determine the crack path is proposed.

7.1 Behaviour of the SIFs

On the microscopic level the propagation of a given crack on a composite linear elastic material is influenced by aspects like the orientation of the material constituents and the existence of internal *defects* such as microcracks, voids and inclusions. Mathematically this can be seen in the way the SIFs vary according to the constitution of the vicinity of the crack tip.

7.1.1 Effects of the local structure

In what follows we investigate how the local structure of a plate influences the SIFs of a pre-existent static crack. To do this consider a cracked plate $\Omega = \Omega_P - \Omega_C$, where $\Omega_P = [-0.5, 0.5] \times [-0.5, 0.5]$ and Ω_C is the crack line $[-0.5, -0.3] \times \{0\}$ of length $a = 0.2$, see Figure 7.1.

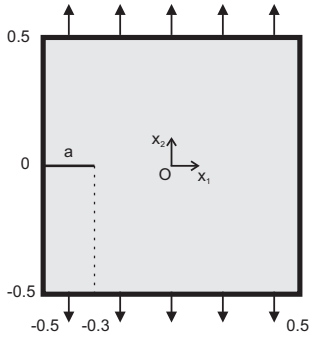

Figure 7.1: Cracked plate.

Assume that the plate is composed of a periodically layered elastic material with isotropic homogeneous components, its behaviour being modelled by (4.2.2). The components of the related elasticity tensor $\widetilde{\mathbf{A}}$ then read

$$\widetilde{a}_{2222}(\mathbf{y}) = \widetilde{a}_{1111}(\mathbf{y}) = \frac{E(\mathbf{y})}{1-\nu^2(\mathbf{y})}, \qquad \widetilde{a}_{2211}(\mathbf{y}) = \frac{E(\mathbf{y})\nu(\mathbf{y})}{1-\nu^2(\mathbf{y})}, \tag{7.1.1}$$

$$\widetilde{a}_{2121}(\mathbf{y}) = \frac{E(\mathbf{y})}{2(1+\nu(\mathbf{y}))}, \qquad \widetilde{a}_{2111}(\mathbf{y}) = \widetilde{a}_{2221}(\mathbf{y}) = 0. \tag{7.1.2}$$

Let the plate be pulled at its upper and lower edges. The remaining boundaries, including the crack edges, are considered to be stress-free, so that the following conditions hold

$$\boldsymbol{\varphi}_N(\mathbf{x}) = \begin{cases} (0,1), & x_2 = 0.5, \\ (0,-1), & x_2 = -0.5, \\ (0,0), & \text{otherwise.} \end{cases} \tag{7.1.3}$$

We assume that the reference cell for this material, given by $Y = [0,1] \times [0,1]$, is the union of the two subdomains $Y_1 = [0,\ 0.5] \times [0,\ 1]$, $Y_2 = [0.5,\ 1] \times [0,\ 1]$, composed respectively by materials A and B, see Figure 7.2. For $i = 1,\ 2$, Y_i is occupied by a material with Young's modulus E_i and Poisson's ratio ν_i and we have

$$E(\mathbf{y}) = E_1\chi_1(y_1) + E_2\chi_2(y_1), \tag{7.1.4}$$

$$\nu(\mathbf{y}) = \nu_1\chi_1(y_1) + \nu_2\chi_2(y_1), \tag{7.1.5}$$

where χ_1 and χ_2 are the characteristic functions of the sets Y_1 and Y_2.

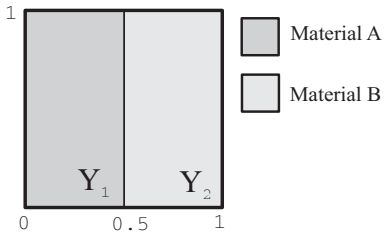

Figure 7.2: Reference cell Y, composed by materials A and B.

Finally let

$$\nu_1 = 0.3,\ \ \nu_2 = 0.1,\ \ E_1 = 10,\ \ E_2 = 1,\ \ \epsilon = 0.02,\ \ \mathbf{f} = \mathbf{0}. \tag{7.1.6}$$

The problem we have described up to now has been set up so that the material layers are orthogonal to the crack line, see Figure 7.3 e). Other material orientations can also be considered. In particular, we look into the five situations depicted in Figure 7.3, representing zoom-ins of the vicinity of the crack tip. The figures labelled a) to e) correspond to various material orientations characterised by the angle θ_0 that the layer boundaries form with the horizontal axis. We assume that the crack tip lays inside material A.

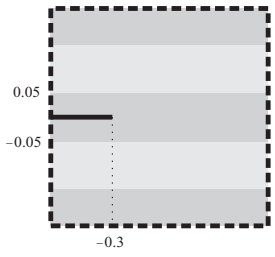

Figure 7.3 - a) $\theta_0 = 0^o$

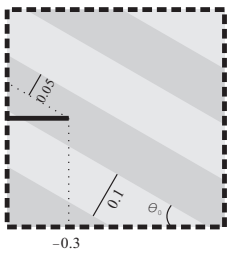

b) $\theta_0 = 30^o$.

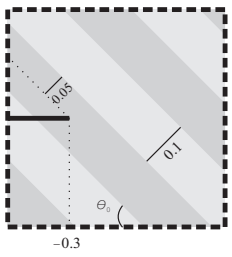

c) $\theta_0 = 45^o$.

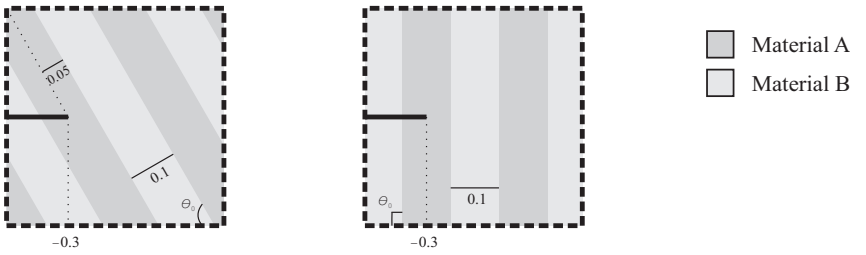

d) $\theta_0 = 60^o$. *e)* $\theta_0 = 90^o$.

We now want to compute the mode I and mode II stress intensity factors. Once this has been done, we may also obtain the propagation angle θ_P for each of these configurations using the maximum circumferential tensile stress criterion. We recall that this is the angle under which the crack will propagate if the loading is large enough for crack growth to occur. Before we can compute the SIFs, we have to solve the elasticity problems (4.2.2) with (7.1.1)-(7.1.6) for the various values of θ_0. For that we employ the finite element method. A fine mesh with quadratic triangular elements in the vicinity of the crack tip and quadratic rectangular elements everywhere else is generated. This allows for the computation of the displacement and stress fields for the different material orientations. The SIFs K_I and K_{II} are then determined using the J-integral method and their values are displayed in Table 7.1. As for the propagation angle θ_P also included in the table, it is zero when $\theta_0 = 0^o$ or $\theta_0 = 90^o$. The other cases are computed using (3.3.10).

θ_0	K_I	K_{II}	θ_P
0^o	2.20	0	0^o
30^o	2.13	$-2.23E-2$	1.2^o
45^o	2.10	$-5.22E-2$	2.8^o
60^o	2.11	$-8.20E-2$	4.4^o
90^o	2.13	0	0^o

Table 7.1: SIFs and propagation angles. The material surrounding the crack tip is characterised by E_1 and ν_1.

Next we interchange the roles of materials A and B. We assume they are now characterised by E_2 and ν_2 and by E_1 and ν_1 respectively. We solve the previous problem with this new assumption. The values we find are shown in Table 7.2.

By comparing the results in the previous two tables, it can be seen that the local structure can influence the value of the SIFs quite dramatically. Indeed, if we take for instance the values of K_I and K_{II} along the second and third columns of Table 7.1 or of Table 7.2 we

θ_0	K_I	K_{II}	θ_P
0^o	$8.16E-1$	0	0^o
30^o	$7.75E-1$	$7.18E-2$	-10.4^o
45^o	$7.10E-1$	$1.07E-1$	-16.4^o
60^o	$6.24E-1$	$1.21E-1$	-20.5^o
90^o	$5.39E-1$	0	0^o

Table 7.2: SIFs and propagation angles. The material surrounding the crack tip is characterised by E_2 and ν_2.

see that the SIFs vary with the material orientation. However, there is a greater difference when we compare the situations in which the roles of the materials A and B are interchanged. The values of the K_I and K_{II} change dramatically when we compare the two tables for the same values of θ_0. This sensitivity of the SIFs to the material structure is particularly relevant for composites or other materials that are very heterogeneous.

We note that we dealt with a heterogeneous periodic plate where the period ϵ of the heterogeneities was rather large. For that accurate numerical approximations of the solutions of the elasticity problems and consequently of the SIFs can be obtained by the finite element method and taken as reference solutions. When ϵ is much smaller, the typical mesh width h must satisfy $h \ll \epsilon$ to yield reasonable results and so prohibitively thin meshes have to be employed. Alternatively, we may adopt a macroscopic approach and replace the heterogeneous medium by a fictitious equivalent homogeneous material. In particular, instead of the layered material with vertically disposed layers for which (7.1.4) and (7.1.5) hold, one may consider the orthotropic material characterised by the elasticity tensor $\overline{\mathbf{A}}$ with components

$$\overline{a}_{1111} = \frac{E_x}{1-\nu_{xy}\nu_{yx}}, \qquad \overline{a}_{2211} = \frac{E_x\nu_{yx}}{1-\nu_{xy}\nu_{yx}}, \tag{7.1.7}$$

$$\overline{a}_{2222} = \frac{E_y}{1-\nu_{xy}\nu_{yx}}, \qquad \overline{a}_{2121} = G_{xy}, \tag{7.1.8}$$

$$\overline{a}_{2111} = \overline{a}_{2221} = 0, \tag{7.1.9}$$

where $\nu_{xy}E_y = \nu_{yx}E_x$, cf. Chapter 4. Homogenisation can also be applied for the remaining material orientations other than for $\theta_0 = 90^o$, by rotating the axes of orthotropy.

The advantage of the homogenisation procedure lays in the very significative simplification of the underlying elasticity equations, as the ϵ-dependent coefficients are replaced by constants. However this comes at the price of losing the effects of locality. Indeed, homogenisation intends to provide the average behaviour of a material in some sense,

not its local behaviour, so it is not as accurate. Moreover, we note that if we are interested in computing the SIFs and propagation angles for the homogenised material it should be taken into account that the homogenised material is *orthotropic*. In particular, the *maximum circumferential tensile stress criterion* should be reformulated, cf. [64].

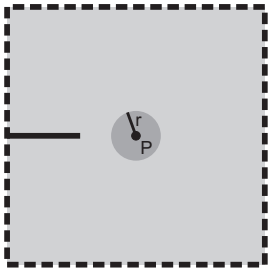

Figure 7.4: Inclusion near the crack tip.

Besides the material orientation, the behaviour of the SIFs is also affected by the presence of defects, as we will illustrate in the following example. Consider again the cracked plate represented in Figure 7.1, and let it now be composed of a linear elastic isotropic homogeneous material with $E = 1$ and $\nu = 0.1$. We assume that it is subject to the boundary conditions (7.1.3), so that a mode I situation arises. Using the finite element method to compute the SIF for this configuration, we find that $K_I = 1.18$.

Now consider the same plate but containing one linear elastic circular inclusion of radius 0.05, centred at the point P and characterised by $E_2 = 10$ and $\nu_2 = 0.3$, cf. Figure 7.4. We take various coordinates for P as listed in Table 7.3, so that the SIF can be measured when the inclusion is closer or further from the crack tip, located at $(-0.3, 0)$.

P	d	K_I
$(-0.2, 0)$	0.05	1.11
$(-0.1, 0)$	0.15	1.16
$(-0.2, 0.2)$	0.17	1.14
$(-0.1, 0.2)$	0.23	1.15
$(0, 0)$	0.25	1.17
$(0.2, 0)$	0.45	1.18

Table 7.3: SIF affected by the proximity of an inclusion.

When the inclusion is at a larger distance d from the crack tip, the SIF is about the same as the one computed for the plate without any inclusion. Conversely, this fracture parameter is affected by a closer proximity of the inclusion, see Table 7.3.

This example illustrates the sensitivity of the stress intensity factors to the local characteristics of the surroundings of the crack tip. Many other authors have also studied this phenomenon, see for example [24, 84, 85]. If one looks for accurate approximations for the SIFs, the local structure in the vicinity of the crack tip may not be disregarded. As we move away from this region, the heterogeneities have much less influence on the crack behaviour.

7.1.2 Computational aspects

The first step in predicting the behaviour of a pre-existing crack in a composite plate lays in solving the related elasticity problem. Doing so using the finite element method without disregarding the heterogeneities is usually too demanding in terms of the computational complexity.

To deal with this problem we would like to have the best of both worlds and design a method that is both accurate - especially in the vicinity of the crack tip - and computationally feasible. This is the goal of the *hybrid approach* presented in the previous chapter. It is a flexible method that allows the region around the crack tip to be treated separately. With this procedure the computational complexity of the original problem is significantly reduced, as the heterogeneities are only resolved where it is relevant to do so.

In what follows we will apply the hybrid approach to a cracked elastic plate $\Omega = \Omega_P - \Omega_C$, where $\Omega_P = [-1, 1] \times [-1, 1]$ and Ω_C is the closed crack line $[-a, a] \times \{0\}$.

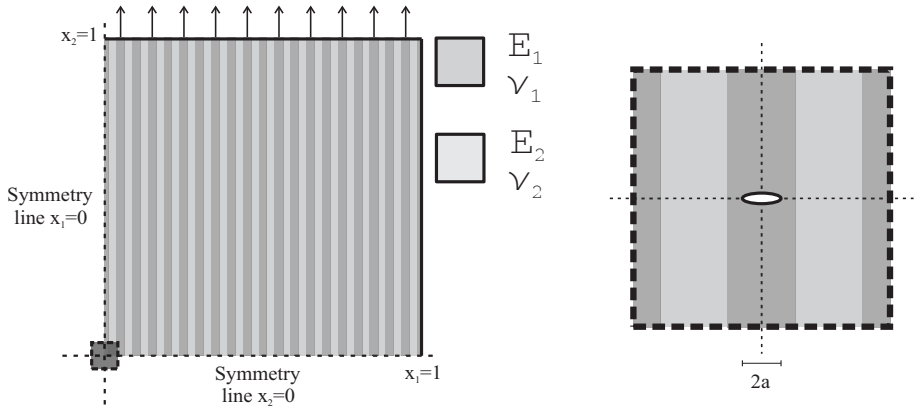

Figure 7.5: Cracked plate (left) and zoom-in around crack region (right).

We assume that the plate is composed of a layered material with isotropic components such that (4.2.2) and (7.1.4)-(7.1.5) hold. The elasticity tensor $\widetilde{\mathbf{A}} = \widetilde{\mathbf{A}}(\mathbf{y})$ depends only on y_1 so that the layers are disposed at a 90° angle with the horizontal axis. Besides this, we take

$$\nu_1 = \nu_2 = 0.3, \;\; E_1 = 3, \;\; E_2 = 1, \;\; \epsilon = 2.5E-2, \;\; \mathbf{f} = \mathbf{0}. \tag{7.1.10}$$

Let the plate be pulled at its upper and lower edges while it remains free of stress along the other boundaries so that we have the following boundary conditions

$$\boldsymbol{\varphi}_N(\mathbf{x}) = \begin{cases} (0,1), & x_2 = 1, \\ (0,-1), & x_2 = -1. \\ (0,0), & \text{otherwise.} \end{cases} \tag{7.1.11}$$

Due to the underlying symmetry of the elasticity problem, it suffices to consider the domain $[0,1] \times [0,1] - ([0,a] \times \{0\})$ represented in Figure 7.5.

Consider the values for a, half of the crack length, included in the first line of Table 7.4. For each of these values a solution is found for the elasticity problem employing finite elements, with very fine meshes. We take these as reference solutions. Using the J-integral method the mode I stress intensity factor K_I is computed. It is included in the second line of the table.

SIF \ a	$2.5E-3$	$5.0E-3$	$7.5E-3$	$1.0E-2$
K_I	$1.33E-1$	$1.93E-1$	$2.46E-1$	$3.24E-1$
K_I^{ha}	$1.31E-1$	$1.90E-1$	$2.47E-1$	$3.18E-1$

Table 7.4: SIF for various crack lengths.

Next, we look for an approximation of the SIF applying the hybrid approach. The computational domain $\Omega_{Cp} = [0,1] \times [0,1]$ is split into the overlapping subdomains $\widehat{\Omega}_1 = [0,0.15] \times [0,0.15]$ and $\Omega_2 = \Omega_{Cp} - ([0,0.1] \times [0,0.1])$. We compute the elasticity problem by Algorithm 6.2, as in the previous chapter, and determine the stress intensity factors K_I^{ha} with the J-integral method. These values are displayed in the last line of Table 7.4.

This example illustrates the computational capabilities and the accuracy of the hybrid approach. We note that similarly accurate results could have been obtained without resorting to domain decomposition as in Algorithm 6.2. Indeed, whilst in the vicinity of the crack tip the original differential equations must be considered, the heterogeneous material can be replaced by an equivalent homogenised material in the remainder of the plate. This gives rise to a problem that may be solved by the finite element method employing a mesh that is finer near the crack tip. In the case of the problem we have just considered such an approach is computationally feasible. It is then a good idea to use it because it is easier to implement than Algorithm 6.2.

Note however that if we had more than one crack or if we wanted the subdomain where

the microscale structure must be resolved to be handled separately then Algorithm 6.2 would have to be used without suppressing domain decomposition.

7.2 Crack paths in layered materials

The problem of the growth of a pre-existent crack on a homogeneous linear elastic plate under plane stress conditions was addressed earlier in Chapter 3. The crack path was determined adopting the incremental approach proposed in Algorithm 3.1, with the direction of propagation being computed at each iteration for the updated plate geometry.

In this section we want to extend the previous analysis to deal with the problem of a crack propagating on a linear elastic plate under plane stress conditions, but now constituted of a highly heterogeneous composite material. This implies that a growing crack will likely interact with more than one material and also with the respective interfaces. At a given moment, we can then distinguish between the situations when the crack tip region is contained inside one of the components of the composite and when the tip is at an interface.

Naturally, these two situations are not likely to be static. A crack that has its tip at the interface may be directed away from it or even continue propagating between the materials, i.e., *delaminating*. Also, any crack propagating through a material component may encounter an interface. When this happens, several situations are possible. The crack may penetrate into the adjacent material, eventually suffering a change in angle, reflect back to the material it was originally propagating in or be deflected along one or both sides of the interface so that delamination occurs, see Figure 7.6 and cf. [29,59,75].

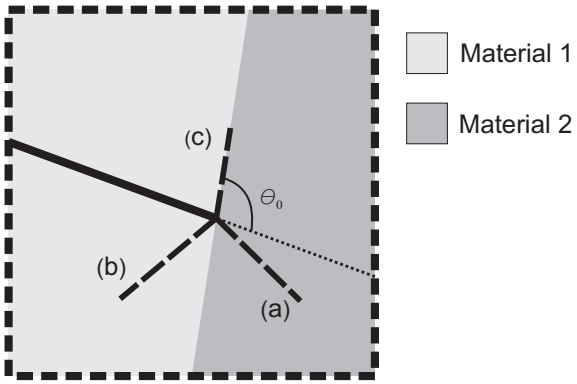

Figure 7.6: The crack (full line) may penetrate (a), be reflected back (b), or deviate along the interface (c).

For reasons of simplicity we will assume that the components of the composite are well bonded so that no delamination may occur in what follows. We will also disregard the

possibility of branching, creation of new cracks or the existence of flaws in the plate as well as of interfaces between more than two materials. One may e.g. consult [9, 24, 63] for this.

Under these assumptions, for a crack present in a linear elastic plate with isotropic homogeneous constituents, the stress and displacement fields are characterised by (3.2.5) and (3.2.14) when the crack tip is laying inside one of the constituents. This is no longer the case when the crack tip is positioned at an interface. Let us consider the situation depicted in Figure 7.6 where the crack penetrates into the adjacent material. The order of the stress singularity is then characterised by the solution λ of the equation

$$\begin{aligned}&\big[\alpha+\beta^2-(1-\beta)(\alpha-\beta)(1-\cos(2\theta_0))\lambda^2\\&+(1-\beta^2)(\pi-2\theta_0)\cos(\lambda\pi)\cos(\lambda)\big]^2\\&+(1-\beta^2)(\pi-2\theta_0)\sin^2(\lambda)\left[(1-\beta^2)\cos^2(\lambda\pi)+\beta^2-\alpha^2\right]=0,\end{aligned}\tag{7.2.1}$$

where α and β are the so-called *Dundurs bimaterial parameters*, cf. [22, 27, 59]. Let us denote by $\sigma^m_{\theta\theta}$ and $\sigma^m_{r\theta}$ the tangential and radial stress fields defined over the material m, $m = 1, 2$, where the axes are positioned as represented in Figure 3.3. Then when λ is a real number these fields satisfy

$$\sigma^m_{\theta\theta}+i\sigma^m_{r\theta}=r^{\lambda-1}\mathbf{F}^m(\theta,\alpha,\beta,K_I,K_{II}).\tag{7.2.2}$$

When $\lambda = \mathrm{Re}(\lambda) + i\,\mathrm{Im}(\lambda)$ is complex, they read

$$\sigma^m_{\theta\theta}+i\sigma^m_{r\theta}=r^{\mathrm{Re}(\lambda)-1}\mathbf{G}^m(\theta,\alpha,\beta,K_I,K_{II}).\tag{7.2.3}$$

The complex functions $\mathbf{F}^m$ and $\mathbf{G}^m$ can be found for example in [19], where the SIFs K_I and K_{II} are also defined for a crack terminating at the interface.

We are now ready to predict the propagation of a crack in a composite material. When the crack growth occurs far from any interface, the incremental approach of Algorithm 3.1 is applicable. This implies solving an elasticity problem at each iteration using the finite element method, finding approximations for the SIFs and computing the propagation angle from these by using the maximum circumferential tensile stress criterion. The crack is then incremented, i.e., the geometry is updated by subtracting the portion of new crack created.

When the crack tip is at the interface, the stress fields display the more complex behaviour described by (7.2.2) or (7.2.3). We assume that the maximum circumferential tensile stress criterion can again be used to predict the direction of propagation. We approximate this direction by averaging the amplitudes of a number of angles, each

maximising $\sigma_{\theta\theta}$ on a small circle centred at the crack tip. The stress fields are again computed by the finite element method.

It is important to note that in the region near an interface the accuracy of the computed stress fields is less than elsewhere, cf. [84]. To deal with this, our strategy is to adjust the size of the new crack increment when the crack tip approaches this critical region. The propagation angle is kept unchanged and the updated crack tip position lays at the interface. This seems to be a good idea for situations when the angle θ_0 represented in Figure 7.6 is not expected to be close to 0^o or 180^o. If the crack may grow nearly parallel to the interface line, a different approach should be used. Not only small errors in the propagation angle may lead to very different updated crack tip positions, but also cracks parallel to layers behave differently from those that propagate through the layers, see for example [84] and references within.

The procedures we have described can be structured in the following algorithm for a composite plate with a pre-existent crack. We denote by Δa and δ_R the length for the crack increments and the minimum distance between the crack tip and the interface for which we assume the stress fields are accurately computed. Moreover, let $\mathbf{x}_{tip}^{(n)}$ denote the crack tip coordinates with respect to a fixed coordinate system at the iteration step n. Finally, $\theta^{(n)}$ is the angle between the crack segment containing the crack tip and the x_1-axis of the coordinate system.

Algorithm 7.1

Set $n = 0$. Given: Δa, δ_R, $\mathbf{x}_{tip}^{(0)}$, $\theta^{(0)}$.

1- Solve the elasticity problem.

2- If $\mathbf{x}_{tip}^{(n)}$ is at an interface, compute $\sigma_{\theta\theta}$ using (3.3.6). Otherwise skip to step 4.

3- Compute the value of the propagation angle θ_P using the maximum circumferential tensile stress criterion. Skip to step 6.

4- Compute the values of the stress intensity factors K_I and K_{II}.

5- Determine the angle of propagation $\theta_P = \theta_P^{(K)}$ using equation (3.3.10).

6- Update the crack angle and the crack tip coordinates

$$\theta^{(n+1)} := \theta^{(n)} + \theta_P, \tag{7.2.4}$$

$$\mathbf{x}_{tip}^{(n+1)} := \mathbf{x}_{tip}^{(n)} + \Delta a(\cos(\theta^{(n+1)}), \sin(\theta^{(n+1)})). \tag{7.2.5}$$

7- Find the coordinates $\mathbf{y}^{(n+1)}$ of the point in the interface that is collinear with the points of coordinates $\mathbf{x}_{tip}^{(n)}$ and $\mathbf{x}_{tip}^{(n+1)}$. If $\|\mathbf{y}^{(n+1)} - \mathbf{x}_{tip}^{(n+1)}\| < \delta_R$ replace $\mathbf{x}_{tip}^{(n+1)}$ by $\mathbf{y}^{(n+1)}$,

$$\mathbf{x}_{tip}^{(n+1)} \to \mathbf{y}^{(n+1)}. \tag{7.2.6}$$

8- Increment n, $n \to n+1$.

9- If required to determine the path further, repeat steps 1 to 9.

We will now consider a periodically layered plate $\Omega = ([-0.5, 0.5] \times [-0.5, 0.5]) \setminus \Omega_C$, displaying a pre-existent crack, the crack line being given by $\Omega_C = [-0.50, -0.49] \times \{0\}$, cf. Figure 7.7. The layers are at a 45º angle with the horizontal axis and the two components of the plate are isotropic, homogeneous and linear elastic, being characterised by $E_1 = 1, \nu_1 = 0.1$ and $E_2 = 10, \nu_2 = 0.3$.

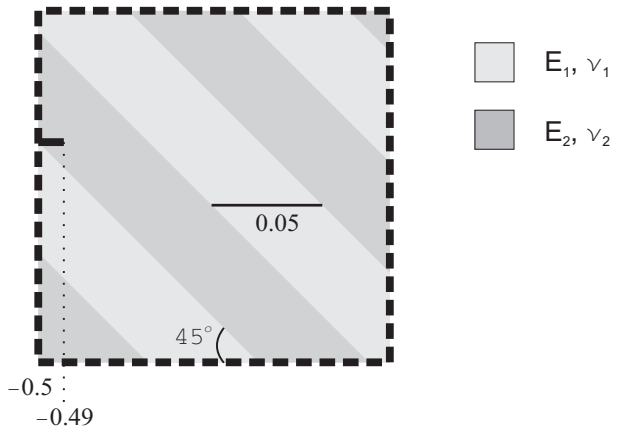

Figure 7.7: Zoom in of the crack tip region.

To complete the problem formulation, we consider the following boundary conditions

$$\boldsymbol{\varphi}_N(\mathbf{x}) = \begin{cases} (0,1), & x_2 = 0.5, \\ (0,-1), & x_2 = -0.5, \\ (0,0), & \text{otherwise}, \end{cases} \tag{7.2.7}$$

and that body forces are absent. Our goal is to predict the path of the crack assuming that the loading is sufficiently large to ensure crack growth. We will employ the previous algorithm with $\Delta a = 0.01$ and $\delta_R = 0.0125$ in two ways that differ in how the first step of the algorithm is done. The first of these consists of computing a reference

solution for the crack path. After this a computationally cheaper approximation will be determined by using the hybrid approach described earlier to solve the elasticity problem in step 1 of the algorithm.

The reference solution is obtained first by solving the elasticity problem by the finite element method using fine meshes, composed of quadratic triangular elements near the crack tip and quadratic rectangular elements elsewhere. The J-integral method is employed to compute the SIFs in the fourth step of the algorithm.

n	$(\Delta a)_{x_1}$	$(\Delta a)_{x_2}$	θ_P
0	$9,89E-3$	$1.48E-3$	8.52^o
1	$9.95E-3$	$-9.90E-4$	-14.20^o
2	$9.82E-3$	$-1.88E-3$	-5.16^o
3	$1.82E-2$	$-7.09E-3$	-9.81^o

n	$(\Delta a)_{x_1}$	$(\Delta a)_{x_2}$	θ_P
4	$9.85E-3$	$1.74E-3$	30.65^o
5	$9.99E-3$	$4.85E-4$	-12.78^o
6	$1.00E-2$	$1.13E-4$	3.43^o
7	$1.65E-2$	$2.29E-3$	7.27

Table 7.5: Crack tip increments.

This procedure enables us to predict the amplitude of the propagation angles θ_P of the new crack segments, as well as the corresponding horizontal and vertical components $(\Delta a)_{x_1}$ and $(\Delta a)_{x_2}$ of the increment vector. These values are displayed in Table 7.5 for the first 8 increments.

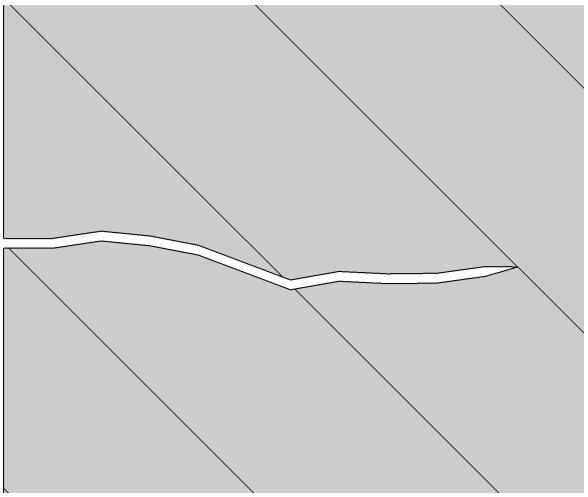

Figure 7.8: Crack propagating through layers.

We note that the lengths of the increments when $n = 3$ and $n = 7$ are greater. This is due to the proximity of the crack tip to the interface. The updated crack tip positions were computed with step 7 of the algorithm. Since the plate is pulled in the vertical direction, the path propagates essentially in a horizontal direction, as can be seen in Figure 7.8.

A second approximation for the crack path is obtained by employing the hybrid approach to solve the first step of Algorithm 7.1. The idea is to reduce the computational complexity of the problem. As we have seen, working with composites often leads to problems that may not be solved efficiently by applying the finite element method in a straightforward manner. Since we considered one crack only, it is not necessary to employ domain decomposition. The hybrid approach procedure then consists of homogenising the material of the plate outside of the rectangle $\Omega_1 = ([-0.5, 0.25] \times [-0.25, 0.25]) \setminus \Omega_C$. Next we solve the elasticity problem for a plate consisting of three distinct materials, the original material components over Ω_1 and the homogenised material over $\Omega \setminus \Omega_1$. The crack path computed using Algorithm 7.1 with the hybrid approach is depicted in dots in Figure 7.9. There we also show the path obtained by using the reference solution, represented as a full line. We can see that the plots almost coincide.

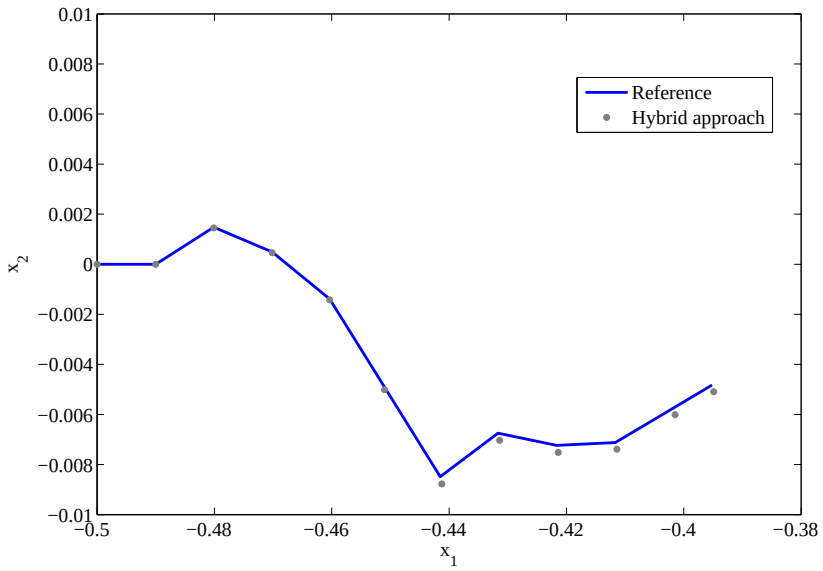

Figure 7.9: Paths determined by application of Algorithm 7.1.

It is then a good strategy to employ the hybrid approach to solve the elasticity problems when one wants to predict crack propagation for highly composite materials. This will actually work better for materials with smaller heterogeneities due to the decrease in the homogenisation error. In that case, the size of the region where we perform a microscopic analysis can be smaller.

Finally, we note that a macroscopic approach can be adopted to find the path for the homogenised plate. Naturally the effects of locality will then be lost, but the procedure is much more straightforward. After employing homogenisation, one can simply apply a modification of Algorithm 3.1. Since the homogenised material is orthotropic, the

maximum circumferential tensile stress criterion needs to be reformulated, see for example [56,64]. One other aspect to consider is that the homogenised model does not take into account the effect of the internal boundaries, so this would have to be incorporated somehow.

Bibliography

[1] M. H. Aliabadi and M. H. López. *Database of stress intensity factors*. Computational Mechanics Publications, 1996.

[2] G. Allaire. *Shape optimization by the homogenization method*. Springer, New York, 2002.

[3] A. Alonso, R. L. Trotta, and A. Valli. Coercive domain decomposition algorithms for advection-diffusion equations and systems. *J. Comput. Appl. Math.*, 96(1):51–76, 1998.

[4] M. F. Ashby and D. R. Jones. *Engineering materials I, an introduction to their properties and applications*. Butterworth Heinemann, 1996.

[5] I. Babuska and J. E. Osborn. Generalized finite element methods: their performance and their relation to mixed methods. *SIAM J. Numer. Anal.*, 20(3):510–536, 1983.

[6] I. Babuska and J. E. Osborn. Finite element methods for the solution of problems with rough data. In *Singularities and constructive methods and their treatment*, pages 1–18. Spring-Verlag, Berlin-New York, 1985.

[7] I. Babuska and T. Strouboulis. *The finite element method and its reliability*. Clarendon Press, Oxford, 2001.

[8] N. Bakhvalov and G. Panasenko. *Homogenization: averaging process in periodic media*. Kluwer Academic, Dordrecht, Boston, London, 1989.

[9] L. Banks-Sills and D. Ashkenazi. A note on fracture criteria for interface fracture. *Int. J. Fract.*, 103(2):177–188, 2000.

[10] E. J. Barbero. *Finite element analysis of composite materials*. CRC Press, 2008.

[11] A. A. Becker. *The boundary element method in engineering*. McGraw-Hill, Maidenhead, 1992.

[12] A. Bensoussan, J. L. Lions, and G. Papanicolaou. *Asymptotic analysis of periodic structures*. North-Holland, Amesterdam, 1978.

[13] P. E. Bjørstad and O. B. Widlund. Iterative methods for the solution of elliptic problems on regions partitioned into substructures. *SIAM J. Numer. Anal.*, 23(6):1097–1120, 1986.

[14] P. E. Bjørstad and O. B. Widlund. To overlap or not to overlap: a note on a domain decomposition method for elliptic problems. *SIAM J. Sci. Stat. Comput.*, 10(5):1053–1061, 1989.

[15] D. Broek. *Elementary engineering fracture mechanics*. Kluwer Academic Publishers, 1986.

[16] L. Ceriolo and A. Tommaso. Fracture mechanics of brittle materials: a historical point of view. *2nd Int. PhD Sympodium in Civil Engineering*, 1998.

[17] T. F. Chan. Domain decomposition algorithms and computational fluid dynamics. *Int. J. High Perform. Comput. Appl.*, 2(4):72–83, 1988.

[18] T. F. Chan and D. Goovaerts. *Schwarz = Schur: overlapping versus nonoverlapping domain decomposition*. CAM 88-21, Department of Mathematics, UCLA, 1988.

[19] J. Chang and J. Xu. The singular stress field and stress intensity factors of a crack terminating at a bimaterial interface. *Int. J. Mech. Sci.*, 49, 2007.

[20] G. P. Cherepanov. *Mechanics of brittle fracture*. MacGraw-Hill, 1979.

[21] D. Cioranescu and P. Donato. *An introduction to homogenization*. Oxford University Press, 1999.

[22] A. Cirello and B. Zuccarello. On the effects of a crack propagating toward the interface of a bimaterial system. *Eng. Fract. Mech.*, 73(9):1264–1277, 2006.

[23] B. Cotterell. The past, present, and future of fracture mechanics. *Eng. Fract. Mech.*, 69:533–553, 2002.

[24] I. Demir, H. M. Zbib, and M. Khaleel. Microscopic analysis of crack propagation for multiple cracks, inclusions and voids. *Theor. Appl. Fract. Mech.*, 36:147–164, 2001.

[25] L. Dickinson. Using fiber to fight delamination: trans-laminar reinforcement out of the lab and into production. *Compos. Manuf.*, 2005.

[26] O. Dubois. *Optimized Schwarz methods for the advection-diffusion equation*. PhD thesis, McGill University, Montréal, 2003.

[27] J. Dundurs. Discussion of edge-bonded dissimilar orthogonal elastic wedges under normal and shear loading. *J. Appl. Mech.*, 36, 1969.

[28] W. E, B. Engquist, L. Li, W. Ren, and E. Vanden-Eijnden. The heterogeneous multiscale method: a review. http://www.math.princeton.edu/multiscale, 2005.

[29] F. Erdogan and T. S. Cook. Antiplane shear crack terminating at and going through a bimaterial interface. *Int. J. Fract.*, 10:227–240, 1974.

[30] F. Erdogan and G. C. Sih. On the crack extension in plates under plane loading and transverse shear. *J. Basic Eng.*, 85:519–527, 1963.

[31] L. B. Freund. *Dynamic fracture mechanics*. Cambridge University Press, 1990.

[32] G. Galilei. *Discorsi e dimonstrazioni matematiche intorno duo nuove scienze*, 1638.

[33] P. Gould. *Introduction to linear elasticity*. Springer-Verlag, 1983.

[34] A. A. Griffith. The phenomena of rupture and flows in solids. *Phil. Trans. Roy. Soc. London*, A221:163–198, 1921.

[35] P. de Haas. *Numerical simulation of nonlinear water waves using a panel method; domain decomposition and applications*. PhD thesis, University of Twente, 1997.

[36] W. Han and B. D. Reddy. *Plasticity mathematical theory and numerical analysis*. Springer, Berlin, 1999.

[37] D. Hegen. *An element-free Galerkin method for crack propagation in brittle materials*. PhD thesis, Technical University of Eindhoven, 1997.

[38] T. Y. Hou and X. H. Wu. A multiscale finite element method for elliptic problems in composite materials and porous media. *J. Comput. Phys.*, 134:169–189, 1997.

[39] T. Y. Hou, X. H. Wu, and Z. Cai. Convergence of a multiscale finite element method for elliptic problems with rapidly oscillating coefficients. *Math. Comp.*, 227(68):913–943, 1999.

[40] G. Houzeaux and R. Codina. An iteration-by-subdomain overlapping Dirichlet / Robin domain decomposition method for advection-diffusion problems. *J. Comput. Appl. Math.*, 158(2):243–276, 2003.

[41] C. E. Inglis. Stresses in a plate due to the presence of cracks and sharp corners. *Proc. Inst. Naval Architects*, 60:219–41, 1913.

[42] G. R. Irwin. Fracture dynamics. *Fracturing of Metals, Proceedings of the ASM Symposium on Fracturing of Metals*, pages 147–166, 1948.

[43] G. R. Irwin. Analysis of stresses and strains near the end of a crack transversing a plate. *Trans. ASME, J. Appl. Mech.*, 24:361–364, 1957.

[44] G. R. Irwin. *Encyclopedia of physics (Handbuch der physic)*, volume IV. Springer, Berlin, 1958.

[45] G. R. Irwin. *Encyclopedia of physics (Handbuch der physic)*, volume VI. Springer, Berlin, 1958.

[46] V. V. Jikov, S. M. Kozlov, and O. A. Oleinik. *Homogenization of differential operators and integral functionals*. Springer-Verlag, Berlin, New York, 1994.

[47] P. K. Jimack. *Engineering computational technology*, chapter Domain decomposition preconditioning for parallel PDE software, pages 193–219. Civil-Comp Press, 2002.

[48] L. Mishnaevsky Jr. *Computational mesomechanics of composites: numerical analysis of the effect of microstructures of composites on their strength and damage resistance*. John Wiley, 2007.

[49] M. Kachanov, B. Shafiro, and I. Trukrov. *Handbook of elasticity solutions*. Kluwer Academic, 2003.

[50] M. F. Kanninen and C. H. Popelar. *Advanced fracture mechanics*. Clarendon Press, 1985.

[51] H. Kishi, Y. Mizuno, and H. Chazono. Base-metal electrode-multilayer ceramic capacitors: past, present and future perspectives. *AAPPS Bulletin*, 14(2), 2004.

[52] A. K. Kulshreshtha and C. Vasile. *Handbook of polymer blends and composites*. Rapra Technology Ltd., 2002.

[53] J. Lancaster. *Engineering catastrophes: causes and effects of major accidents*. Abington Publishing, 2000.

[54] F. F. Lange. Fiber and laminar composites with strong interfaces. *Silic. Indus.*, 63, 1998.

[55] R. W. Lewis and B. Koosha. A mixed mode rock fracture model for the prediction of crack path. *Int. J. Numer. Anal. Meth. Geomech.*, 23:281 – 294, 1999.

[56] W. Lim, S. Choi, and B. Sankar. Biaxial load effects on crack extension in anisotropic solids. *Eng. Fract. Mech.*, 68:403–416, 2001.

[57] J. R. Lund and J. P. Byrne. Leonardo da Vinci's tensile strength tests: Implications for the discovery of engineering mechanics. *Civ. Eng. Environ. Syst.*, 18(3):243–250, 2001.

[58] A. I. Lurie and A. Belyaev. *Theory of elasticity*. Springer, Berlin, 2005.

[59] K. Madani, M. Belhouari, B. Bachir Bouiadjra, B. Serier, and M. Benguediab. Crack deflection at an interface of alumina/metal joint: A numerical analysis. *Comput. Mater. Sci.*, 38:625–630, 2006.

[60] A. L. Madureira. *Métodos numéricos para equações diferenciais parciais com múltiplas escalas*. Notas de aula de Minicurso no Seminário brasileiro de Análise, Vol: 31, No. 2, 2005.

[61] L. E. Malvern. *Introduction to the mechanics of a continuous medium*. Prentice-Hall, 1969.

[62] R. Mattheij, S. Rienstra, and J. ten Thije Boonkamp. *Partial differential equations: modelling, analysis, computation*. SIAM, 2005.

[63] M. A. Meggiolaro, A. C. O. Miranda, J. T. P. Castroa, and L. F. Martha. Stress intensity factor equations for branched crack growth. *Eng. Fract. Mech.*, 72:2647–2671, 2005.

[64] L. Nobile and C. Carloni. Fracture analysis for orthotropic cracked plates. *Compos. Struct.*, 68:285–293, 2005.

[65] E. Orowan. Energy criteria of fracture. *Weld J. Res. Suppl.*, 30:157–160, 1955.

[66] D. R. J. Owen and A. J. Fawkes. *Engineering fracture mechanics: numerical methods and applications*. Pineridge Press, 1983.

[67] M. Patrício and R. Mattheij. Crack propagation analysis. *CASA report 07-03*, 2007.

[68] M. Patrício, R. Mattheij, and G. de With. Homogenisation with application to layered materials. *To appear in Math. Comput. Simulat.*, 2008.

[69] M. Patrício, R. Mattheij, and G. de With. Solutions for periodically distributed materials with localised imperfections. *ICCES'08: International Conference on Computational & Experimental Engineering and Sciences*, 2008.

[70] M. Patrício, R. Mattheij, and G. de With. Solutions for periodically distributed materials with localised imperfections. *To appear in Comput. Model. Eng. Sci.*, 2008.

[71] G. A. Pavliotis and A. M. Stuart. *Multiscale methods: averaging and homogenization*. Springer, 2008.

[72] A. Quarteroni and A. Valli. *Domain decomposition methods for partial differential equations*. Clarendon Press, Oxford, 1999.

[73] J. R. Rice. *Fracture: an advanced treatise*, volume 2, chapter Mathematical analysis in the mechanics of fracture. Academic Press, 1968.

[74] J. R. Rice. A path independent integral and the approximate analysis of strain concentration by notches and cracks. *Transactions of ASME, J. Appl. Mech.*, 35:79–386, 1968.

[75] S. Roham, K. Hardikar, and P. Woytowitz. Crack penetration and deflection at a bimaterial interface in a four-point bend test. *J. Mater. Res.*, 19:3019–3027, 2004.

[76] H. Roos, M. Stynes, and L. Tobiska. *Numerical methods for singularly perturbed differential equations*. Spring-Verlag, 1991.

[77] H. P. Rossmanith. Fracture mechanics and materials testing: forgotten pioneers of the early 20th century. *Fatigue Fract. Eng. Mater. Struct.*, 22:781–797, 1999.

[78] Sanchez-Palencia. *Non-homogeneous media and vibration theory*, volume 127. Springer Verlag, Berlin, 1980.

[79] H. A. Schwarz. Über einen grenzübergang durch alternierendes verfahren. *Vierteljahrsschrift der Naturforschenden Gesellschaft in Zürich*, (15):272–286, 1870.

[80] B. Smith, P. Bjørstad, and W. Gropp. *Domain decomposition: parallel multilevel methods for elliptic partial differential equations*. Cambridge University Press, 1996.

[81] B. F. Smith. *Domain decomposition algorithms for the partial differential equations of linear elasticity*. PhD thesis, New York, 1990.

[82] S. Spagnolo. Sul limite delle soluzioni di problemi di Cauchy relativi all'equazione del calore. *Ann. Sc. Norm. Sup. Pisa*, (21):657–699, 1967.

[83] H. Tada, P. C. Paris, and G. R. Irwin. *The stress analysis of cracks handbook*. ASME Press, 2000.

[84] M. T. Tilbrook, R. Moon, and M. Hoffman. Crack propagation in graded composites. *Compos. Sci. Technol.*, 65:201–220, 2005.

[85] M. T. Tilbrook, K. Rozenburg, E. Steffler, L. Rutgers, and M. Hoffman. Crack propagation paths in layered, graded composites. *Composites Part B*, 37(6):490–498, 2006.

[86] S. P. Timoshenko. *History of the strength of materials*. MacGraw-Hill, 1953.

[87] A. A. F. van de Ven. *Field theory for continuous media*. Lecture notes (Technical University of Eindhoven).

[88] H. M. Versieux and M. Sarkis. Numerical boundary corrector for elliptic equations with rapidly oscillating periodic coefficients. *Commun. Numer. Meth. Eng.*, 22, 2006.

[89] L. da Vinci. Codice Atlantico. Folio 82 recto-B, date unknown.

[90] J. C. W. van Vroonhoven. *Dynamic crack propagation in brittle materials: analyses based on fracture and damage mechanics*. PhD thesis, Technical University of Eindhoven, 1996.

[91] H. M. Westerngaard. Bearing pressures and cracks. *Trans. ASME, J. Appl. Mech.*, 1939.

[92] T. Wilshaw. *Fracture of brittle solids*. Cambridge University Press, 1975.

[93] G. de With. Structural integrity of ceramic multilayer capacitor materials and ceramic multilayer capacitors. *J. Eur. Ceram. Soc.*, 12, 1993.

[94] G. de With. *Structure, deformation and integrity of materials*. Wiley-VCH Verlag, 2006.

[95] A. Zehnder. *Lecture notes on fracture mechanics*. Cornell University, 2007.

Index

Summary

In this thesis we study the problem of crack growth on highly heterogeneous periodically distributed composites. The material components are assumed to be linearly elastic, isotropic and homogeneous. Depending on the length scale at which the problem is viewed, several points of view can be adopted. The simplest approach is given by looking at the macroscale. It is assumed that the propagation occurs on a homogeneous material and we are within the scope of linear elastic fracture mechanics. Predicting the behaviour of a growing crack then involves solving the elasticity problems for the cracked structure as the propagation occurs and having a fracture criterion available.

Instead, when the scale of the constituents is considered, the composites are seen to have complex microstructures. This microscopic point of view gives rise to complicated elasticity problems that can be simplified by employing homogenisation. The heterogeneous material is replaced by a homogenised material that has an equivalent behaviour on the macroscopic scale. Mathematically this means that the highly oscillatory coefficients that characterise the behaviour of the heterogeneous material are replaced by constant coefficients.

Homogenisation allows us to look at a heterogeneous composite at the macroscale as if it were homogeneous. This means that we have less computational complexity but also less accuracy. As the purpose of this thesis is to look at the problem of fracture from the scale of the constituents, homogenisation per se is not an option. However, the prohibitive complexity of elasticity problems for composites has to be addressed somehow, and so we look for other techniques. Domain decomposition methods can be considered as a valid alternative. They solve the original problem by dividing the computational domain in smaller subdomains. This divide and conquer logic certainly looks promising, even allowing parallel implementations, but it requires the microscale to be resolved throughout which seems unnecessary. Indeed, when a crack propagates, we focus on the crack tip and its vicinity. Elsewhere the heterogeneous nature of the material does matter, but it is not as relevant.

This leads us to consider a hybrid approach combining homogenisation and domain decomposition techniques. The idea is to look at the problem of crack propagation at a microscopic length scale only in the vicinity of the crack tip and at the macroscale everywhere else. This approach makes the problems of elasticity of periodically distributed

composites feasible and we show that it provides the desired microscopic accuracy. In particular, with this technique we are able to set up a procedure to predict the path that a crack propagating on a layered composite will follow. Naturally, the interaction of the crack with the material interfaces also has to be addressed.

Samenvatting

In dit proefschrift bestuderen we het probleem van scheurpropagatie (scheurgroei) in extreem heterogene, periodiek verdeelde, composietmaterialen. De componenten van het materiaal worden lineair elastisch, isotroop en homogeen verondersteld. Afhankelijk van de schaal waarop het probleem wordt bekeken kunnen verschillende aanpakken worden toegepast. De eenvoudigste aanpak wordt verkregen door naar de macroschaal te kijken. Hierbij gaat men uit van een scheur die propageert in een homogeen materiaal en die beschreven kan worden met de theorie van lineair elastische breukmechanica. Het gedrag van een groeiende scheur kan dan voorspeld worden door de elasticiteitsproblemen op te lossen in het domein waarin de scheur propageert en door een breukcriterium te gebruiken.

Als daarentegen op de schaal van de materiaalcomponenten wordt gekeken, dan wordt duidelijk dat de composietmaterialen een ingewikkelde microstructuur hebben. Deze microschaal introduceert lastige elasticiteitsproblemen die vereenvoudigd kunnen worden door gebruik te maken van homogenisatietechnieken. Het heterogene materiaal wordt dan vervangen door een homogeen materiaal dat hetzelfde gedrag vertoont op de macroschaal. Wiskundig gezien betekent dit dat de sterk fluctuerende coëfficiënten die het gedrag van het heterogene materiaal beschrijven, worden vervangen door constante coëfficiënten.

Via homogenisatie kunnen we naar heterogene composietmaterialen kijken als ware deze homogeen. Dit betekent dat de complexiteit van de berekening omlaag gaat maar tegelijkertijd ook minder nauwkeurig wordt. Omdat het doel van dit proefschrift is om te kijken naar breuken op de schaal van de materiaalcomponenten, is simpelweg toepassen van homogenisatie geen optie. Daarentegen is de complexiteit van het elasticiteitsprobleem voor de composietmaterialen te hoog en zal dip op de één of ander manier aangepakt moeten worden. Dit is de reden dat we naar andere technieken kijken en domein decompositie biedt hier een mogelijk alternatief. Deze techniek lost het oorspronkelijke probleem op door het rekenkundig domein op de splitsen in kleinere subdomeinen. Deze verdeel en heers strategie ziet er veelbelovend uit, met de mogelijkheid tot parallellisatie in de implementatie, maar vereist wel dat de microschaal overal opgelost moet worden wat gevoelsmatig niet erg zinvol lijkt te zijn. Wanneer namelijk een scheur propageert focussen we op het uiteinde van de scheur en diens directe omgeving. In de rest van het domein is het heterogene aspect van het materiaal wel

aanwezig, maar minder belangrijk.

Dit in gedachte hebbende zet ons ertoe om een hybride methode te bekijken dat een combinatie is van homogenisatie en domein decompositie technieken. Het idee is nu om het probleem van de scheurpropagatie op de microschaal alleen bij het uiteinde van de scheur en diens directe omgeving te bekijken en op de macroschaal in de rest van het domein. Deze aanpak maakt het mogelijk om de elasticiteitsproblemen van periodiek verdeelde composietmaterialen op te lossen. Bovendien laten we zien dat ook aan de gewenste nauwkeurigheid op de macroschaal wordt voldaan. In het bijzonder is het mogelijk om een procedure op te stellen dat het pad van een scheur voorspeld wanneer deze propageert in een gelaagd composietmateriaal. Uiteraard wordt ook de nodige aandacht besteed aan de interactie tussen de scheur en de raakvlakken van de gelaagde materialen.

Curriculum vitae

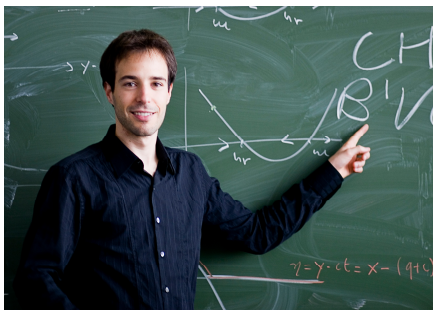

Miguel Patrício was born in Coimbra (Portugal) on October 24, 1980. He finished his pre-university education at the Escola Secundária de Avelar Brotero in his home city in 1998. After that he enrolled at the Department of Mathematics of the University of Coimbra where he graduated in 2003 in (Pure) Mathematics.

Subsequently, Miguel moved to The Netherlands where he joined the Centre for Analysis, Scientific Computing and Applications (CASA) for a period of eight months. He was then granted a four years scholarship by the Fundação para a Ciência e a Tecnologia to work on a different project still at CASA, leading to this thesis.